DYNAMIC SHEAR AMPLIFICATION IN SEISMIC RESPONSE OF STRUCTURAL WALL SYSTEMS

by

Umut Utku CELEP

B.S., Civil Engineering, Dokuz Eylül University, 1998

M.S., Earthquake Engineering, Boğaziçi University, 2001

Submitted to the Kandilli Observatory and
Earthquake Research Institute in partial fulfillment of
the requirements for the degree of
Doctor of Philosophy

Graduate Program in Earthquake Engineering
Boğaziçi University
2008

To my precious wife Beyza CELEP

ACKNOWLEDGEMENTS

I would like to express my deepest gratitude to Professor Nuray Aydınoğlu for his invaluable guidance and help during the preparation of this dissertation, who had been a father to me as well as a wise mentor when I need. I would like to thank for his patience and understanding for the times I had to split focus to my job as a practicing engineer.

I would like to express my sincere gratefulness to my dear wife Beyza Celep for her support and encouragement. This dissertation would not have been completed without her presence.

I would also like to mention my special gratitude to my boss and mentor Osman Müyesser for his support and understanding.

Finally, special thanks to my old friend and colleague Göktürk Önem for his valuable discussions and feedback.

ABSTRACT

DYNAMIC SHEAR AMPLIFICATION IN SEISMIC RESPONSE OF STRUCTURAL WALL SYSTEMS

Previous research indicates that, shear force demand in yielding walls are not proportional to the design moments calculated by code procedures and higher shear force demands develop along the wall with respect to code predictions as a consequence of the higher mode effects after the plastic hinge formation at the base of the wall. 2007 version of the Turkish Seismic Design Code takes the dynamic shear amplification phenomena into account with a constant base shear amplification factor of 1.5 regardless of the first mode period and ductility level of the wall. However, results obtained from extensive non-linear time history analyses performed on generic walls in this study indicate that dynamic shear amplifications increase with increasing first mode period, Strength Reduction Factor (R) and ground motion intensity. A dynamic base shear amplification relationship as a function of the first mode period and strength reduction factor has been proposed for the Turkish Seismic Design Code (2007), based on the regression analysis of the non-linear time history analysis. A story shear force profile has been suggested for the Turkish Seismic Design Code (2007), which is intended for not only preventing shear failures at the base but also along the height of the wall. As a side product of the non-linear time history analyses, a moment profile has also been proposed for use in the Turkish Seismic Design Code (2007). A modal decomposition technique is presented in this study for demonstrating the effects of the higher modes on the dynamic shear amplification phenomenon.

ÖZET

PERDE SİSTEMLERDE DEPREM NEDENİYLE OLUŞAN DİNAMİK KESME KUVVETİ BÜYÜTMESİ

Geçmiş çalışmalar, perde tabanında plastik kesit oluşması sonrasında ortaya çıkan yüksek mod etkileri nedeniyle kesme kuvveti talebinin yönetmelik yöntemleri ile elde edilen tasarım kesme kuvvetlerinden büyük olduğunu ve tasarım momentleri ile uyumsuz olduğunu göstermiştir. 2007 Türk Deprem Yönetmeliği dinamik kesme kuvveti büyütmesini periyot ve deprem yükü azaltma katsayısından (R) bağımsız olarak tasarım taban kesme kuvvetlerine uygulanan 1.5 katsayısı ile dikkate almaktadır. Fakat temsili perde duvarlar üzerinde yapılan zaman tanım alanında doğrusal olmayan analizlerinin sonucunda, dinamik kesme kuvveti büyütmelerinin artan birinci mod periyodu ve deprem yükü azaltma katsayısı ile arttığını göstermektedir. Zaman tanım alanında doğrusal olmayan analizlerden elde edilen sonuçlara yapılan regresyon analizlerinden; 2007 Türk Deprem Yönetmeliği'nde kullanılabilecek, periyot ve deprem yükü azaltma katsayısının fonksiyonu olan bir dinamik taban kesme kuvveti büyütmesi ilişkisi önerilmiştir. Bunun yanında, 2007 Türk Deprem Yönetmeliği'nde kullanılabilecek perde yüksekliği boyunca kesme göçmelerini de engellemek amacıyla bir kat kesme kuvveti dağılımı önerilmiştir. Yapılan zaman tanım alanında doğrusal olmayan analizlerin bir yan ürünü olarak, 2007 Türk Deprem Yönetmeliği için bir perde moment profili önerilmiştir. Çalışmada, yüksek modların dinamik kesme kuvveti büyütmesi üzerindeki etkisi bir modal ayrıştırma tekniği ile gösterilmiştir.

TABLE OF CONTENTS

LIST OF FIGURES

LIST OF TABLES

LIST OF SYMBOLS

R	Strength reduction factor
T_1	First mode period of the wall corresponding to gross section stiffness
T_{1-cr}	First mode period of the wall corresponding to cracked section stiffness
H_w	Total wall height
ω_1	Natural vibration frequency of the wall
EI_g	Bending stiffness of the wall corresponding to gross section properties
$m(y)$	Mass per unit length of the wall
β^b	Dynamic base shear amplification factor
l_w	Dimension of the wall perpendicular to major bending axis
Ψ^o	Flexural overstrength factor
V_e^b	Design base shear obtained by using code procedures
V_a^b	Amplified design base shear
M_e^b	Moment demand at the base of the wall obtained from code procedures
M_r^b	Provided moment strength of the section at the base of the wall
M_E^b	Elastic moment demand at the base of the wall obtained from code procedures
M_n^b	Nominal moment strength of the section at base of the wall associated with characteristic material strengths.
V_f^b	Sliding shear strength at the base of the wall provided by dowel action of the longitudinal reinforcement
A_{sw}	Total longitudinal reinforcement area in the web of the section at the base of the wall

f_{yk}	Characteristic yield strength of reinforcement.

1. INTRODUCTION

Structural walls systems constitute a noteworthy share in high rise building stock built in seismic zones. Structural walls offer advantages not only to structural engineers such as their considerable lateral stiffness and strength and consequent reduction of seismic deformation demands; but also to architects by whom the structural system can also be used as partitioning elements with reduced disturbance.

On the other hand structural walls exhibit the disadvantage of redundancy problems under seismic attack unless they are designed to respond fully elastic, which would be impractical and uneconomical if not impossible. Thus, general design trend is to incorporate Strength Reduction Factors (hereinafter will be called as R factors) to reduce seismic demands on the walls by taking the risk of an acceptable damage that is deemed to develop under design ground motion levels. Traditionally strength reduction factors uniformly apply to all design seismic effects including wall moments and shear forces, that is, wall design shear forces are assumed to be proportional to design moments. However, previous nonlinear time history analyses by various researchers revealed that, this is not the case for wall structures designed to respond the seismic attack in the nonlinear range and shear force demands are greater than the demands expected in the usual design process. This amplification with respect to design shear forces have been attributed to the higher mode effects after yielding occurring at the base of the wall; however quantified explanation of this phenomenon and the range of amplification is still an open field of research.

Current rationale of most seismic design codes is to inhibit brittle shear failure modes while attaining the flexural capacity at the base of the wall, which stems from capacity design principles. However, amplified shear forces, particularly at the base of the wall, may cause unexpected premature brittle shear failure modes of diagonal tension, diagonal compression and sliding before the plastic hinge development if required measures are not taken. This may cause destructive consequences for the structural wall systems designed for high ductility demands since adequate reinforcement and detailing might not be provided for an extra shear force demand.

1.1. Motivation of the Study

Despite the fact that the effect of higher modes are held responsible for shear force amplification after the plastic hinge formation at the base of the wall, analytical demonstration of the problem is rather limited in the literature.

Dynamic shear force amplification is generally taken into account in design by means of base shear amplification factors applied to the design base shear derived from code procedures. Most countries have incorporated base shear amplification factors in their national seismic design codes based on their perspectives to the problem. These amplification factors are presented principally as a function of first mode period and/or strength reduction factors. 1997 version of the Turkish Seismic Design Code (1997) did not incorporate such a factor in the shear design of structural walls; however the 2007 version takes the base shear amplification phenomena into account with a constant base shear amplification factor of 1.5 regardless of the first mode period and ductility level of the wall. It is believed that this must be revised with more rigorous base shear amplification factors consistent with the expected behavior of structural walls in the non-linear range. It is also believed that a shear force profile is also necessary in the Turkish Seismic Design Code (2007) not only for preventing shear failures at the base but also along the height of the structural wall.

1.2. Scope of Work

This work comprises a parametric study performed on generic walls for deriving a dynamic base shear amplification factor relationship, which could be proposed for in lieu of the constant base shear amplification in the Turkish Seismic Design Code (2007). A modal decomposition technique has been presented to demonstrate the responsibility of higher modes in dynamic shear amplifications.

Previous studies on dynamic shear amplification have been covered in Chapter 2, with emphasis given to various country perspectives on the subject. Design and characteristics of the generic walls that will be the basis of the numerical findings in this study are presented in Chapter 3. Effect of higher modes on the dynamic shear

amplifications has been demonstrated in Chapter 4 by using a modal decomposition technique. Subsequently, a relationship for dynamic base shear amplification factors and shear force as well as bending moment profile along the wall height have been suggested for the Turkish Seismic Design Code (2007) in Chapter 6 based on the results of extensive non-linear time history analyses described in Chapter 5.

2. LITERATURE REVIEW

Dynamic shear amplification of structural wall systems designed to respond non-linearly during seismic attack has been documented by limited number of researchers in the past. Majority of the researchers had focused on the base shear amplification as the maximum shear forces develop at the base of the wall. Inevitably, research objectives on the subject have been founded on a particular code perspective since the motivation was the code development for inhibiting premature shear failure of structural walls. Majority of the shear amplification recommendations by researchers are based on parametric non-linear time history analyses and presented in the form of base shear amplification factors. However, descriptive research on the analytical demonstration of the effect of higher modes on the base shear amplification is scarce. The dynamic shear amplification is principally explained in the literature by the deviation of the centroid of inertia forces in the non-linear phase with respect to the centroid of inertia forces prescribed by the triangular code distribution as illustrated in Figure 2.1.

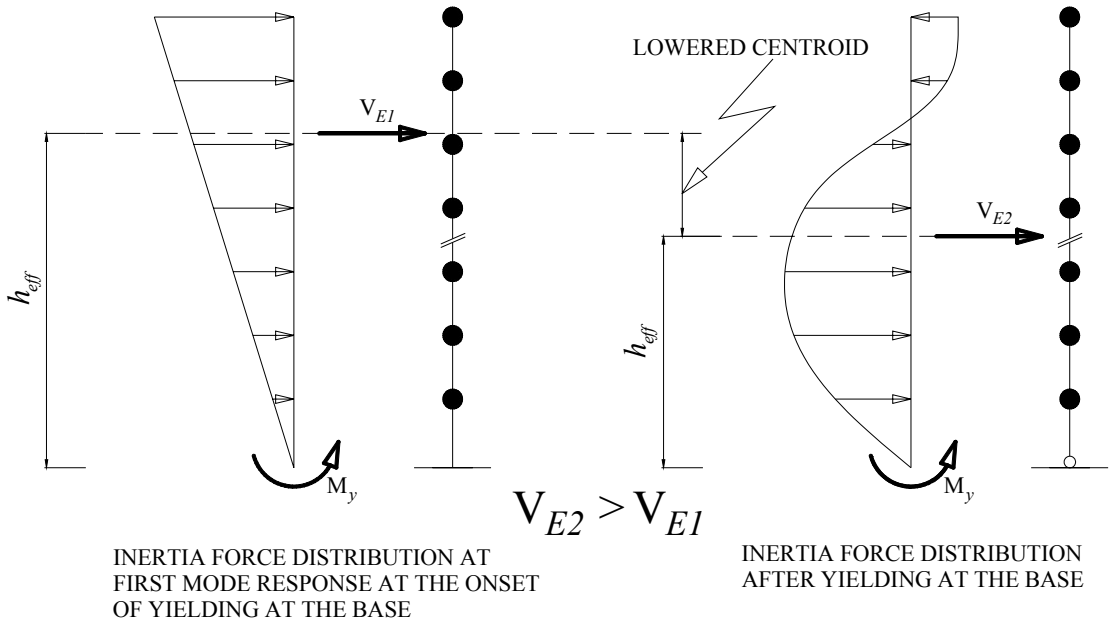

Figure 2.1. Inertia forces before and after yielding at the base of the wall

Dynamic base shear amplification effect is generally presented by researchers in the form of a factor (presented as β^b in this study) that is multiplied with the base shear

derived from conventional code procedures (V_e^b) to obtain the expected base shear demand (V_a^b)as given in Equation (2.1).

$$V_a^b = \beta^b V_e^b \tag{2.1}$$

Dynamic base shear amplification has not been recognized until the work of Blakeley *et al.* (1975), who pioneered the idea that higher mode effects amplify the base shear with respect to the base shear obtained from conventional code procedures after the formation of a plastic hinge at the base of the wall. They stated that after a plastic hinge formation at the base of the wall, the center of lateral inertial loading becomes lower or higher with respect to the center predicted by the code distribution, effectively causing higher shear forces than predicted by the code. Blakely *et al.* (1975) performed non-linear time history analyses on various structural wall models and recommended base shear amplification factors as a function of number of stories (n) of the wall structure. Based on these recommendations the provisions of New Zealand seismic code NZS3101 (Standards New Zealand 1982) have changed in 1982 and formed the basis of the New Zealand code perspective for the base shear amplification factors as given in Equation (2.2) which is still in use (Standards New Zealand 2006).

$$\begin{aligned} \omega_n &= 0.9 + \frac{n}{10} && \text{n} \le 6 \\ \omega_n &= 1.3 + \frac{n}{30} \le 1.8 && \text{n} > 6 \end{aligned} \tag{2.2}$$

It is seen from Equation (2.2) that, New Zealand perspective on the base shear amplification is dependent on the first mode period (fundamental period) of the wall, which is implicitly related to the number of stories of the wall (n).

A parametric investigation study carried out by Derecho and Corley (1984) revealed the increasing dependency of base shear amplification not only to the first mode period but also to the ductility level of the wall. The authors presented their base shear amplification results in the form of a chart format as shown in Figure 2.2. Derecho and Corley also stated

that there is a linear relationship between the base shear amplification factor and intensity of the ground motion.

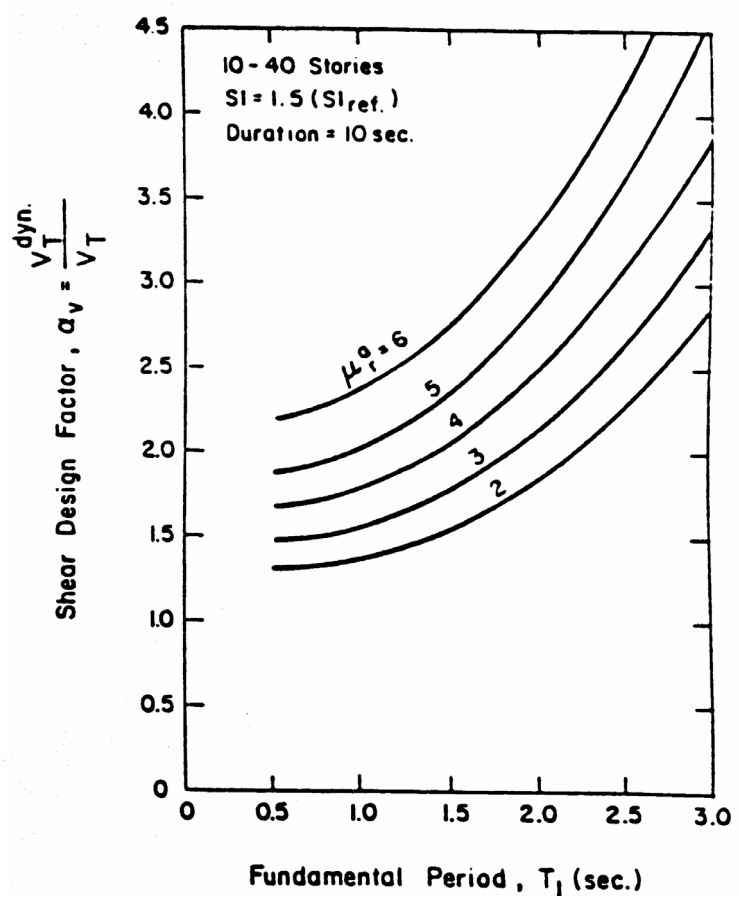

Figure 2.2. Base shear amplification factors suggested by Derecho and Corley (1984)

Kabeyasawa (1987) proposed base shear amplification factors, as given in Equation (2.3), based on the analytical verification of observed data from full scale pseudo dynamic test of a seven story model structure:

$$V_{\max} = V_{\mathrm{n}} + c \times W \times PGA \tag{2.3}$$

in which V_n is the base shear capacity for the structure calculated by ultimate limit state analysis assuming a triangular force distribution, c represents a coefficient that stands for the higher mode effects varying between 0.25 and 0.30, W is the seismic weight of the wall and PGA is the design peak ground acceleration. Kabeyasawa concluded that maximum dynamic shear in a wall under seismic attack is higher than the statically computed shear

due to the higher mode effects and the additional shear force demand in the non-linear range is a function of the peak ground acceleration.

A study by Eibl and Keintzel (1988) has also shown that base shear amplification is both functions of the first mode period and expected ductility level. The authors have proposed a base shear amplification factor relationship as given in Equation (2.4), which later formed the basis of the Eurocode 8 EN 1998-1 (CEN, 2004) provisions for base shear amplifications of wall systems designed for high ductility. Eibl and Keintzel have stated in their study that the first term under the square root denotes the contribution the first mode that is reduced by the strength reduction factor and the second term implicitly denotes the importance of the second mode in yielding systems.

$$\varepsilon = q\sqrt{\left(\frac{\gamma_{\mathrm{rd}}}{q}\frac{M_{\mathrm{rd}}}{M_{\mathrm{Ed}}}\right)^2 + 0.1\left(\frac{S_e(T_{\mathrm{C}})}{S_e(T_1)}\right)^2} \le q \tag{2.4}$$

in which ε is the base shear amplification factor, q is the strength reduction factor, γ_{Rd} the overstrength factor, M_{Rd} the design flexural strength at the wall base, M_{Ed} the design moment at the wall base, T_C the upper limit period of the spectral acceleration plateau in the design spectrum and $S_e(T)$ is the ordinate of the elastic response spectrum.

Ghosh and Markevicius (1990) has concluded in their parametric study that no dependence with the first mode period could be established and claimed that dynamic shear amplification is likely to be a function of ground motion intensity. The authors has suggested a relationship for the maximum base shear demand after yielding at the base of the wall, in which the first term is a function of the intensity of the ground motion and the second term is the base shear corresponding to plastic hinge formation at the base wall as presented in Equation (2.5).

$$V_{\max} = 0.25 \times W \times \frac{PGA}{g} + \frac{M_{\mathrm{y}}}{0.67H} \tag{2.5}$$

where W is the seismic weight of the wall, PGA the design peak ground acceleration, M_y the yield moment capacity at the base of the wall and H is the total wall height.

Experimental investigations on nine small-scale reinforced concrete structural models by Eberhard and Sozen (1993) revealed that base shear response of structural walls are very sensitive to higher mode effects. The authors observed that story inertial-forces differed increasingly from the triangular distribution assumed by the code provisions after yielding initiates at the base of the wall. Eberhard and Sozen demonstrated that modal stiffness of the first mode will practically be zero after yielding at the base and incremental shear force demand in this stage will be due to higher mode effects.

Seneviratna and Krawinkler (1994) have emphasized the dependency of the shear amplification of structural walls on both strength level and the first mode period of the structure as shown in Figure 2.3. The authors stated that shear amplifications increase for longer periods and lower strength levels, which can be attributed to the higher mode vibrations, particularly the second mode, of the elastic portion of wall above the plastic hinge at the base. They also compared their results with the relationship proposed by Ghosh and Markevicius (1990) and concluded that Ghosh and Markevicius relationship predicts the base shear amplifications in good agreement with their results for medium-high walls with relatively low strength levels, however underestimates amplifications for tall structures due to the lack of a term related to the period of the structure.

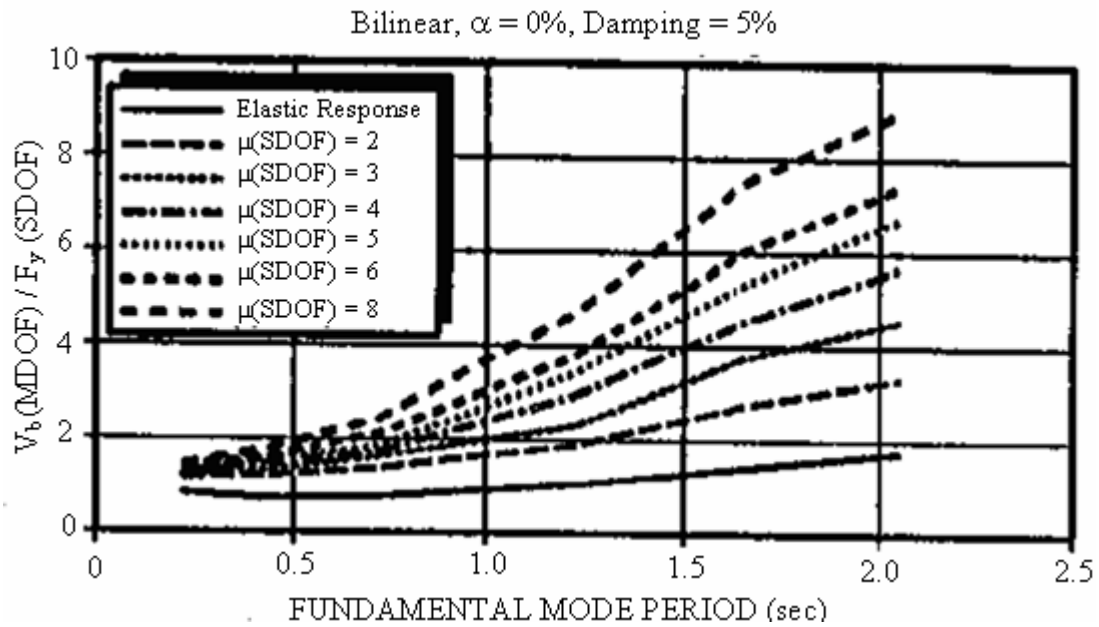

Figure 2.3. Base shear amplification factors suggested by Seneviratna and Krawinkler (1994)

Filiatrault *et al*. (1994) have studied the problem from the Canadian code approach and concluded that brittle shear failures are possible for ductile walls designed by the Canadian seismic code provisions. Based on a parametric study of walls designed according the Canadian code, they suggested seismic zone dependent strength reduction factors of 1.0 or 1.5 for shear design to account for base shear amplifications.

Rutenberg and Nsieri (2006) have studied the problem through Eurocode 8 perspective and claimed that current provisions of Eurocode 8 are in need of revision since they do not predict the shear amplifications realistically for the medium and high ductility classes of structural walls. Based on a parametric study by using non-linear time history analyses, the authors recommended the relationship given in Equation (2.6) in lieu of the current Eurocode relationship for dynamic base shear amplifications.

$$\varepsilon = 0.75 + 0.22 \times (T + q + Tq) \tag{2.6}$$

in which q is the strength reduction factor and T is first mode period of the structure. Rutenberg and Nsieri (2006) concluded that modification is necessary to Eurocode 8 base shear amplification relationship, which should increase with increasing period and strength reduction factors and should take into account the distribution of plasticity along the wall height.

Krawinkler (2006) expressed that "O*nce a plastic hinge forms at the base of a wall structure, the dynamic response characteristics of the structure above the base change radically. Different 'modes' become predominant and the effective lever arm (M/V ratio) becomes smaller, and for relatively tall and slender structures it becomes much smaller. Correspondingly, the dynamic shear force that can be generated may become much larger than that indicated by a static M/V concept in which the resultant lateral force is applied approximately at 2/3 of the structure height (or higher).*" The author emphasized that despite the detrimental reality that base shear demand is higher than predicted by traditional code provisions, higher actual shear strength of walls than recommended by code equations may be compensating this negative effect. The author also pointed out a very critical issue of wall behavior based on the recent test results, where wall response is

often controlled by sliding at the base and shear force distribution may be totally different than predicted by analytical methods.

It is interesting to note that USA has been rather hesitant to apply dynamic shear amplification factors in the national seismic design codes, despite several researchers in the USA have stressed the fact on shear amplifications in their studies. As an exception, Commentary to the Recommended Lateral Force Requirements of the Structural Engineers Association of California (SEAOC, 1999) recommended adopting the amplification factors advocated by the New Zealand code.

Turkish Seismic Design Code (1997) did not take into account the dynamic base shear amplifications in structural walls at any level of ductility, and the design for shear was based on the shear forces corresponding to the lateral force distribution used for flexural design. Present version of the code (2007) takes the base shear amplification phenomena into account with a constant base shear amplification factor of 1.5 regardless of the first mode period and ductility level of the wall.

Seismic design codes could prefer utilizing base shear amplification factors suggested by researchers, as long as they are practical to implement in design practice. However they have a serious drawback of being related to the intensity of ground motion records they are derived from. Research on shear amplification of structural walls is still continuing and there is limited global consensus between the researchers (also between the codes) on the degree of base shear amplifications, despite the fact that the source of this amplification is recognized as the higher mode effects initiating after the plastic hinge formation at the base of the wall.

3. DESIGN OF THE GENERIC STRUCTURAL WALLS

The numerical and statistical findings in this study are based on the results obtained from the analysis of generic structural walls that are intended to represent the structural wall systems in the building stock. Thus, generic structural walls with 8, 12, 16, 20 and 30 stories and typical story heights of 3.0m have been considered as illustrated in Figure 3.1, in order to cover a broad range of wall characteristics in terms of flexibility and strength.

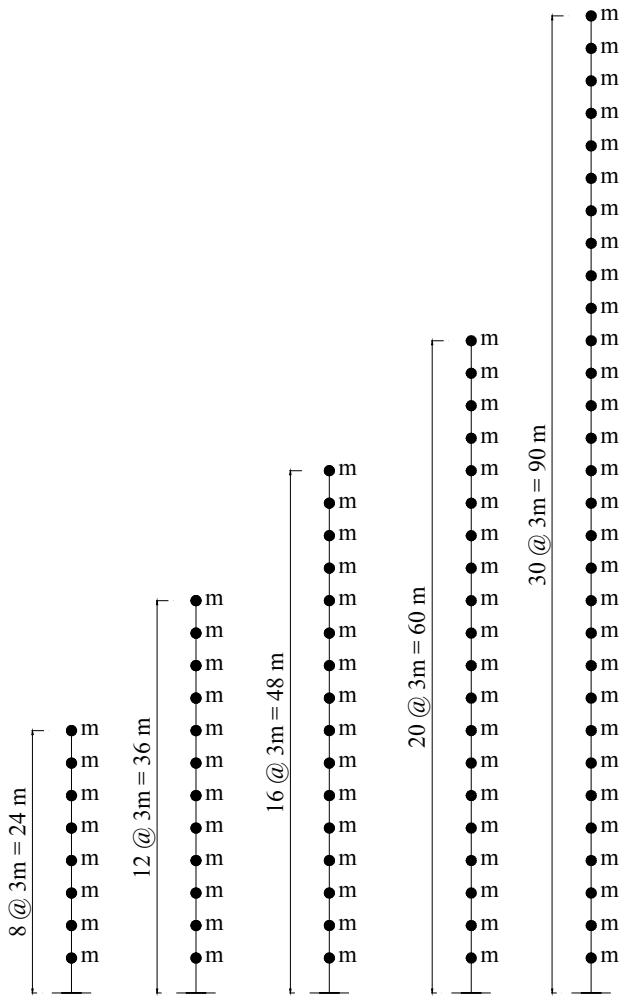

Figure 3.1. Illustration of generic walls considered in this study

Firstly generic walls have been pre-designed to provide section dimensions. Subsequently, the traditional design procedure as applied in practice has been followed

where possible so as not to deviate from realistic results. Details of the pre-design and design steps are presented in the following sections of this chapter.

Analysis and design effects obtained herein have been computed by using SAP 2000 v11 (CSI, 2006) structural analysis software licensed to the Department of Earthquake Engineering of Boğaziçi University.

3.1. Pre-Design of Generic Structural Walls

A simple approach has been utilized to determine the section dimensions of the generic walls. It has been assumed that the first mode period corresponding to gross (uncracked) stiffness shall approximately satisfy an old empirical relation correlated with the total building height (H) as given in Equation (3.1) (Turkish Seismic Design Code, 1997).

$$T_1 = 0.05 H_w^{3/4} \tag{3.1}$$

Thus, by assigning building heights to Equation (3.1), first mode periods have been determined for each generic wall in concern. Assuming that the wall mass and stiffness are uniformly distributed along the wall height, the natural vibration frequency of the system can be estimated by Equation (3.2) (Chopra 2006);

$$\omega_1 = \frac{3.516}{H_w^2}\sqrt{\frac{EI_g}{m(y)}} \tag{3.2}$$

where I_g is the moment of inertia of the gross section properties and $m(y)$ is the mass per unit length of the wall.

Thus the first mode period of the system will be;

$$T_1 = \frac{2\pi}{\omega_1} \tag{3.3}$$

Substituting Equation (3.1) in Equation (3.3) will result in Equation (3.4) to be solved for $I_g/m(y)$, provided that modulus of elasticity for concrete (E) is assumed as $3x10^7$ kN/m^2.

$$0.05H_w^{3/4} = \frac{2\pi}{\frac{3.516}{H_w^2}\sqrt{\frac{EI_g}{m(y)}}} \tag{3.4}$$

Solution of Equation (3.4) for the generic walls resulted in the following first mode period, section dimensions and typical story masses, as given in Table 3.1.

Table 3.1. Generic wall characteristics

WALL	H_w (m)	T_1 (sec)	$b(m)$	$d(m)$	$m_{typical}$ (t)
8 STORY	24	0.54	0.30	4.00	30.95
12 STORY	36	0.73	0.30	5.75	30.12
16 STORY	48	0.91	0.30	7.50	29.68
20 STORY	60	1.08	0.30	9.30	29.88
30 STORY	90	1.46	0.30	13.85	29.73

3.2. Design of Generic Structural Walls

Subsequent to the determination of characteristics of generic structural walls as above, structural design procedure based on response spectrum method has been utilized.

Design basis acceleration response spectrum given in Turkish Seismic Design Code (2007) corresponding to 10 percent probability of exceedence in 50 years has been used for the representation of ground motion (Figure 3.2). The design acceleration response spectrum has been assumed to be based on local site conditions with site class Z3 (corner periods of T_A = 0.15sec and T_B = 0.60 sec) and Seismic Zone 1 (Effective peak ground acceleration of 0.40g), respectively.

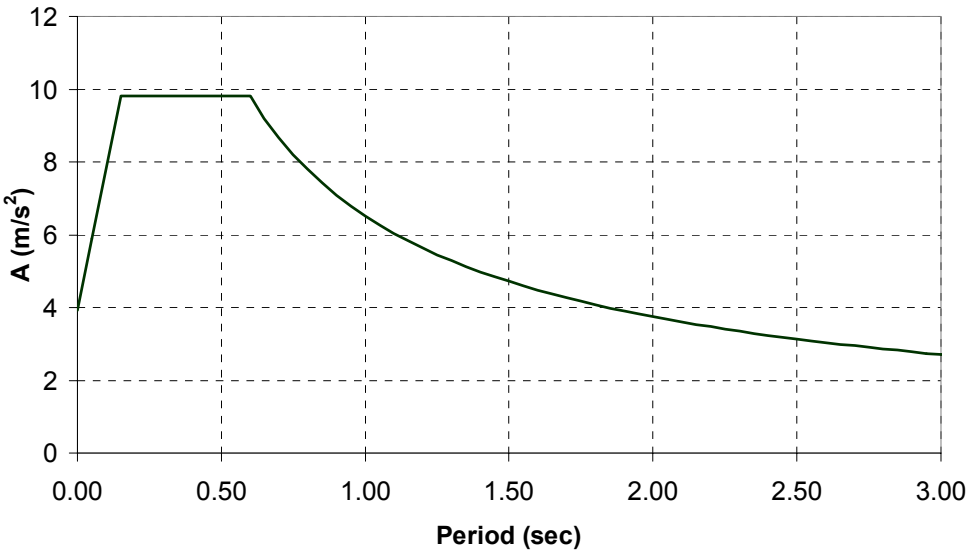

Figure 3.2. Design acceleration response spectrum used in the study

Generic structural walls have been modeled with frame (beam) elements in terms of stiffness and lumped masses at each story level as shown in Figure 3.3. Flexural stiffness of the walls has been reduced by a factor 0.50 to obtain cracked section stiffness, approximating the cracking and softening of linear stiffness under seismic attack.

The boundary conditions at the base of the walls have been assumed to be fixed, thus rotations arising from the foundation or soil stiffness have been neglected.

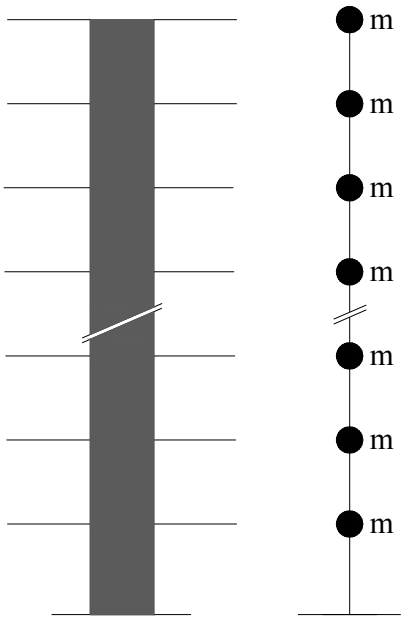

Figure 3.3. Modelling representation of structural walls

Response spectrum analyses have been performed for each generic wall in order to obtain the design story moments and shear forces along the wall height. All modes of the structure exhibiting modal amplitudes in the lateral direction, that is equal to the number of stories of the wall in concern, have been taken into account during response spectrum analysis, and critical damping ratio has been assumed as 5 percent.

Each generic wall has been analyzed by taking into account Strength Reduction Factors R = 2, 4, 6, 8 and 10 in order to provide a strength range. These Strength Reduction Factors have been incorporated into response spectrum analyses by reducing the design spectrum as per the requirements of the Turkish Seismic Design Code 2007. It can be argued that realistic wall buildings in practice are not designed for strength reduction factors of 8 or 10, which would result in drastically under-designed structures. However, it is intended that high values of R may have some merit in cases of seismic assessment of old structural walls designed with lesser seismic demands and weaker capacities.

Modal response quantities derived from response spectrum analyses have been combined with the CQC modal combination method to obtain the design effects, namely the story moments and shear forces, which are presented in Appendix A for each generic wall with their corresponding strength reduction factors.

Design moments obtained at the base of the wall from response spectrum analyses with the corresponding strength reduction factor have been hypothetically assumed as equal to the design moment capacity or yield moment strength of the section at the base of the generic walls. Thus, story moment and shear force profiles along the wall height have also been supposed to be equal to the profiles obtained from the response spectrum analyses as the yield moment is attained at the base.

4. A NOVEL MODAL DECOMPOSITION TECHNIQUE FOR IDENTIFYING HIGHER MODE EFFECTS IN DYNAMIC SHEAR AMPLIFICATION

As with systems exhibiting cantilever like behavior, structural wall systems are statically unstable but dynamically stable structures when flexural yielding occurs at their bases. During seismic excitation, as the system alters from linear to nonlinear behavior mode, a plastic hinge or a series of hinges develop at the base of the wall and the structural wall loses its redundancy for a time interval until it is stabilized back by inertia forces. During this time interval, a new system with a completely unique dynamic characteristics prevail until the system velocity becomes zero, and the linear phase initiates with unloading. Status of the structural wall before and after the plastic development at the base of the wall shall be called hereinafter as "*the linear phase*" and "*the non-linear phase*", respectively, for the ease of understanding.

It has been observed in this study and by various researchers described in Chapter 2 that greater shear forces are obtained from nonlinear time history analyses than the shear forces expected from design. It is a general consensus that higher mode effects in the non-linear phases causes this amplification of shear forces with respect to the ones obtained from linear design, however studies demonstrating individual contribution of higher mode effects to dynamic amplification are very limited in the literature. Kabeyasawa (1987) has called the response of second mode effects as "residual fluctuating forces". Based on a triangular first mode shape, he predicted the second mode shape from orthogonality condition with the first mode and extracted the second mode response by eliminating the triangular first mode effects from the non-linear time history analyses.

A modal decomposition technique is presented in this study for demonstrating the individual effects of the higher modes on the dynamic shear amplification phenomenon. The technique is based on inverse extraction of modal responses from non-linear time history analyses results by using the mode superposition method. A computer program has been coded in MATLAB (The MathWorks Inc., 2004) for the numerical presentation of

the technique. The technique has been demonstrated on the non-linear time history results of 16 story generic wall designed with a Strength Reduction Factor of R=6 which have been obtained from the Whittier Narrows 1987 - Brea Dam (Downstream) record in Group 2 analysis as explained in Chapter 5. (single plastic hinge at the base of the wall with elasto-plastic moment-curvature hysteretic characteristics-see Section 5.2).

4.1. Linear and Non-Linear Modes of Vibration

Modal characteristics of the wall in the linear and non–linear phases should be determined prior to the implementation of the modal decomposition technique. Vibration modes before the plastic hinge development will be denoted as the *linear modes,* whereas vibration modes in the non-linear phases of the plastic hinge will be referred to as the *non-linear modes*. Eigenvalues and mode shapes both for linear and non-linear phases of the walls have been obtained by using a built-in feature of MATLAB. This feature utilizes the Jacobi Method (Bathe, 1996) that converge accurate eigenvalues regardless of the stiffness matrix conditions, as is the case for the wall systems in the non-linear phase.

General expression for the dynamic eigenvalue problem can be derived from the equation of motion of an undamped multi degree of freedom system having a mass matrix of M and a stiffness matrix of K as:

$$\mathbf{K}\boldsymbol{\Phi}_n = \omega_n^2 \mathbf{M}\boldsymbol{\Phi}_n \tag{4.1}$$

where, Φ_n and ω_n^2 denote the eigenvector and eigenvalue of the n'th mode of the system, respectively.

Solution of Equation (4.1) is straightforward for the linear phase of the wall, however the system is theoretically unstable in the nonlinear phase due the plastic hinge formation and thus eigenvalues can not be obtained through classical methods.

It is interesting to note that the Jacobi Method is able to provide the eigenvalues of the system even in the non-linear phase since the solution of the eigenvalue problem by the Jacobi Method does not contain any division by any number. Hence, the method always

converges and yields an accurate solution for positive, zero or negative eigenvalues. (Bathe, 1996; Wilson, 2006)

All linear and non-linear eigenvalues and corresponding eigenvectors having components in the direction of earthquake excitation are necessary to be computed in this technique for accurate calculation of modal accelerations. Thus, for an *n* story wall subjected to unidirectional horizontal ground motion *n* eigenvalues and associated eigenvectors in the lateral direction should be computed.

Figure 4.1 to Figure 4.3 shows the first three of the computed 16 linear and non-linear mode shapes (eigenvectors) of the 16 story generic wall, respectively.

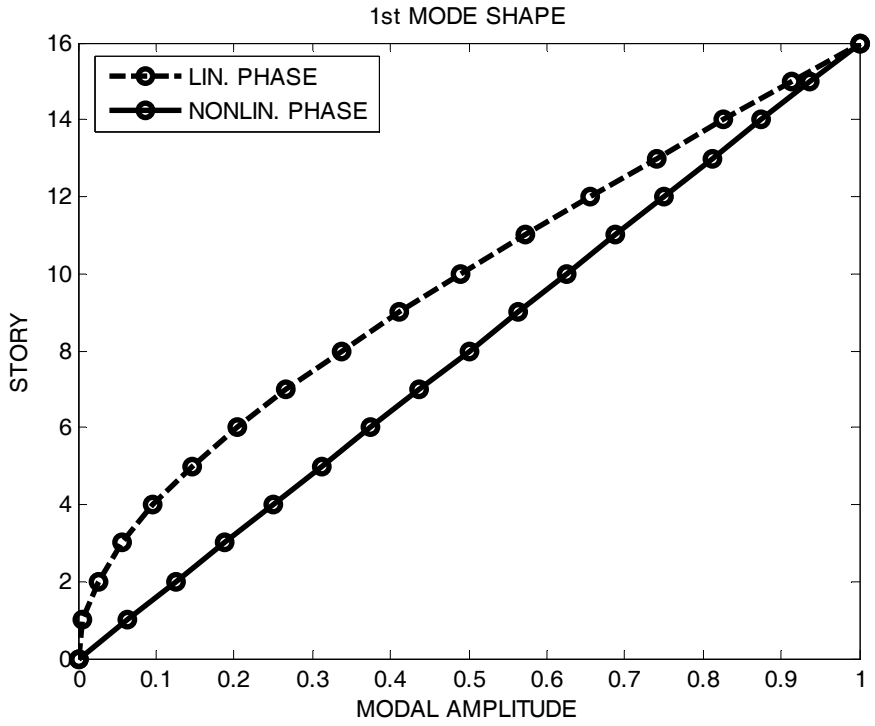

Figure 4.1. Linear and non-Linear 1st mode shapes of the 16 story generic wall

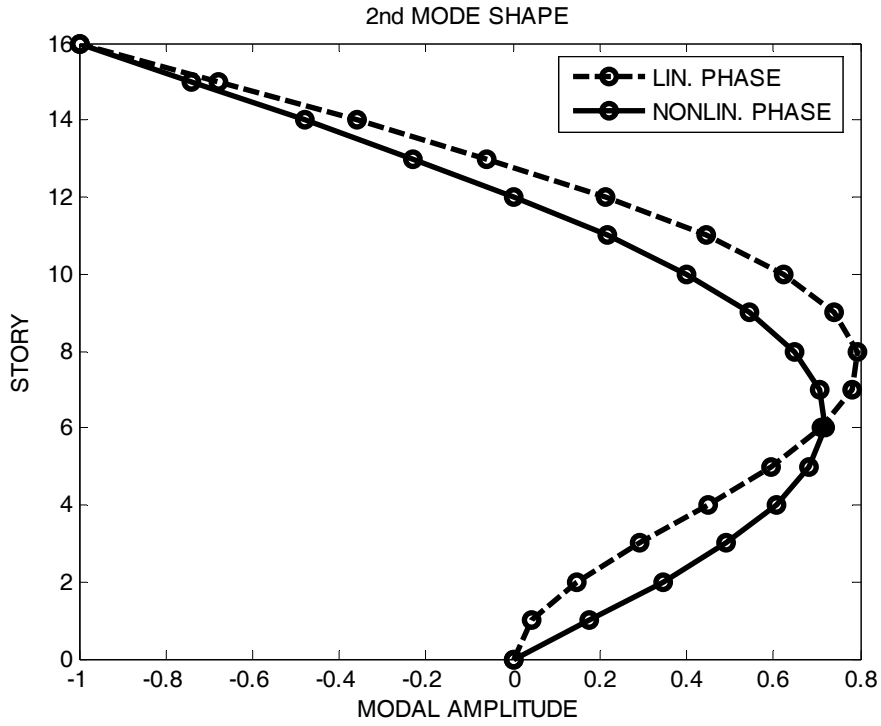

Figure 4.2. Linear and non-linear 2nd mode shapes of the 16 story generic wall

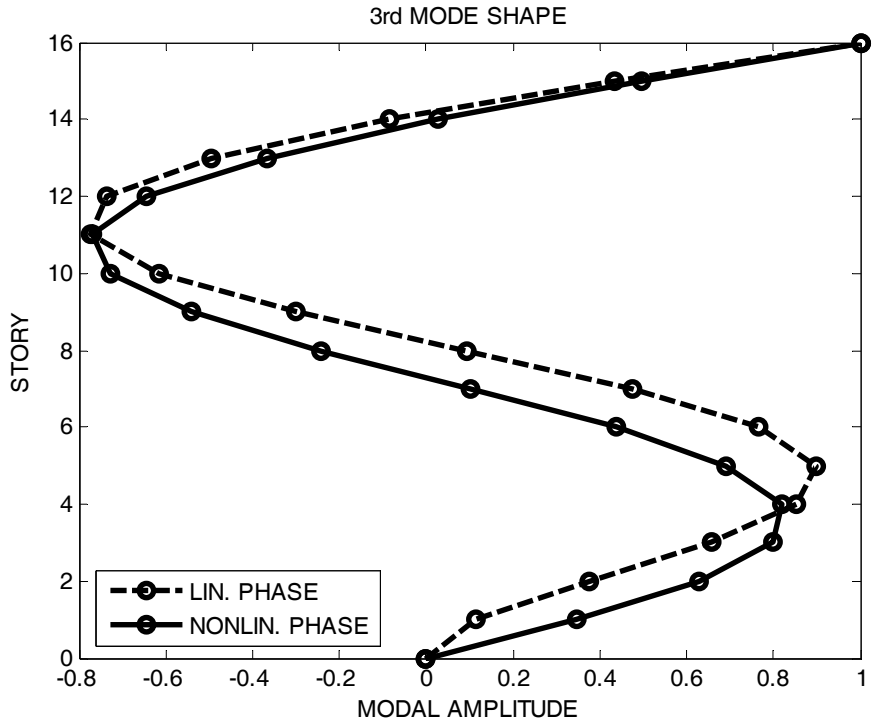

Figure 4.3. Linear and non-linear 3rd mode shapes of the 16 story generic wall

Figure 4.1 reveals a transformation of the first mode shape pattern from parabolic to straight line as a consequence of the plastic hinge development at the base of the wall in the non-linear phase. Period of vibration in the first mode has been calculated as 1.30 sec in the linear phase, whereas in the non-linear phase it is infinite (ω_1=0). The zero natural frequency indicates that modal stiffness for the first mode becomes effectively zero after yielding takes place provided that no hardening is assumed for the moment-curvature relationship at plastic hinge forming at the base. Thus, non-linear first mode can be called as the *unstable mode* of the system, which would be stabilized by the inertia forces during seismic excitation.

However, the non-linear first mode of the system has a definite Modal Participation Factor, since eigenvectors are definite

$$\Gamma_1^* = \frac{\boldsymbol{\Phi}_1^* \mathbf{M} \mathbf{T}_x}{\boldsymbol{\Phi}_1^{*T} \mathbf{M} \boldsymbol{\Phi}_1^*} \tag{4.2}$$

where the superscript asterisk indicate the non-linear mode.

It is also interesting to note that, non-linear first mode of the system satisfy the orthogonality conditions with the non-linear second mode as reported by Kabeyasawa (1987):

$$\boldsymbol{\Phi}_1^{*T} \mathbf{M} \boldsymbol{\Phi}_2^* = 0 \tag{4.3}$$

Modification of the second and third mode shapes in the non-linear phase has been observed as a shift of the bulk of the mode shape downwards as shown in Figure 4.2 and Figure 4.3, due to the hinge development at the base of the wall. Similar behavior has been observed for higher modes of the wall above the third non-linear mode. In order to demonstrate the eigenvectors of the other generic walls buildings with 8, 12, 16, 20 and 30 stories, first two mode shapes, both in the linear and non-linear phases, are presented in Appendix B.

Non-zero periods of vibration have been computed for the higher modes as shown in Table 4.1. Those modes can be called as *stable modes* regardless of the plastic hinge formation at the base of the wall.

Table 4.1. Linear and non-linear higher mode periods of the 16 story generic wall

	LINEAR PHASE	NON-LINEAR PHASE
	T (sec)	T (sec)
MODE 2	0.2145	0.3064
MODE 3	0.0767	0.0947
MODE 4	0.0392	0.0454
MODE 5	0.0237	0.0266
MODE 6	0.0159	0.0174
MODE 7	0.0114	0.0123
MODE 8	0.0086	0.0092
MODE 9	0.0067	0.0071
MODE 10	0.0054	0.0057
MODE 11	0.0045	0.0047
MODE 12	0.0038	0.0039
MODE 13	0.0033	0.0034
MODE 14	0.0030	0.0030
MODE 15	0.0027	0.0028
MODE 16	0.0026	0.0026

4.2. Modal Decomposition Technique

4.2.1. Modal Expressions in The Linear Response

Static-equivalent m'th mode seismic force at time *t* can be expressed as:

$$\mathbf{f}_{\mathrm{m}}(t) = \mathbf{M}\,\boldsymbol{\Phi}_{\mathrm{m}}\,\Gamma_{\mathrm{m}}\,a_{\mathrm{m}}(t) \tag{4.4}$$

where $a_{\mathrm{m}}(t)$ refers to m'th mode pseudo-acceleration response history. $\boldsymbol{\Phi}_{\mathrm{m}}$ represents m'th mode shape vector and Γ_{m} is the corresponding modal participation factor:

$$\Gamma_{\mathrm{m}} = \frac{\boldsymbol{\Phi}_{\mathrm{m}}^{\mathrm{T}}\mathbf{M}\,\mathbf{1}}{\boldsymbol{\Phi}_{\mathrm{m}}^{\mathrm{T}}\mathbf{M}\,\boldsymbol{\Phi}_{\mathrm{m}}} \tag{4.5}$$

in which **1** refers to the vector of ones.

Define scaled mode shape vectors as:

$$\begin{aligned} \bar{\boldsymbol{\Phi}}_{\mathrm{m}} &= \boldsymbol{\Phi}_{\mathrm{m}}\,\Gamma_{\mathrm{m}} \\ \bar{\boldsymbol{\Phi}} &= [\bar{\boldsymbol{\Phi}}_1 \quad \bar{\boldsymbol{\Phi}}_2 \quad \ldots\ldots \quad \bar{\boldsymbol{\Phi}}_{\mathrm{m}} \quad \ldots\ldots \quad \bar{\boldsymbol{\Phi}}_{\mathrm{n}}] \end{aligned} \tag{4.6}$$

where n refers to total number of degrees of freedom in the direction of seismic excitation. Effective mass matrix can be defined as:

$$\bar{\mathbf{M}} = \mathbf{M}\,\bar{\boldsymbol{\Phi}} \tag{4.7}$$

Thus, mode-superposition can be applied to the seismic force vector given in Equation (4.4) for the m'th mode:

$$\mathbf{f}(t) = \bar{\mathbf{M}}\,\mathbf{a}(t) \tag{4.8}$$

where pseudo-acceleration vector is defined as:

$$\mathbf{a}(t) = \langle a_1(t) \quad a_2(t) \quad .... \quad a_m(t) \quad .... \quad a_n(t) \rangle^T \tag{4.9}$$

4.2.2. Incremental Form of Modal Expressions in The Non-Linear Response

Equation (4.4) can be written in incremental form at the (i)'th step representing the response increment in between the time stations t_i and t_{i+1} :

$$\Delta \mathbf{f}_m^{(i)} = \mathbf{M}\, \mathbf{\Phi}_m^{(i)} \Gamma_m^{(i)} \Delta a_m^{(i)} \tag{4.10}$$

In this case $\mathbf{\Phi}_m^{(i)}$ represents either linear or non-linear m'th mode shape vector prevailing in the (i)'th step, depending on whether the base plastic hinge response is along loading/unloading lines or on the yielding plateau of the response hysteresis. Now $\Delta a_m(t)$ refers to m'th mode pseudo-acceleration response increment in the (i)'th step.

Thus Equation (4.8) can be written in incremental form as,

$$\Delta \mathbf{f}^{(i)} = \bar{\mathbf{M}}^{(i)}\, \Delta \mathbf{a}^{(i)} \tag{4.11}$$

where,

$$\bar{\mathbf{M}}^{(i)} = \mathbf{M}\, \bar{\mathbf{\Phi}}^{(i)} \tag{4.12}$$

$$\bar{\mathbf{\Phi}}_m^{(i)} = \mathbf{\Phi}_m^{(i)} \Gamma_m^{(i)}$$
$$\bar{\mathbf{\Phi}}^{(i)} = [\bar{\mathbf{\Phi}}_1^{(i)} \quad \bar{\mathbf{\Phi}}_2^{(i)} \quad ..... \quad \bar{\mathbf{\Phi}}_m^{(i)} \quad ..... \quad \bar{\mathbf{\Phi}}_n^{(i)}] \tag{4.13}$$

Thus, in nonlinear response, two different *n* by *n* effective mass matrices, $\bar{\mathbf{M}}^{(i)}$, are defined, one each corresponding to linear and non-linear modes, respectively.

In the implementation of modal decomposition technique, seismic force increment $\Delta f_k^{(i)}$ acting on any story *k* is obtained as the difference of the story shear demand increments at consecutive stories *k* and *k–1* as follows:

$$\Delta f_k^{(i)} = \Delta V_k^{(i)} - \Delta V_{k-1}^{(i)} \tag{4.14}$$

From plastic rotation time-history response at the base of the wall, the time steps associated with loading/unloading and the non-linear phases of the hysteretic response of the base plastic hinge can be detected as illustrated in Figure 4.4.

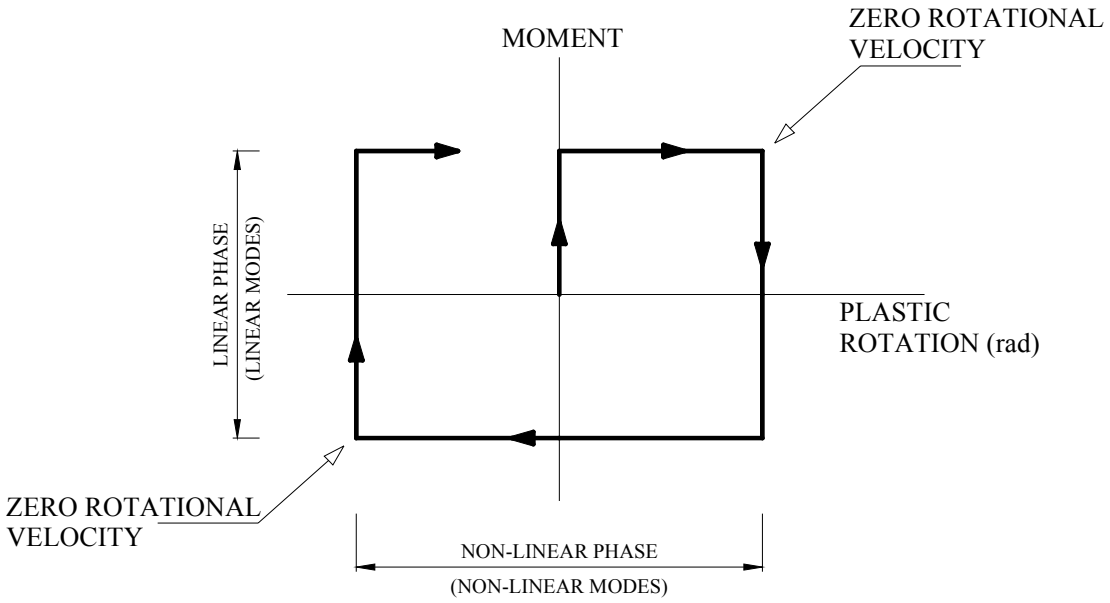

Figure 4.4. Identification of linear and non-linear phases of the wall through plastic hinge rotations at the base

Utilizing the appropriate $\bar{\mathbf{M}}^{(i)}$ matrix (corresponding to linear or non-linear modes), increment of pseudo-acceleration vector at any (i)'th step can be obtained from Equation (4.11) as:

$$\Delta\mathbf{a}^{(i)} = \bar{\mathbf{M}}^{(i)\,-1}\,\Delta\mathbf{f}^{(i)} \tag{4.15}$$

$$\Delta\mathbf{a}^{(i)} = \left\langle \Delta a_1^{(i)} \quad \Delta a_1^{(i)} \quad .... \quad \Delta a_m^{(i)} \quad .... \quad \Delta a_n^{(i)} \right\rangle^{T} \tag{4.16}$$

Thus modal increments of seismic forces, $\Delta\mathbf{f}_m^{(i)}$, can be readily obtained from Equation (4.10). Further, base shear and base bending moment modal increments can be obtained as:

$$\Delta V_m^{b(i)} = \langle \mathbf{1} \rangle \Delta\mathbf{f}_m^{(i)} \tag{4.17}$$

$$\Delta M_m^{b(i)} = \langle \mathbf{y} \rangle \Delta\mathbf{f}_m^{(i)} \tag{4.18}$$

Adding to those at the previous time station t_i, m'th mode base shear and base bending moment at time station t_{i+1} can be obtained as:

$$V_m^b(t_{i+1}) = V_m^b(t_i) + \Delta V_m^{b(i)} \tag{4.19}$$

$$M_m^b(t_{i+1}) = M_m^b(t_i) + \Delta M_m^{b(i)} \tag{4.20}$$

Final quantities at time station t_{i+1} are obtained by mode superposition:

$$V^b(t_{i+1}) = V_1^b(t_{i+1}) + V_2^b(t_{i+1}) + \ .... + V_m^b(t_{i+1}) + \ .... + V_n^b(t_{i+1}) \tag{4.21}$$

$$M^b(t_{i+1}) = M_1^b(t_{i+1}) + M_2^b(t_{i+1}) + \ .... + M_m^b(t_{i+1}) + \ .... + M_n^b(t_{i+1}) \tag{4.22}$$

which should be exactly equal to those directly obtained from the nonlinear response history analysis of the wall.

Equation (4.10) can also written in terms of incremental modal displacements as shown in Equation (4.23):

$$\Delta \mathbf{f}_m^{(i)} = \mathbf{M}\,\boldsymbol{\Phi}_m^{(i)}\Gamma_m^{(i)}\Delta d_m^{(i)}\left(\omega_m^{(i)}\right)^2 \tag{4.23}$$

Increments of modal seismic forces for the first non-linear mode should be obtained as zero from Equation (4.23) since the frequency associated with the first non-linear mode is obtained as zero provided that there is no strain hardening at the base plastic hinge. Thus, increments of modal base shear and modal overturning moment associated with the first non-linear mode should also be zero from Equations (4.17) and (4.18). This finding indicates that first mode of the wall in the non-linear phase do not contribute to any force related response. However, non-linear first mode contribute to increments of modal deformations as the associated incremental displacements will be non-zero as shown in Equation (4.24).

$$\Delta \mathbf{u}_1^{(i)} = \boldsymbol{\Phi}_1^{(i)}\Gamma_1^{(i)}\Delta d_1^{(i)} \tag{4.24}$$

On the contrary, higher modes in the non-linear phases will maintain their contribution to base shear and deformation response as their frequencies and incremental

displacements are non-zero. On the other hand, it is interesting to note that increments of modal overturning moments associated with non-linear higher modes shall also be zero at the base since the product

$$\langle \mathbf{y} \rangle \boldsymbol{\Phi}_{m}^{(i)} \Gamma_{m}^{(i)} \Delta d_{m}^{(i)} \left(\omega_{m}^{(i)} \right)^{2} \tag{4.25}$$

is calculated as zero for these modes. Thus, it can be stated that non-linear higher modes initiates non-zero incremental shear forces, which also satisfy zero increments of modal overturning moments at the base of the wall. Hence, during time intervals of non-linear phase, incremental shear forces shall continue to develop on the structural wall until the commencement of unloading in the plastic hinge, which modify the proportionality assumed between the base shear forces and overturning moments by code procedures.

Figure 4.5 shows the plastic rotation history of the 16 story generic wall designed with R=6, which has been arranged to demonstrate only the non-linear phases of the wall with non-zero plastic rotations (linear phases of the wall are shown with zero rotations). The wall has exhibited the first non-linear response at time t = 4.62 seconds of the record and sustained this phase for 0.04 seconds with plastic rotations in the positive direction. A total of 40 non-linear phases has been noted throughout the response history of the generic wall with 38 of them are associated with plastic rotations in the negative direction which indicates a response around a residual deformation developed after t = 5.0 seconds.

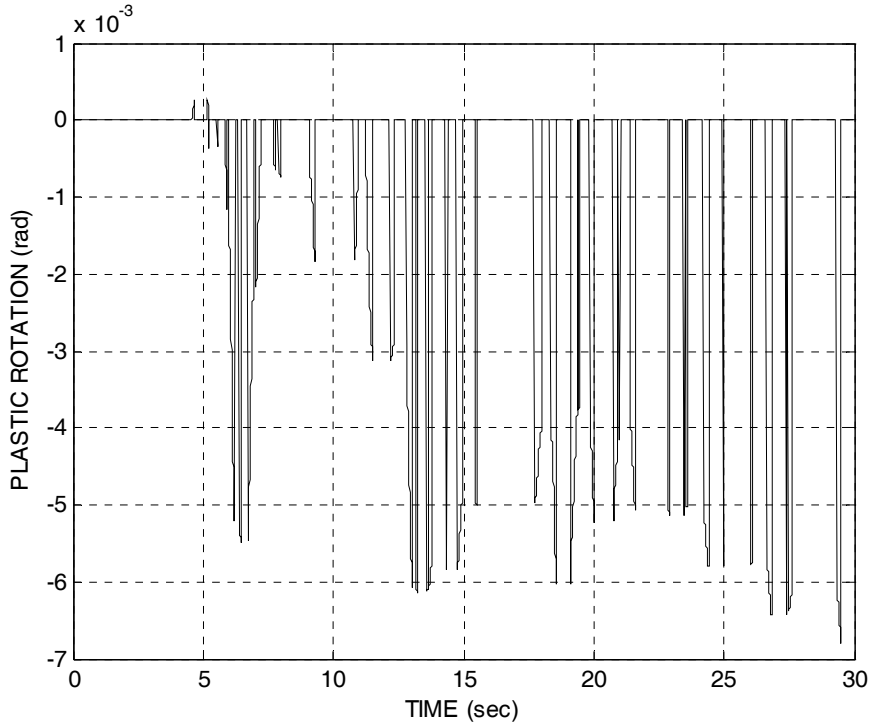

Figure 4.5. Plastic rotation history at the base of 16 story generic wall (R=6) obtained from non-linear time history analysis (Whittier Narrows, 1987-Brea Dam Record)

Modal base shear history of the 16 story generic wall, decomposed with the technique explained above, is given in Figure 4.6 for the first five modes of the wall. Base shear response combined with mode superposition method is also provided in last pane of Figure 4.6. With reference to Figure 4.5, maximum base shear response of the 16 story generic wall has been observed in the first non-linear phase of the wall which occurred at t = 4.65 seconds (hereinafter called "*the peak response instant*") of the response history as indicated in Figure 4.6 with a dark circle. This non-linear phase has been observed to initiate at t = 4.62 seconds and continued through 0.04 seconds to switch to a linear phase with unloading in the plastic hinge. It is evident from Figure 4.6 that, modal base shear of the second mode also reaches its first peak value at the peak response instant, where the contribution of the first mode is comparatively lower. Effect of third and higher modes has been observed to be negligible at peak response instant as shown in Figure 4.6, indicating the significant role of the second mode on the base shear response.

Base shear and overturning moment response histories of the 16 story generic wall computed by the superposition of decomposed modal responses have been compared with the actual base shear and overturning moment response histories obtained from the Group

2 non-linear time history analysis in order to verify the accuracy of the technique as shown in Figure 4.7. and Figure 4.8, respectively. Both Figure 4.7 and Figure 4.8 demonstrate an almost perfect match between the responses obtained from mode superposition and non-linear time history analysis, which indicates that non-linear response can be decomposed into modal responses by using modal characteristics of the structural walls in an incremental fashion.

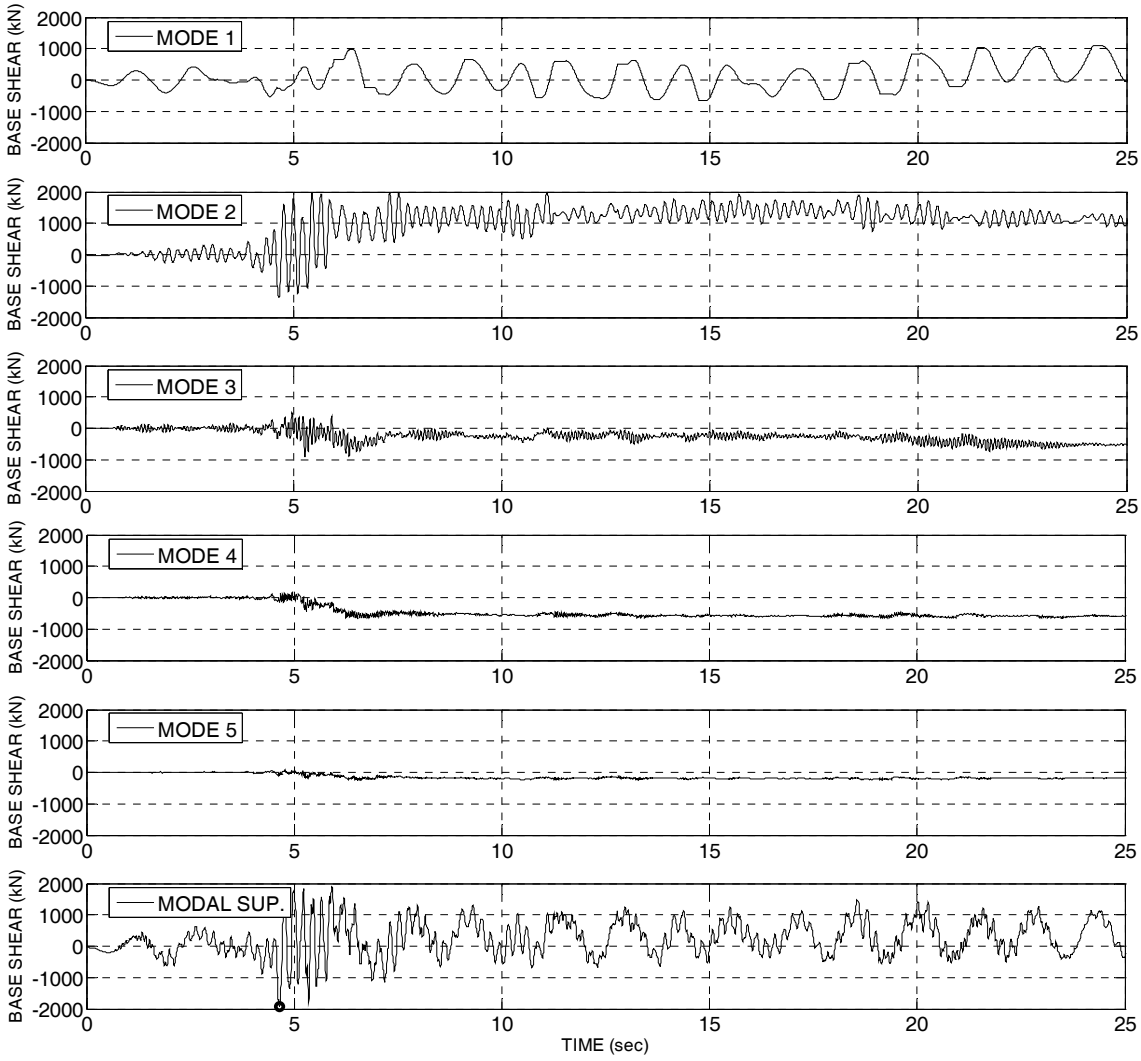

Figure 4.6. Modal and superposed base shear history of the 16 story generic wall designed with R=6

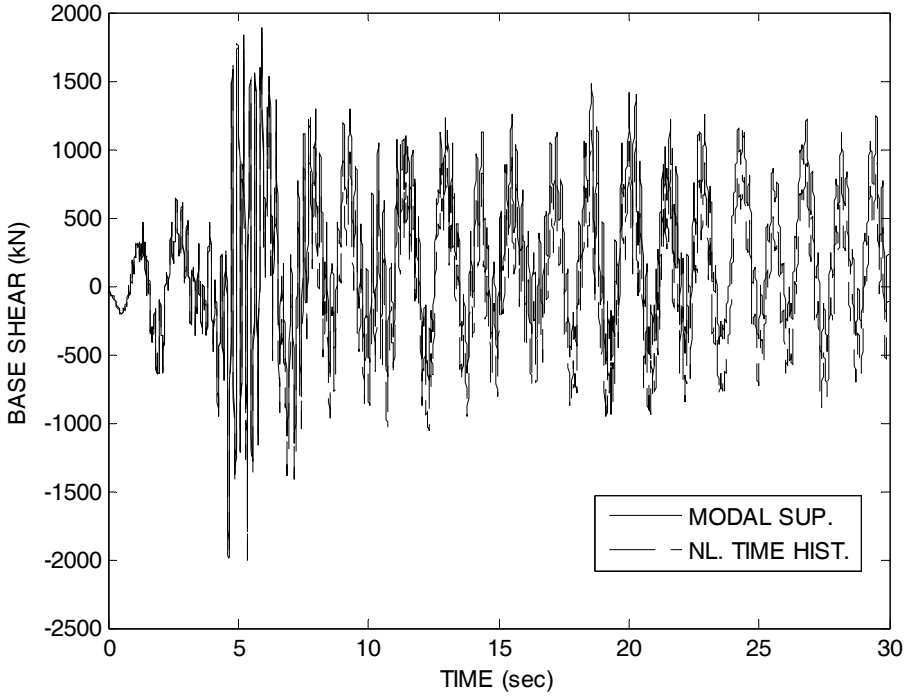

Figure 4.7. Agreement between the base shear of the 16 story generic wall obtained from mode superposition and Group 2 non-linear time history analysis

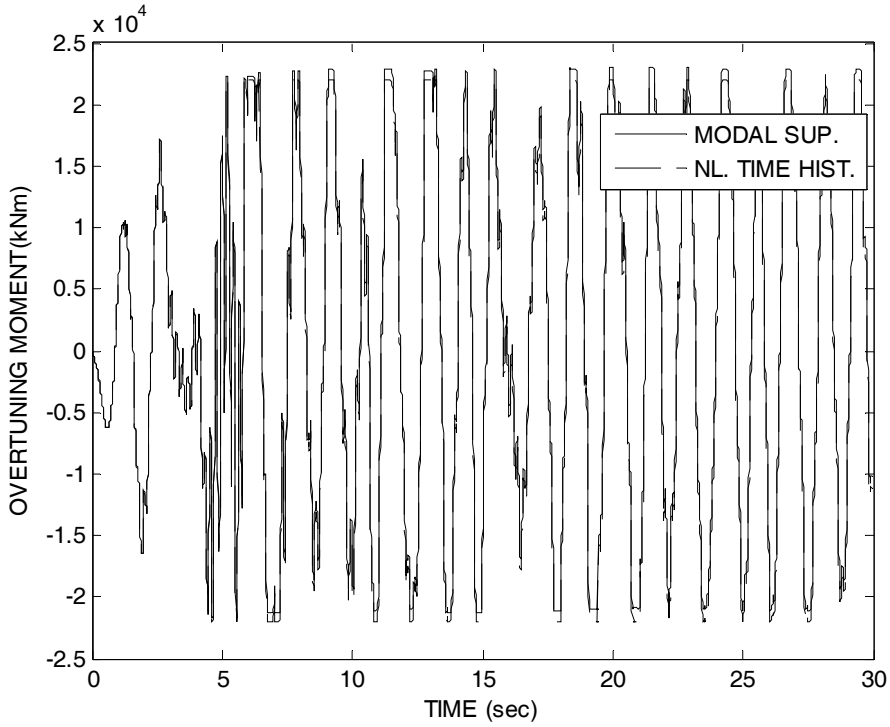

Figure 4.8. Agreement between the overturning moment of the 16 story generic wall obtained from mode superposition and Group 2 non-linear time history analysis

Modal increment of seismic forces associated with the first three modes of the 16 story generic wall obtained immediately before the peak response instant are shown in Figure 4.9.

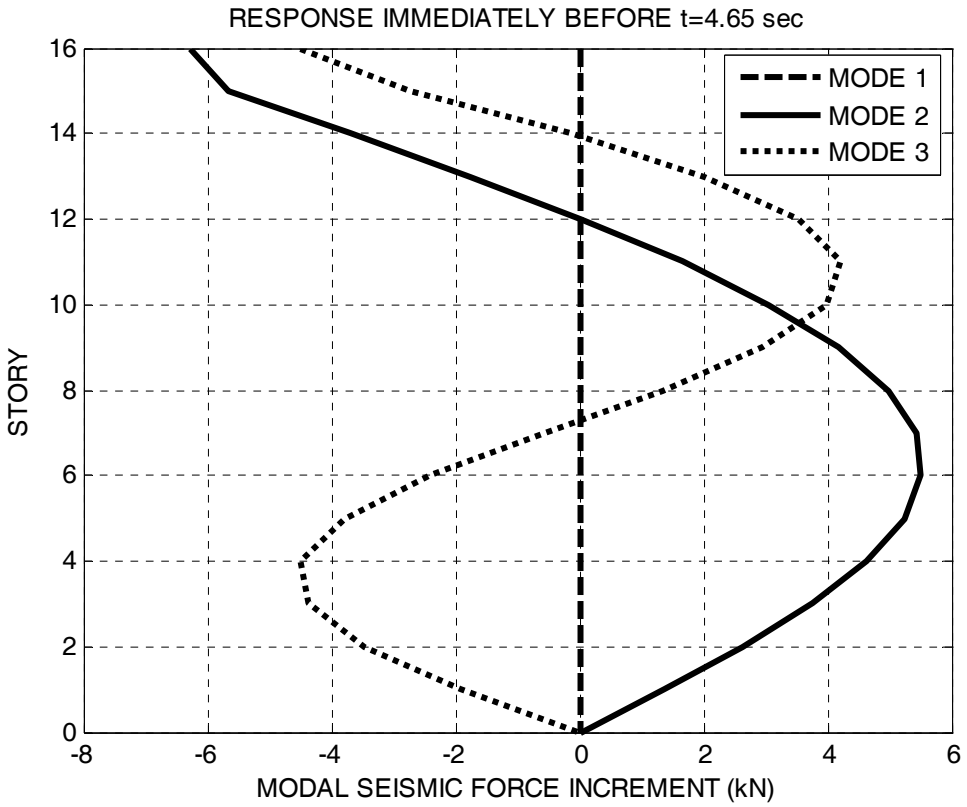

Figure 4.9. Increment of modal seismic forces of the 16 story generic wall designed with R=6 (Immediately before the peak response instant)

Figure 4.9 demonstrates zero increment of seismic forces corresponding to non-linear first mode of the structural wall, where modal increments of seismic forces associated with the higher modes are non-zero regardless of the plastic hinge formation at the base of the wall.

Modal seismic force pattern of the wall at the peak response instant is shown in Figure 4.10, which emphasizes considerably higher modal seismic forces provided by the non-linear second mode with respect to other modal contributions.

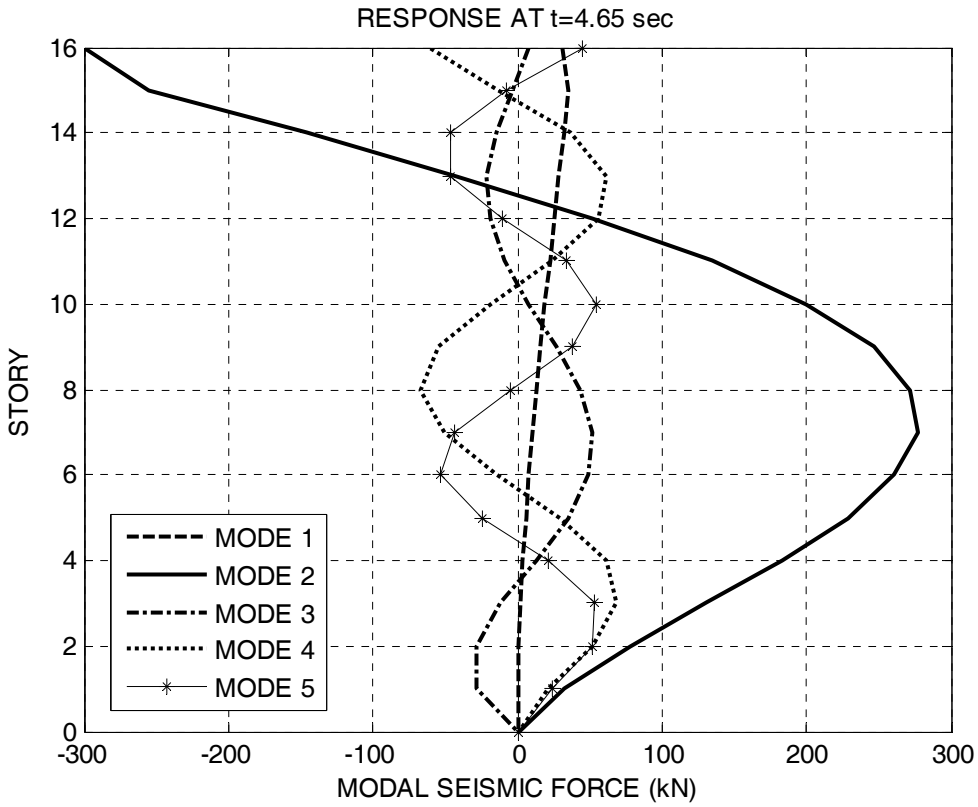

Figure 4.10. Modal seismic forces of the 16 story generic wall designed with R=6 (at the peak response instant)

Figure 4.11 demonstrates the significant effect of the non-linear second mode to story shear forces combined with mode superposition at the peak response instant. Story shear force quantities are given as absolute values in Figure 4.11 for the ease of interpretation. It is evident from Figure 4.11 that majority of story shear forces in the non-linear phases of the wall are provided by the non-linear second mode. Story shear forces associated with the first mode at the peak response instant shown in Figure 4.11 are those retained from the prior linear phase, since increments of seismic forces associated with the first mode are zero in this phase as demonstrated in Figure 4.9. Contribution of the third and higher modes to story shear force response are virtually negligible based on the observation that modal increments of seismic forces associated with these modes tend to reduce the modal shear response in the non-linear phase contrary to the case for the second non-linear mode.

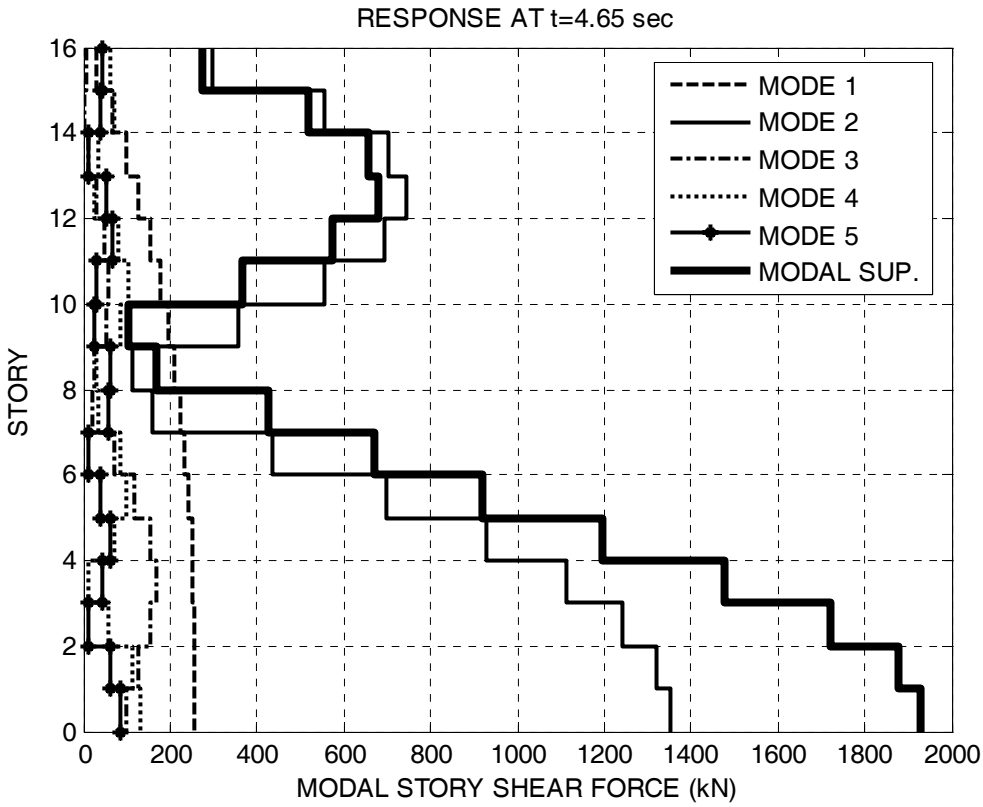

Figure 4.11. Modal and superposed story shear forces of the 16 story generic wall designed with R=6 (at the peak response instant)

Effect of the non-linear second mode has also been observed on the moment response of the 16 story generic wall as shown in Figure 4.12 in terms of modal increment of moments obtained immediately before the peak response instant. Increment of modal moments associated with the first non-linear mode has been obtained as zero due to zero increment of seismic forces associated with this mode. However, second non-linear mode, with zero modal moment increment at the base, has been observed to induce moments at upper story levels. This effect may contribute to the spread of plasticity at the upper levels of the wall in the non-linear phases as observed in Group 1 and Group 3 non-linear time history analysis (See Chapter 5).

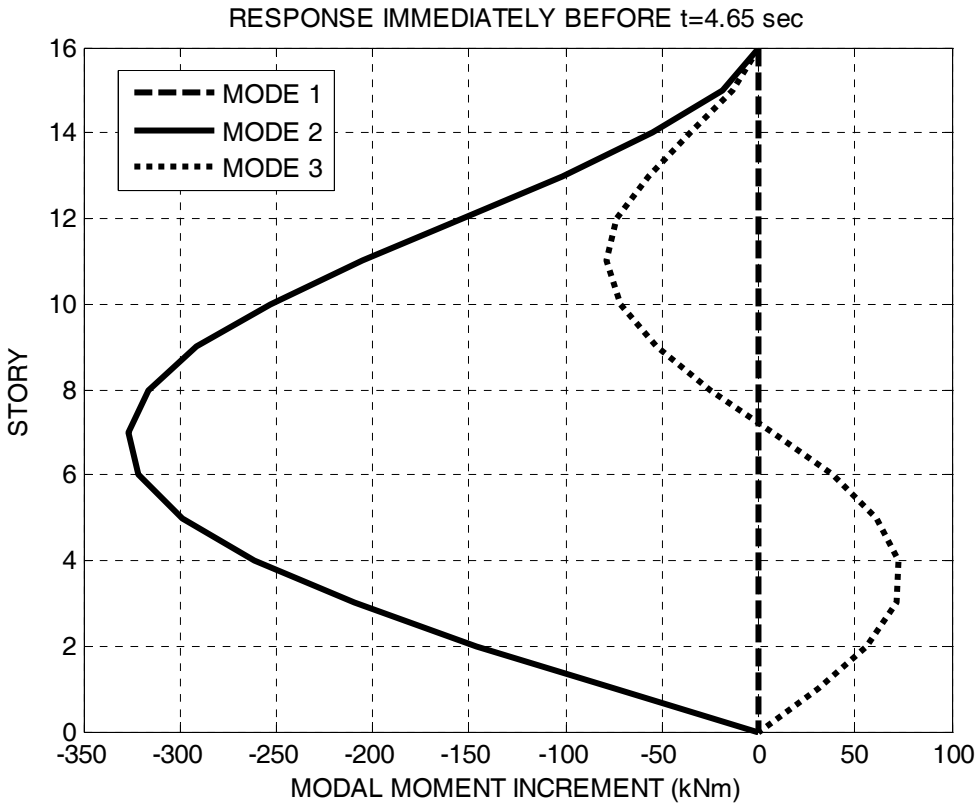

Figure 4.12. Increment of modal moments of the 16 story generic wall designed with R=6 (Immediately before the peak response instant)

Dynamic base shear amplification factors can also be presented in terms of modal contributions. Figure 4.13 shows first ten seconds of modal dynamic amplification factor history of the 16 story generic wall, obtained by dividing each modal base shear to the design base shear of the wall. Dynamic base shear amplification factor combined with mode superposition method is also provided in last pane of Figure 4.13 and dynamic amplification factor at the peak response instant has been marked with a dark dot for the ease of understanding.

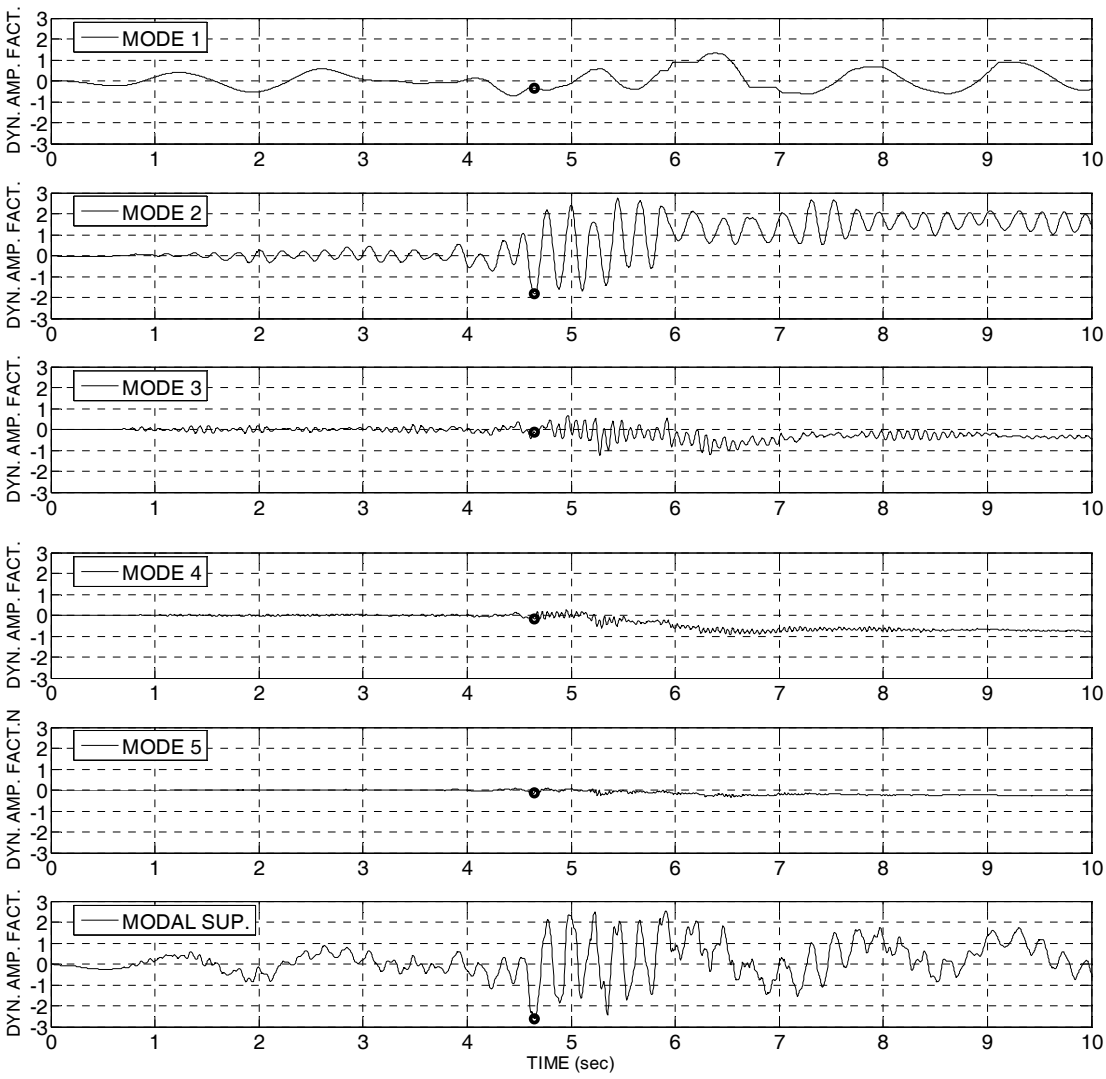

Figure 4.13. First ten seconds of the modal and superposed dynamic base shear amplification factor history of the 16 story generic wall designed with R=6

Figure 4.13 indicates that, non-linear second mode is chiefly responsible for the dynamic base shear amplifications, where effect of higher modes above the second mode has been found to be negligible at the peak response instant. Dynamic base shear amplification factor associated with the first mode has been computed greater than unity between 6.30 seconds and 6.40 seconds of the response history (Figure 4.13), due to slight numerical errors in the decomposition process.

Based on the results of this study, it is believed that dynamic amplification phenomenon should be related to second mode effect rather than higher mode effects.

Significant role of the second mode on dynamic shear amplifications has been demonstrated in this study by utilizing a modal decomposition technique. It has been shown that, response of yielding structural walls can be decomposed into modal response contributions by using the modal decomposition technique explained above.

5. NON-LINEAR TIME HISTORY ANALYSES OF GENERIC WALLS

Owing to the cantilever-like characteristics of structural wall systems, maximum shear force effects occur at the base of the wall. Thus, focusing on the amplification factors of the base shear forces has a merit for inhibiting brittle modes of failure associated with shear, such as the diagonal tension failure, diagonal compression failure and sliding at the cold joints.

In this chapter, base shear amplification factors and their relation with the first mode period of walls and the strength reduction factors have been investigated through a parametric study based on non-linear time history analyses. Base shear amplification factors are proposed based on regression analyses of the parametric time history analysis results, which are indented to be used in Turkish Seismic Design Code (2007) for shear design of walls. Furthermore, a story shear force envelope along the wall height is recommended and interrelated with the amplified base shear.

The generic walls with geometric characteristics given in Chapter 3 have been analyzed with non-linear time history analyses by using step-by-step integration procedure in the time domain. Each wall has been consecutively analyzed for the strength levels corresponding to strength reduction factors of R=2, 4, 6, 8 and 10 with 20 strong ground motion acceleration records scaled to fit the Turkish Seismic Design Code (2007) Acceleration Response Spectrum as explained in Appendix C.

Newmark's average acceleration method (γ=1/2 and β=1/4) has been used as an unconditionally stable algorithm in step-by-step integration of non-linear time history analyses. In order to avoid the accuracy problems, time steps has been chosen as 0.005 sec, which is below 1/10 of the third mode period of all generic walls.

Damping matrix of the system has been constructed with Rayleigh method that is, the damping matrix has been assumed to be proportional to the stiffness and mass matrices of the walls. Damping ratios for the first and the third modes have been chosen to be 1 per

cent, so as not to over emphasize the damping effects in the second mode as illustrated in Figure 5.1

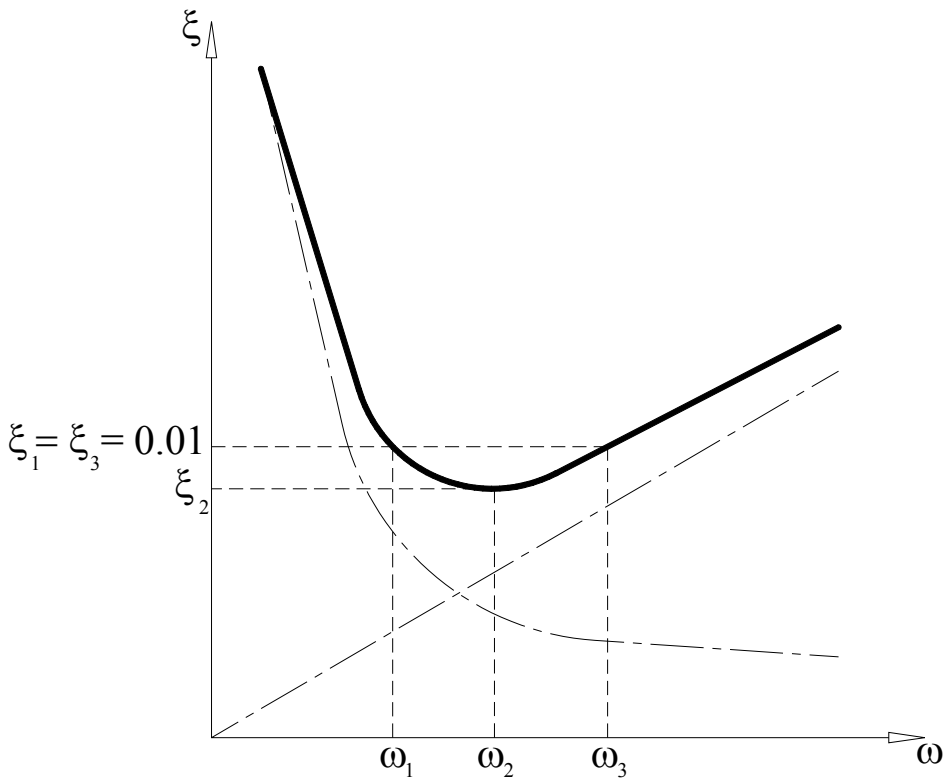

Figure 5.1. Illustration of damping ratio assumption in time history analyses

Non-linear time history analyses has been executed under four groups (hereinafter called Group 1, Group 2, Group 3 and Group 4) in order to investigate the sensitivity of the base shear amplification factors to the distribution of plastic hinges along the wall height and the hysteresis characteristics of the plastic hinges. Modeling details and base shear amplification results for each group are presented in the subsequent sections. Due to vast number of analyses performed in this study, only the moment and story shear force diagrams along the wall height, that have been obtained from the generic 16 story wall with strength reduction factor of R=6 has been presented.

Group 1 and Group 2 non-linear time history analyses have been performed by using SAP 2000 v11 (CSI, 2006) structural analysis software, whereas Group 3 and Group 4 non-linear time history analyses have been performed by using RUAUMOKO (Carr, 2000)

structural analysis software, which are both licensed to the Department of Earthquake Engineering of Boğaziçi University.

5.1. Group 1 Analyses and Results

Group1 analyses involve the generic wall analytical models of multiple plastic hinge distribution along the wall height with elastoplastic moment-curvature hysteresis relations as shown in Figure 5.2. Other structural modeling assumptions described in Chapter 3 are also valid for the Group 1 models.

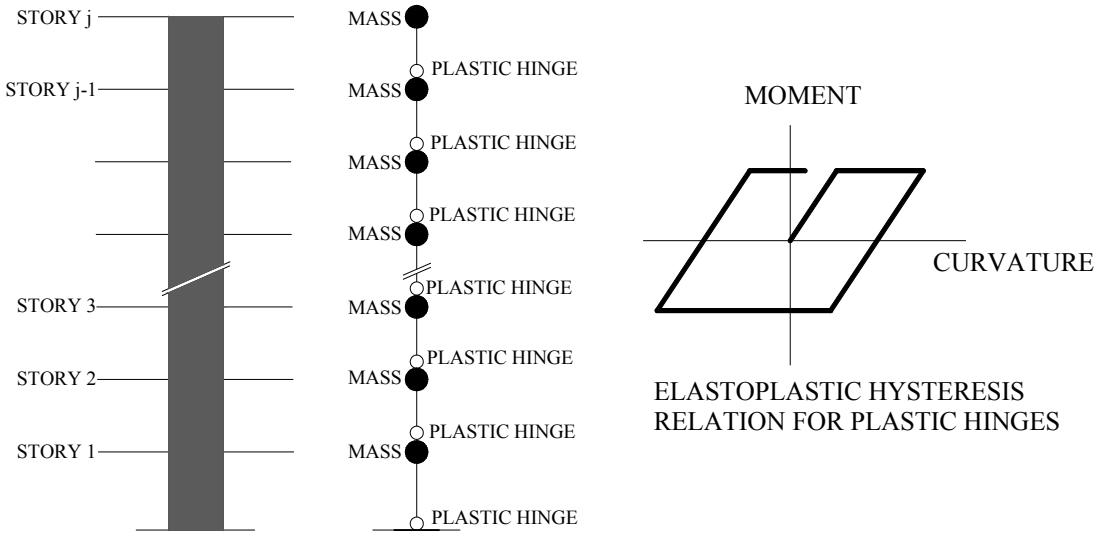

Figure 5.2. Illustration of analytical model for Group 1 analyses

It has been assumed that yield moment capacity is uniform along the wall, being equal to base design moment corresponding to the strength reduction factors as described in Chapter 3. Actually, reinforced concrete wall sections do not exhibit perfectly elastoplastic hysteresis characteristics during flexure as reversals due to seismic attack become significant, and some degree of stiffness degradation should be expected. Yet, elastoplastic plastic hinges are customarily used in most non-linear time history analyses and it is believed that reliable results can be obtained for the benchmarking of studies with more complex hysteresis relationships.

Non-linear time history analyses have been performed for generic wall models of 8, 12, 16, 20 and 30 stories with strength levels corresponding to R = 2, 4, 6, 8 and 10. For

each generic wall model with the aforementioned strength level, maximum story moments and shear forces have been obtained for each of 20 ground motion record as shown in Figure 5.3 and Figure 5.4 for 16 story wall with strength level of R = 6.

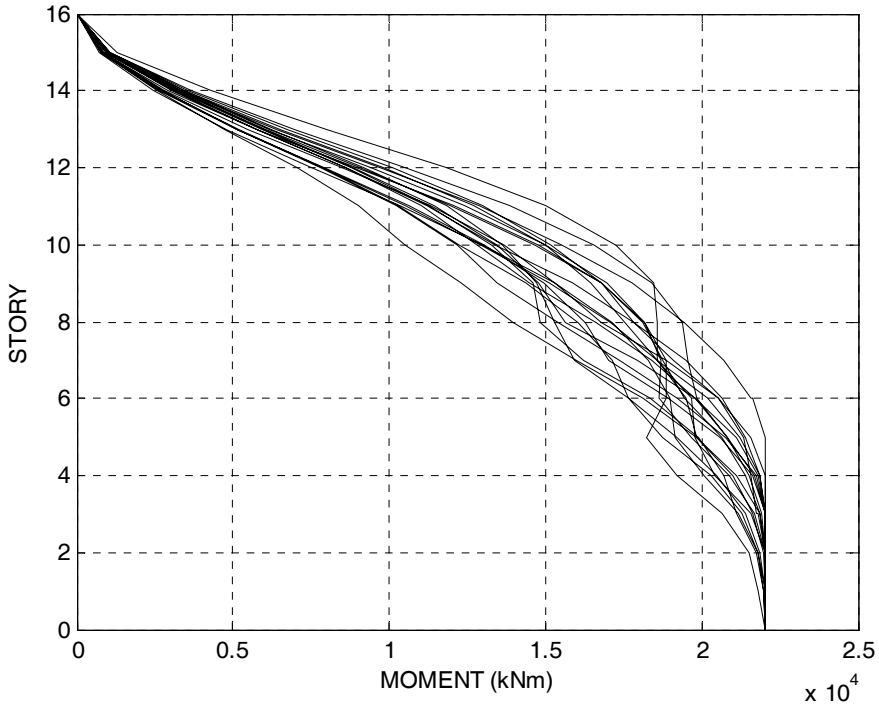

Figure 5.3. Story moment diagrams of 16 story wall with strength level R=6 (Group 1 time history analyses)

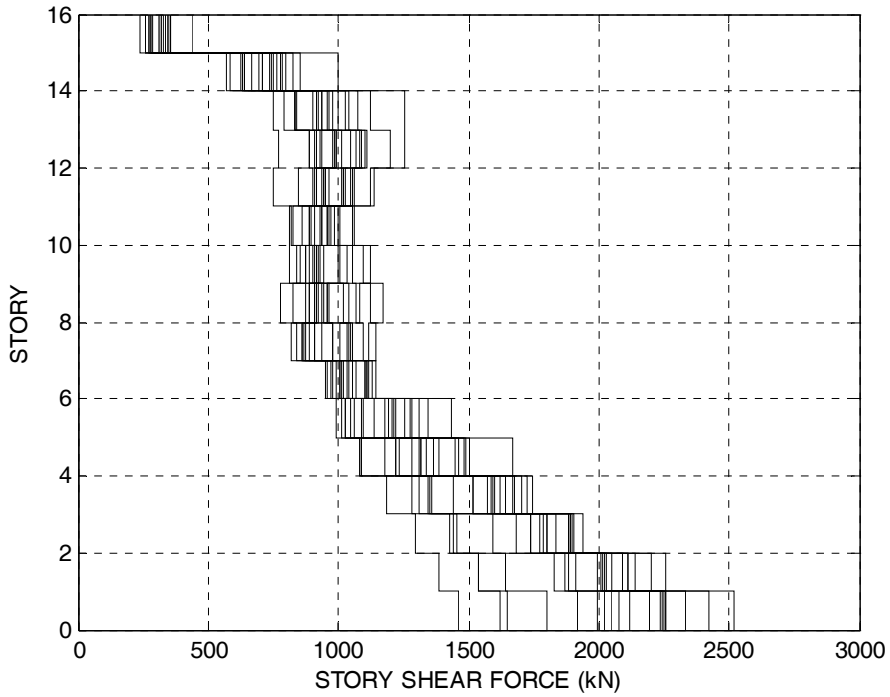

Figure 5.4. Story shear force diagrams of 16 story wall with strength level R=6 (Group 1 time history analyses)

Subsequently story moment and shear forces have been averaged to obtain mean story moment and story shear force diagrams, as shown in Figure 5.5 and Figure 5.6 for 16 story wall with R = 6 strength level with comparison to the design moment and shear force diagrams.

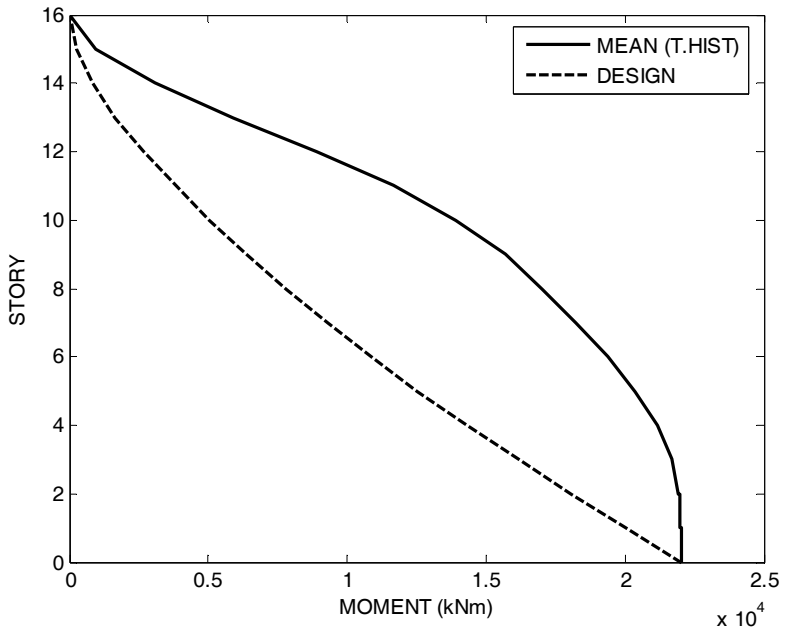

Figure 5.5. Mean story moment diagram of 16 story wall with strength level R=6 (Group 1 time history analyses)

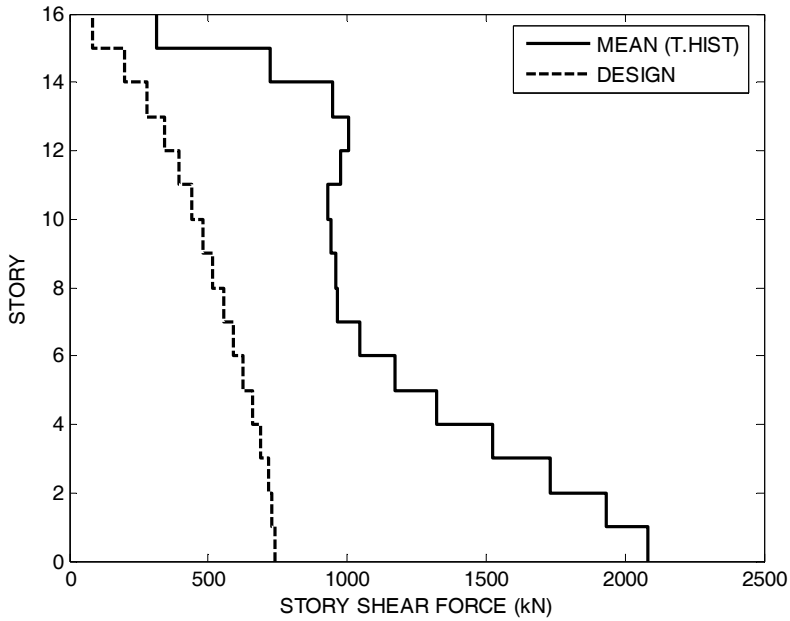

Figure 5.6. Mean story shear force diagram of 16 story wall with strength level R=6 (Group 1 time history analyses)

Consequently mean story shear forces obtained from time history analyses have been divided to design story shear forces in order to obtain story shear force amplification factors as shown in Figure 5.7 for the 16 story wall with R = 6 strength level.

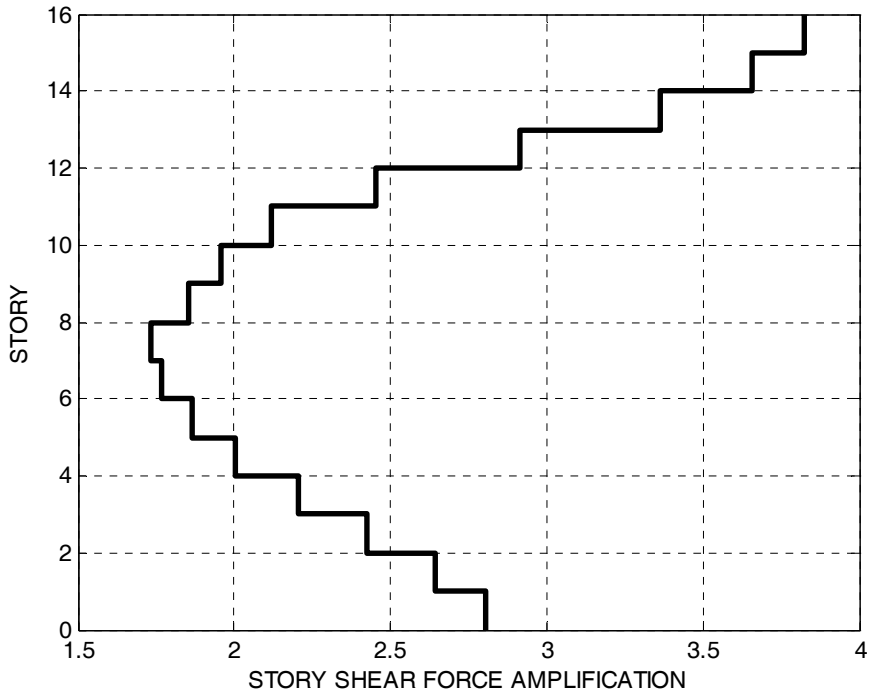

Figure 5.7. Mean story shear force amplification factors computed for the 16 story wall with strength level R=6 (Group 1 time history analyses)

As shown in Figure 5.4, there is a scatter of story shear forces due to the different characteristics of the ground motion in spite of scaling has been applied to fit a target response spectrum. This scatter has been observed at all generic walls and corresponding strength levels and is obviously reflected to the base shear amplification factors; however it is believed that averaging time history results from 20 ground motion records is justifiable due to the sufficient number of samples in the group.

Mean base shear amplification factors derived from Group 1 non-linear time history analyses have been collected in a single diagram (β^b – T – R diagram) related with the first mode periods of the wall corresponding the cracked section stiffness and strength reduction factors as shown in Figure 5.8

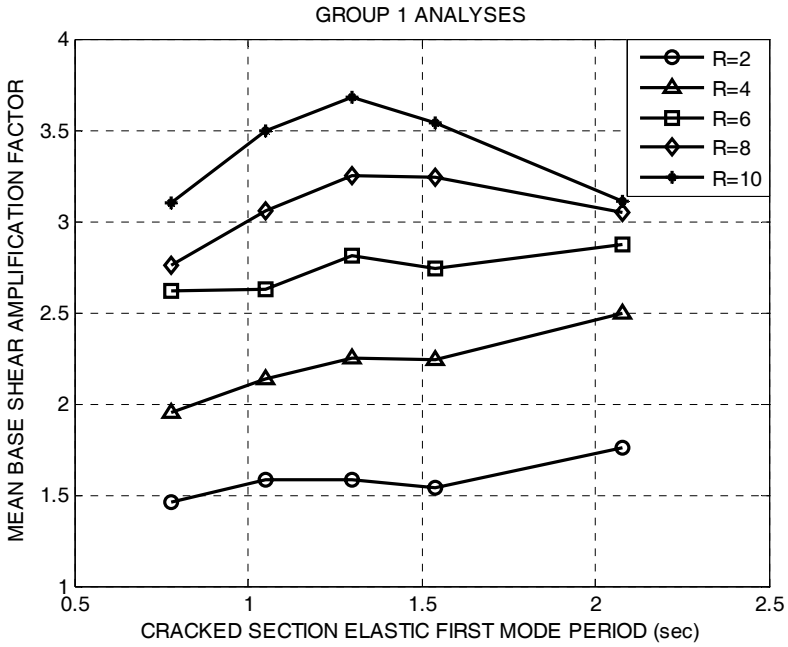

Figure 5.8. Mean base shear amplification factors obtained from Group 1 time history analyses

5.2. Group 2 Analyses and Results

Group 2 analyses include the generic wall analytical models with a single plastic hinge at the base of the wall with elastoplastic moment-curvature hysteresis relation as shown in Figure 5.9. Other structural modeling assumptions described in Chapter 3 are also valid for the Group 2 models.

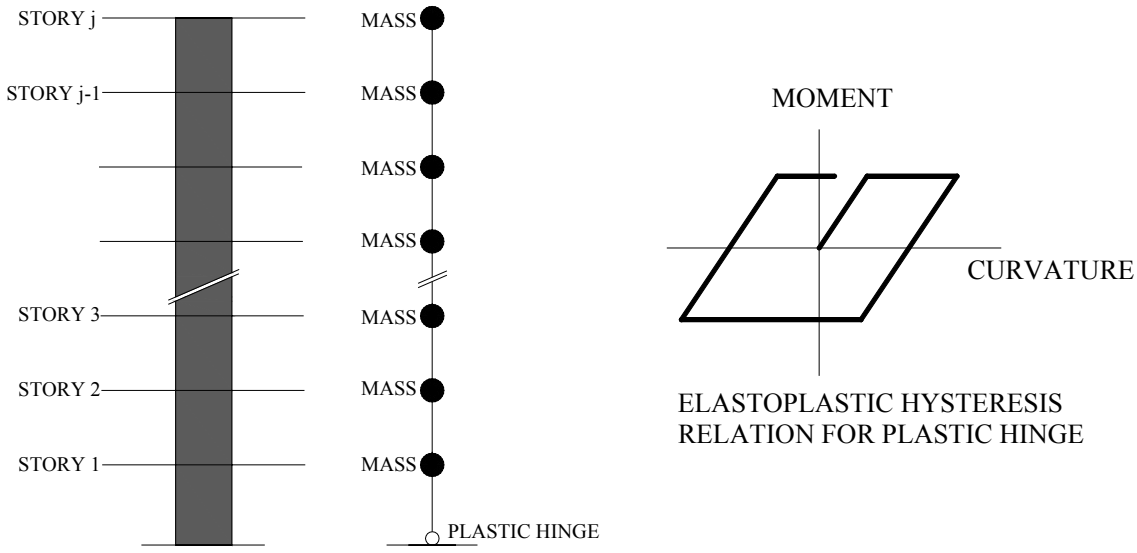

Figure 5.9. Illustration of analytical model for Group 2 analyses

It is expected in real wall structures that a single plastic hinge formation at the base of the wall is not possible and the plasticity spreads upwards from the base with increasing seismic demand. However, it is intended that Group 2 analyses shall provide insight on the effect of spread of plasticity on structural response with respect to Group 1 analyses.

Non-linear time history analyses have been performed for Group 2 generic wall models similar to the Group 1 analyses. Similarly, for each generic wall model with the corresponding strength level, maximum story moments and shear forces have been obtained for each of 20 ground motion record. Subsequently mean story moments, story shear forces and base shear amplification factors have been computed as shown in Figure 5.9 to Figure 5.14 for the 16 story wall with R = 6 strength level.

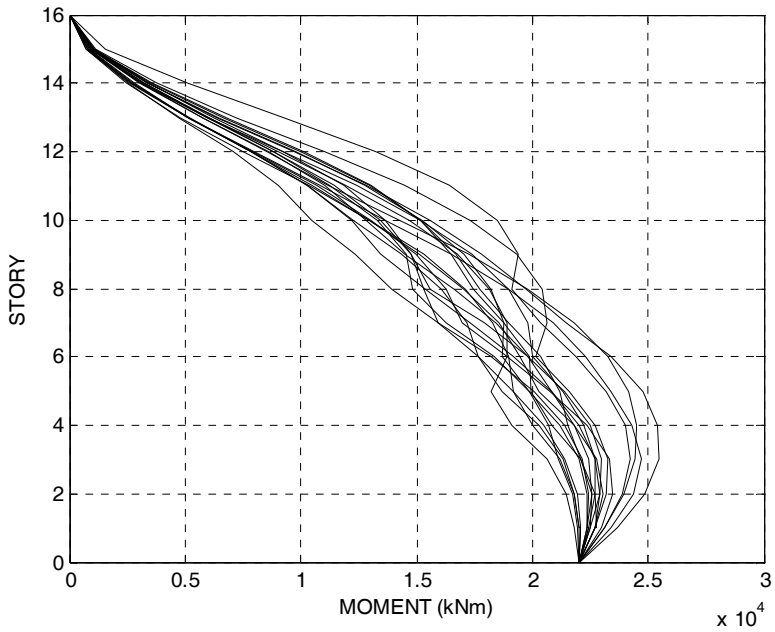

Figure 5.10. Story moment diagrams of 16 story wall with strength level R=6 (Group 2 time history analyses)

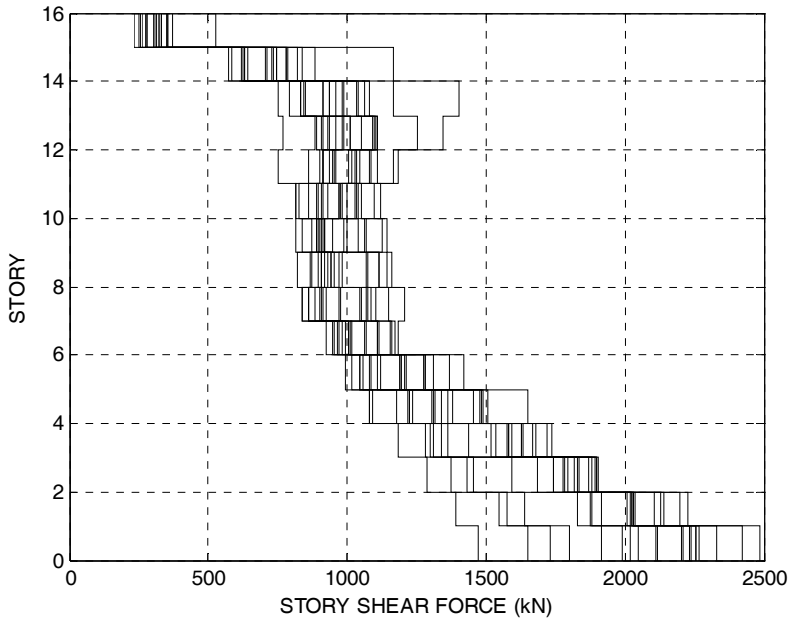

Figure 5.11. Story shear force diagrams of 16 story wall with strength level R=6 (Group 2 time history analyses)

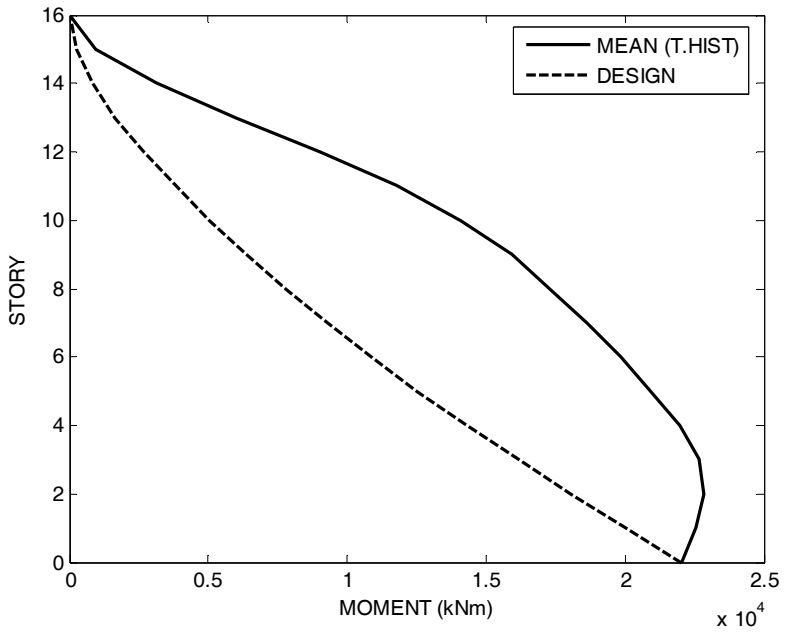

Figure 5.12. Mean story moment diagram of 16 story wall with strength level R=6 (Group 2 time history analyses)

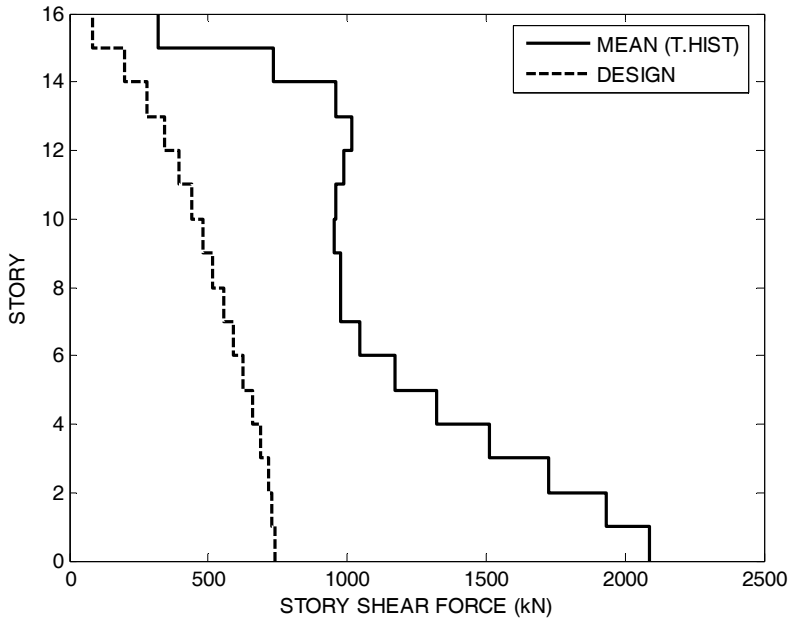

Figure 5.13. Mean story moment diagram of 16 story wall with strength level R=6 (Group 2 time history analyses)

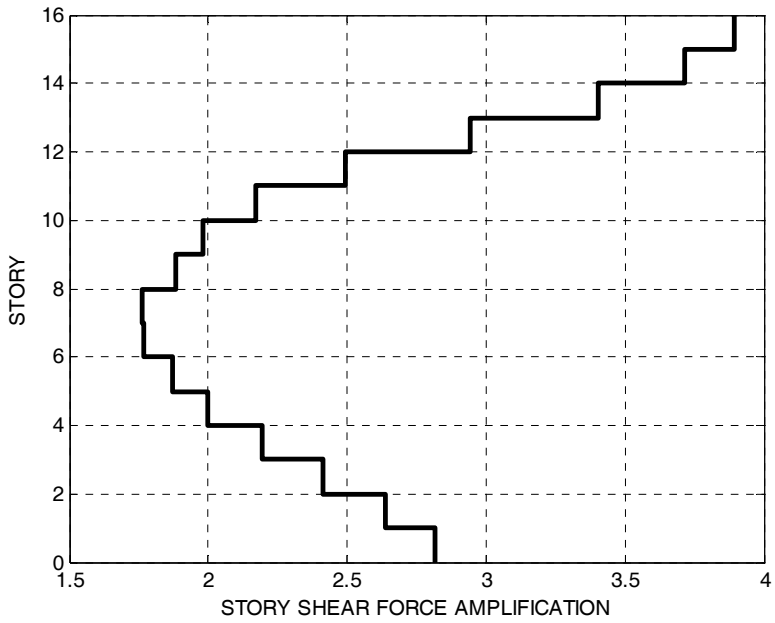

Figure 5.14. Mean story shear force amplification factors computed for the 16 story wall with strength level R=6 (Group 2 time history analyses)

β^b – T – R diagram derived from Group 2 non-linear time history analyses are presented in Figure 5.15

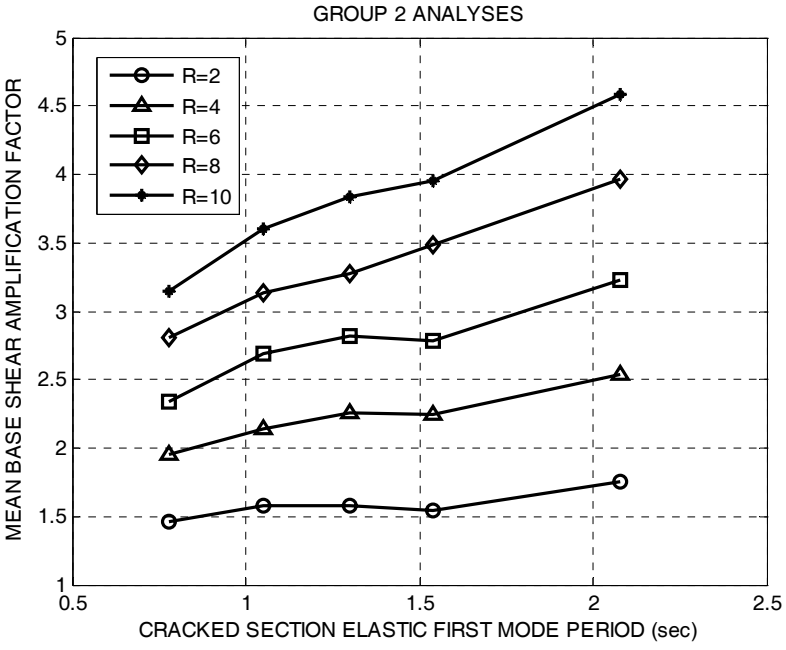

Figure 5.15. Mean base shear amplification factors obtained from Group 3 time history analyses

5.3. Group 3 Analyses and Results

Group 3 analyses involve the generic wall analytical models with multiple plastic hinge distribution along the wall height with Takeda (1970) degrading stiffness moment-curvature hysteretic relationships as shown in Figure 5.16. Other structural modeling assumptions depicted in Chapter 3 are also valid for the Group 3 models.

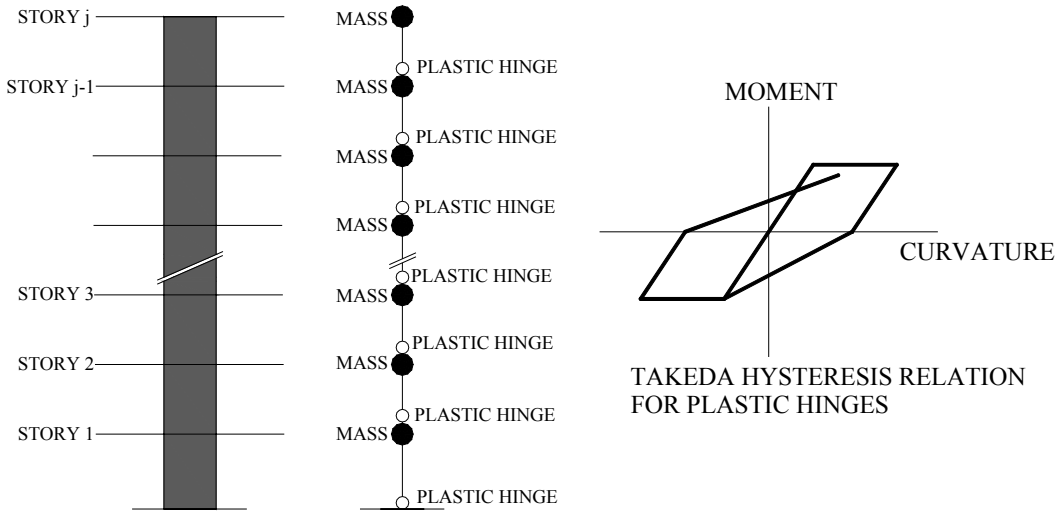

Figure 5.16. Illustration of analytical model for Group 3 analyses

It has been intended that Group 3 analyses shall reflect the effect of degrading stiffness moment-curvature hysteretic relationship with respect to the Group 1 analyses that were performed with elastoplastic hysteretic relationship.

Non-linear time history analyses have been performed for the generic wall models in the Group 3 analyses similar to Group 1 and Group 2 analyses. For each generic wall model with the corresponding strength level, maximum story moments and shear forces have been obtained for each of 20 ground motion records. Subsequently mean story moments, story shear forces and base shear amplification factors have been computed as shown in Figure 5.17 to Figure 5.21 for the 16 story wall with R = 6 strength level.

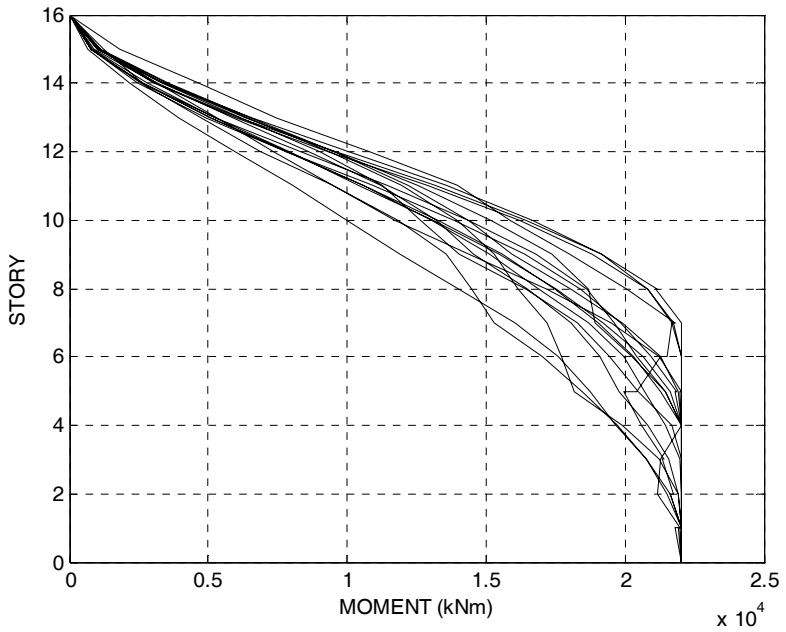

Figure 5.17. Story moment diagrams of 16 story wall with strength level R=6 (Group 3 time history analyses)

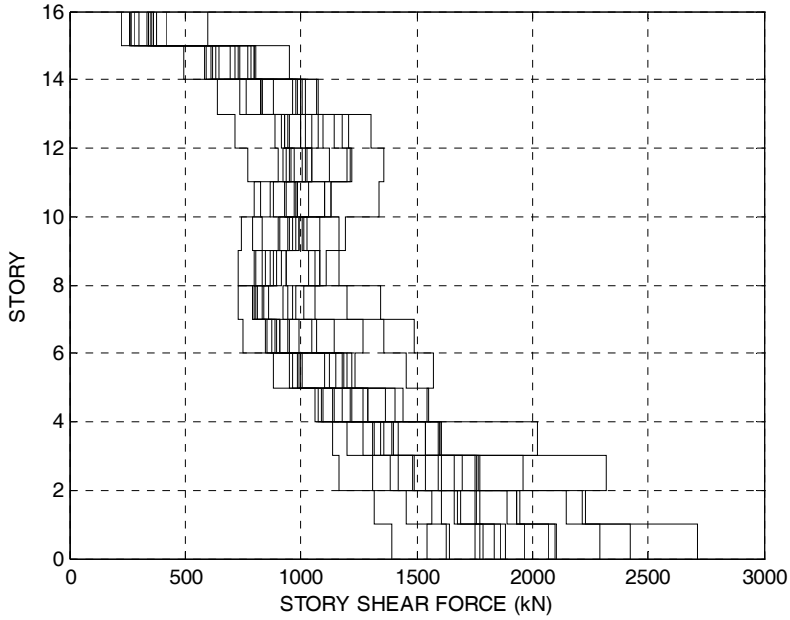

Figure 5.18. Story shear force diagrams of 16 story wall with strength level R=6 (Group 3 time history analyses)

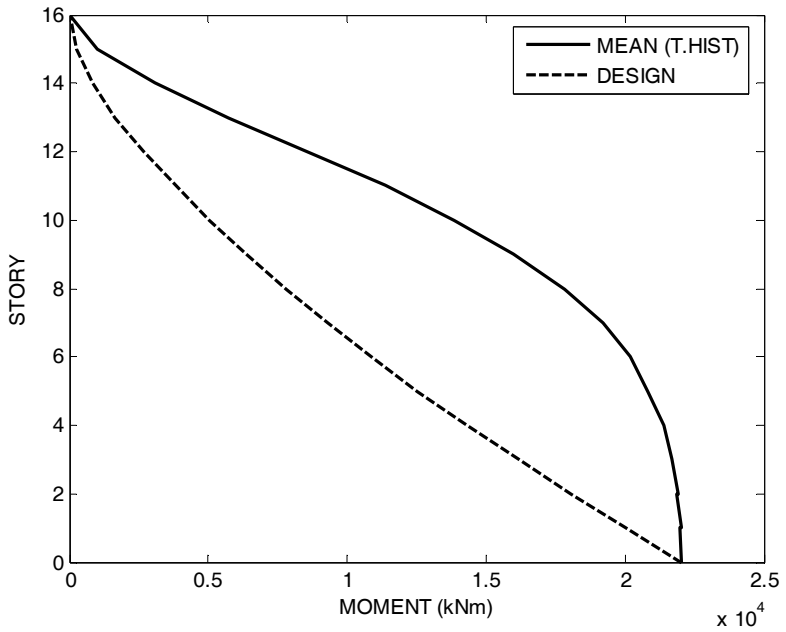

Figure 5.19. Mean story moment diagram of 16 story wall with strength level R=6 (Group 3 time history analyses)

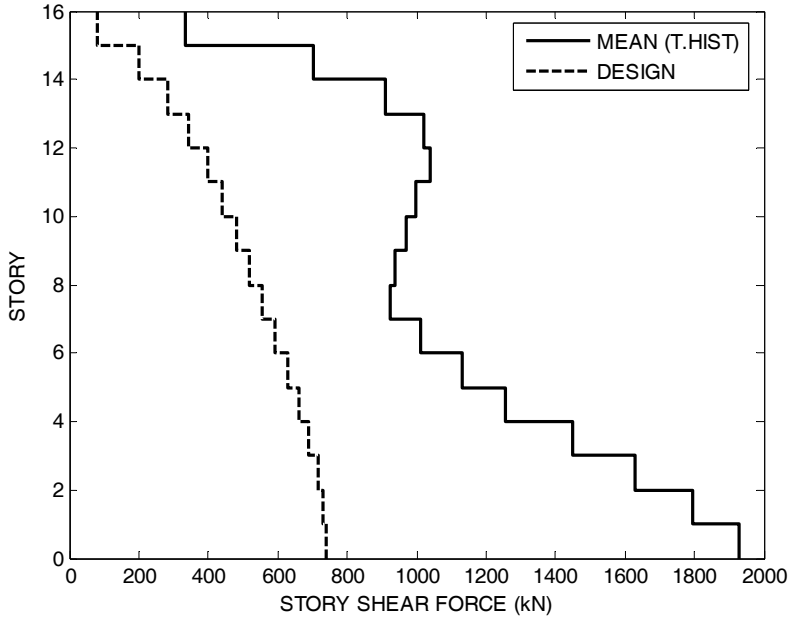

Figure 5.20. Mean story shear force diagram of 16 story wall with strength level R=6 (Group 3 time history analyses)

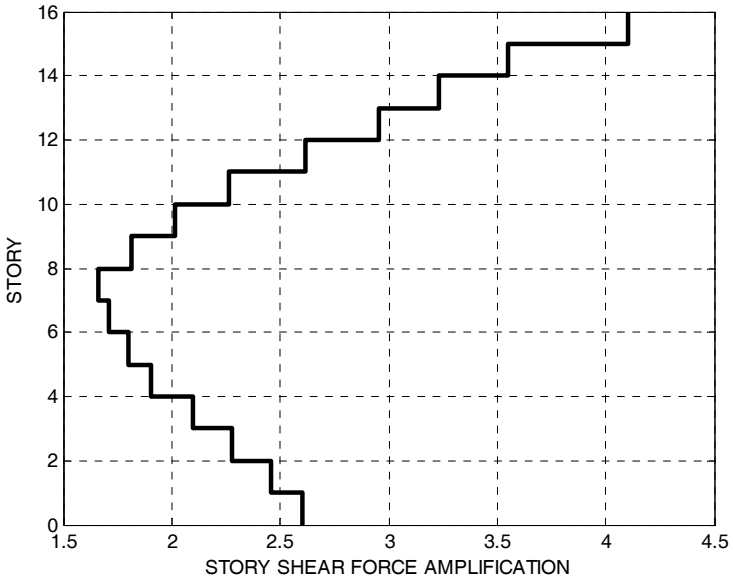

Figure 5.21. Mean story shear force amplification factors computed for the 16 story wall with strength level R=6 (Group 3 time history analyses)

β^b – T – R diagram derived from Group 3 non-linear time history analyses are presented in Figure 5.22

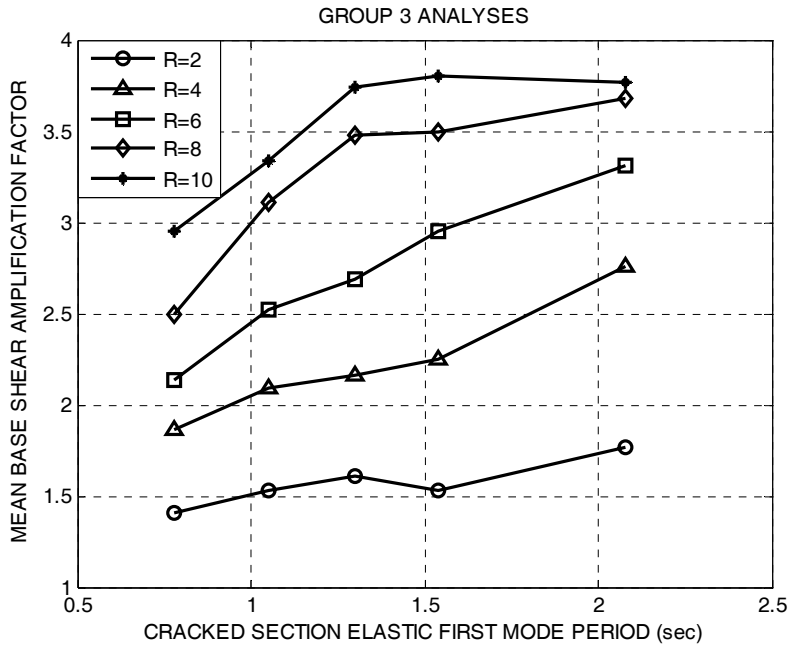

Figure 5.22. Mean base shear amplification factors obtained from Group 3 time history analyses

5.4. Group 4 Analyses and Results

Group 4 analyses constitute the generic wall analytical models with a single plastic hinge at the base of the wall height Takeda (1970) degrading stiffness moment-curvature hysteresis relations as shown in Figure 5.23. Other structural modeling assumptions described in Chapter 3 are also valid for the Group 4 models.

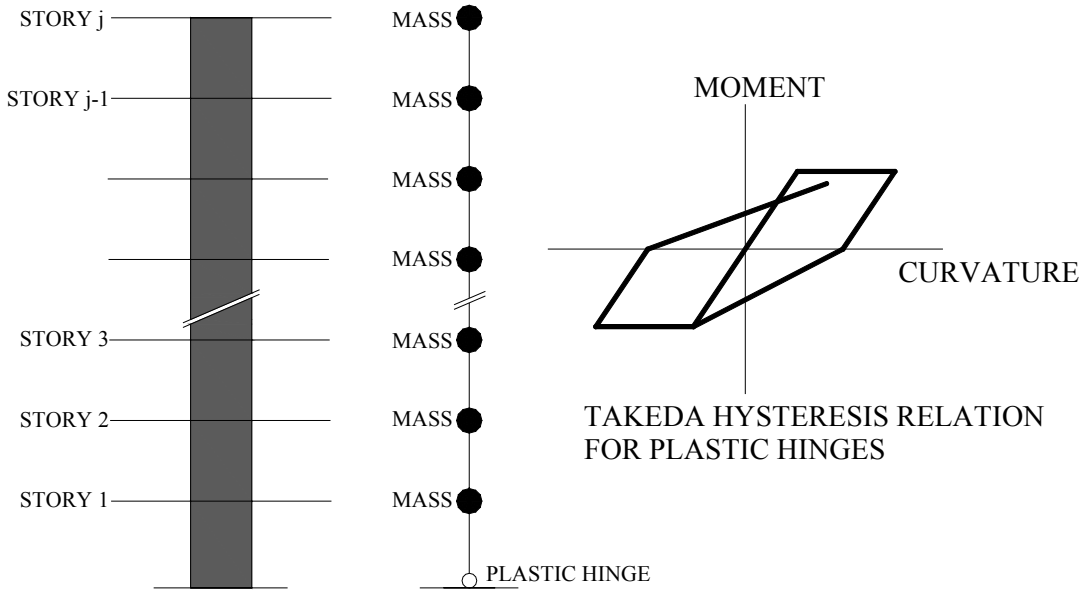

Figure 5.23. Illustration of analytical model for Group 3 analyses

In spite of an unrealistic behavior expected with a single plastic hinge at the base of the wall, it has been anticipated that Group 4 analyses shall provide insight on the effect of spread of plasticity on structural response with respect to Group 3 analyses.

Similar to the other analysis groups, non-linear time history analyses have been performed for the generic wall models in the Group 4 analyses. For each generic wall model with the corresponding strength level, maximum story moments and shear forces have been obtained for each of 20 ground motion record. Subsequently mean story moments, story shear forces and base shear amplification factors have been computed as shown in Figure 5.24 to Figure 5.28 for the 16 story wall with R = 6 strength level.

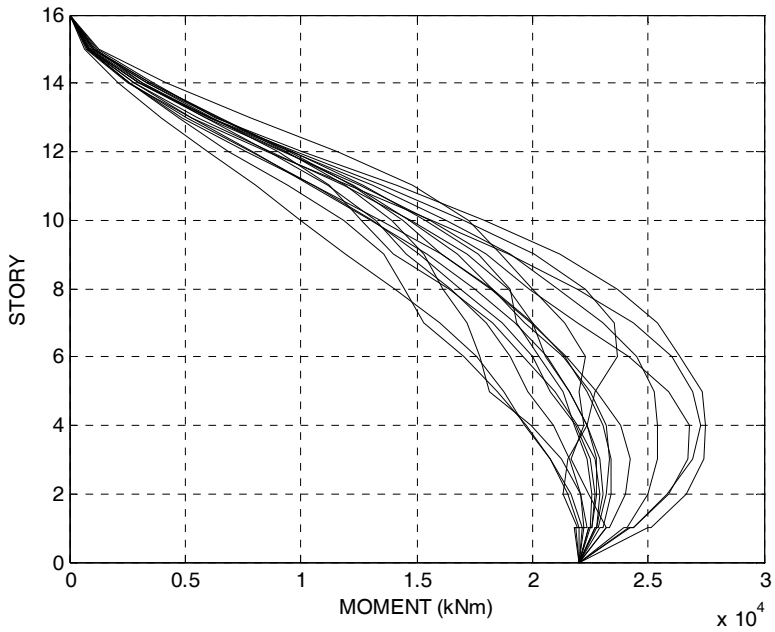

Figure 5.24. Story moment diagrams of 16 story wall with strength level R=6 (Group 4 time history analyses)

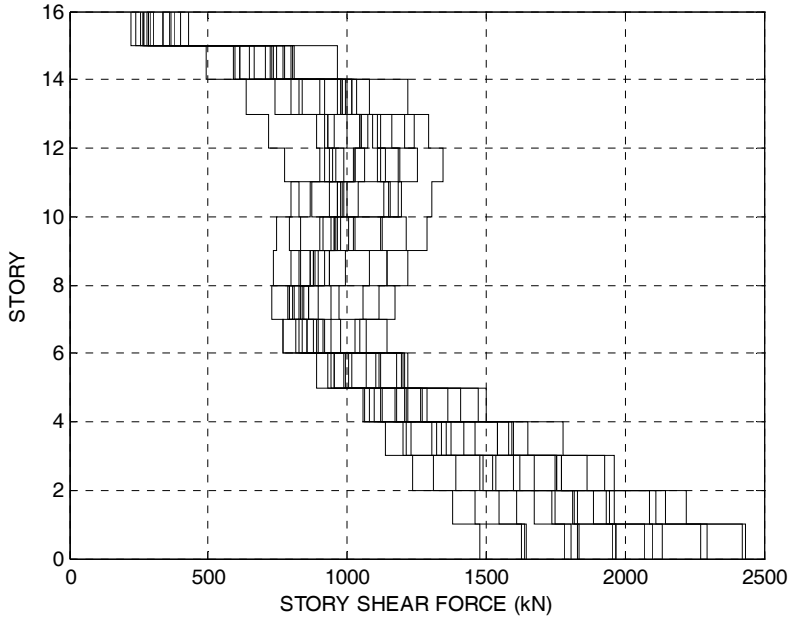

Figure 5.25. Story shear force diagrams of 16 story wall with strength level R=6 (Group 4 time history analyses)

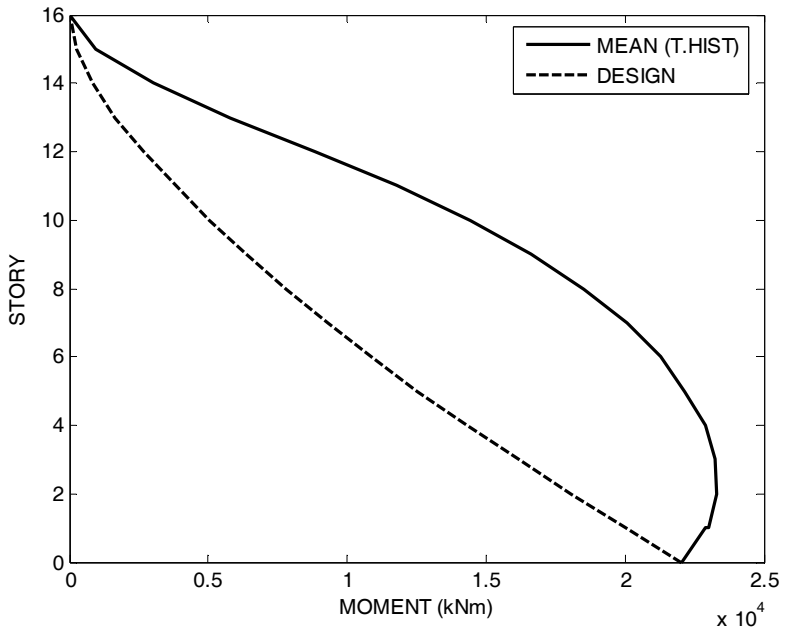

Figure 5.26. Mean story moment diagram of 16 story wall with strength level R=6 (Group 4 time history analyses)

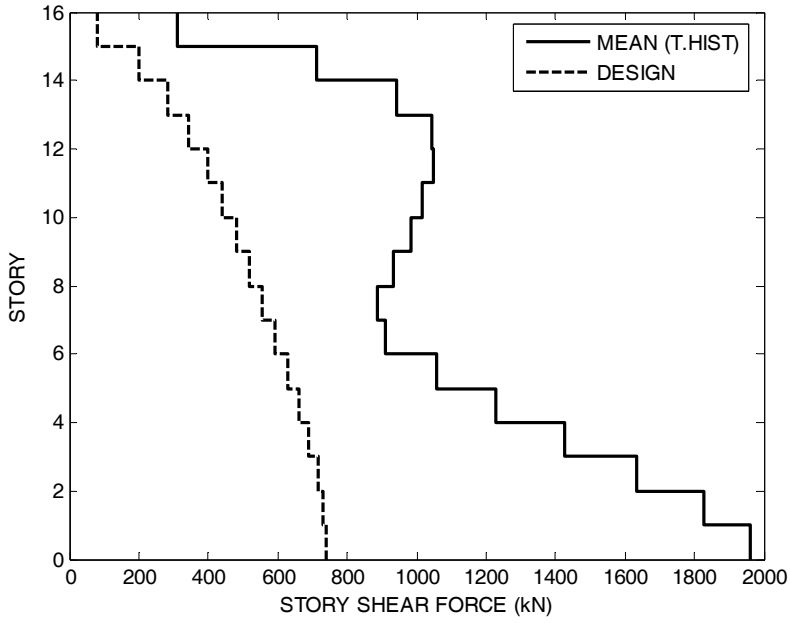

Figure 5.27. Mean story shear force diagram of 16 story wall with strength level R=6 (Group 4 time history analyses)

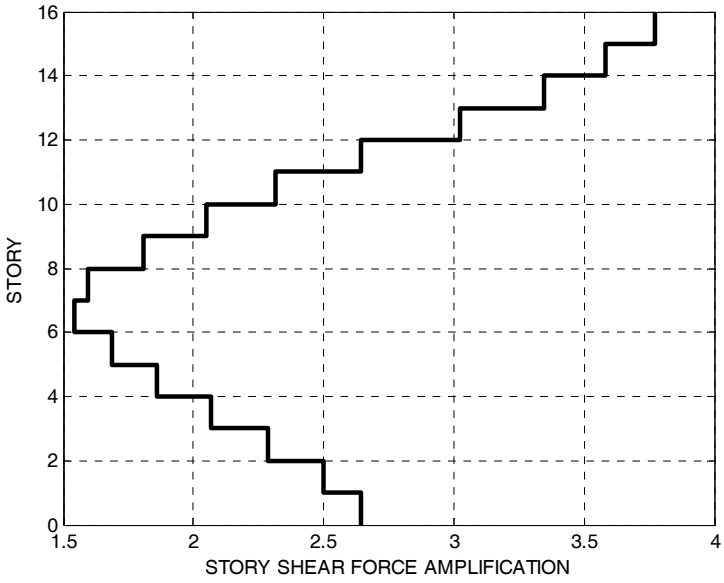

Figure 5.28. Mean story shear force amplification factors computed for the 16 story wall with strength level R=6 (Group 4 time history analyses)

β^b – T – R diagram derived from Group 3 non-linear time history analyses are presented in Figure 5.29

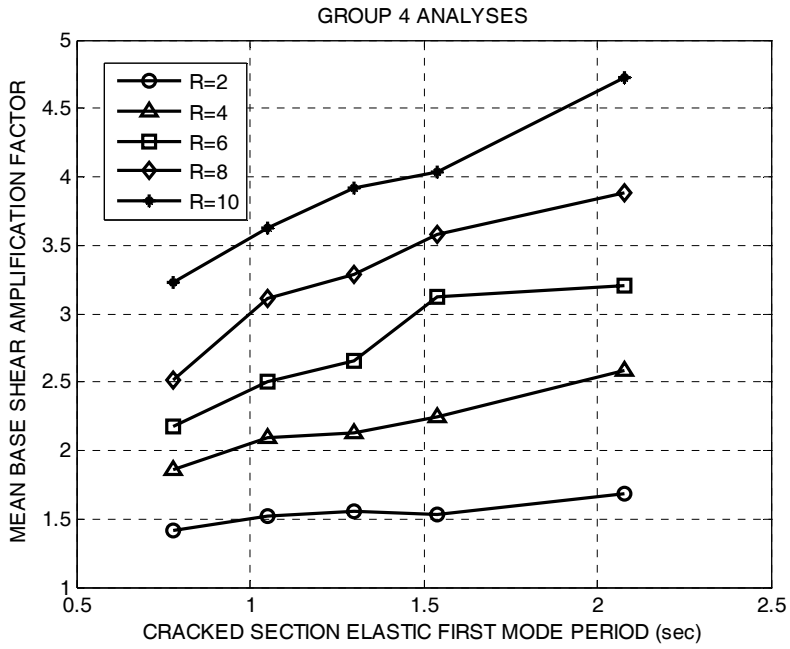

Figure 5.29. Mean base shear amplification factors obtained from Group 4 time history analyses

5.5. Remarks on Results Obtained from Non-Linear Time History Analyses

Based on the information gathered from the Group 1, Group 2, Group 3 and Group 4 non-linear time history analyses results, the following points have been observed;

- Maximum shear forces develop at the base of the wall as expected.
- Story shear forces are noticeably amplified with respect to the design values regardless of the distribution of the plastic hinges in the model or the hysteretic characteristics of the plastic hinges.
- Single hinge models (Group 2 and Group 4) resulted in comparatively higher story shear force amplification factors with respect to the distributed hinge models (Group 1 and Group 3), particularly for the models with elastoplastic plastic hinge properties. It is believed that due to the multiple plastic hinge formations along the wall, complex mode shapes occur, which reduce seismic forces.
- Single hinge models (Group 2 and Group 4) provide incorrect moment quantities and patterns above the base of the wall after the plastic hinge formation, where these quantities are higher than the yield moment capacity of the plastic hinge.
- Difference between the story shear force amplification factors obtained from Group 1 and Group 3 are barely noticeable and it is believed that analyses using elastoplastic moment-curvature hysteresis properties can provide reasonable estimations with respect to analyses using degrading stiffness hysteresis characteristics in cases the analyst lacks software with such complex hysteresis libraries.
- Both Group 1 and Group 3 analyses results indicate that, there is a tendency of reduction in base shear amplification factors for walls with low strength levels (R=8 and R=10) and with high first mode periods, which has not been observed in the single hinge model analyses (Group 2 and Group 4). This can be attributed to the multiple plastic hinge formations along the wall and associated complex mode shapes.
- Base shear amplification factors tend to increase with increasing Strength Reduction Factors (or decreasing strength levels) and with increasing first mode period, except for the wall with high first mode periods and considerably low strength levels.

6. PROPOSED DYNAMIC SHEAR AMPLIFICATION FACTOR RELATIONSHIP AND STORY SHEAR PROFILE

Based on the remarks stated in Chapter 5, it has been concluded that multiple hinge distribution along the wall better present the expected wall behavior during seismic attack. Moreover, it is believed that Takeda (1970) degrading stiffness hysteresis model is more suitable to represent realistic reinforced concrete flexural behavior. Thus, regression analysis have been performed for the base shear amplification factors derived from Group 3 non-linear time history analyses in order to propose a relationship between the base shear dynamic amplification factor, first mode period of the wall corresponding to cracked section stiffness and the strength reduction factor. It is suggested that the relationship proposed herein can be used for the design and evaluation of structural wall systems in accordance with Turkish Seismic Design Code (2007) provisions.

Prior to regression analyses, an expression as given in Equation (6.1) has been suggested as the initial structure of the proposed relationship.

$$\beta^{b} = 1 + (aT_{1\text{-cr}} + b)(R - 1.5)^{c} \tag{6.1}$$

Consequent to regression analyses, regression variables a, b and c has been calculated as:

$$a = 0.281 \qquad b = 0.394 \qquad c = 0.553$$

which formed the proposed expression given in Equation (6.1) for the dynamic base shear amplification factors as presented in Equation (6.2);

$$\beta^{b} = 1.0 + (0.281 \times T_{1\text{-cr}} + 0.394) \times (R - 1.5)^{0.553} \tag{6.2}$$

$$1.0 \le \beta^{b} \le R \tag{6.3}$$

The coefficient of multiple determination of the regression (R^2) has been computed as 0.9743 over 1.0000, which suggested a successful fit of the proposed relationship to the samples. The agreement between the obtained mean dynamic base shear amplification

factors and the proposed dynamic base shear amplification relationship is shown in Figure 6.1.

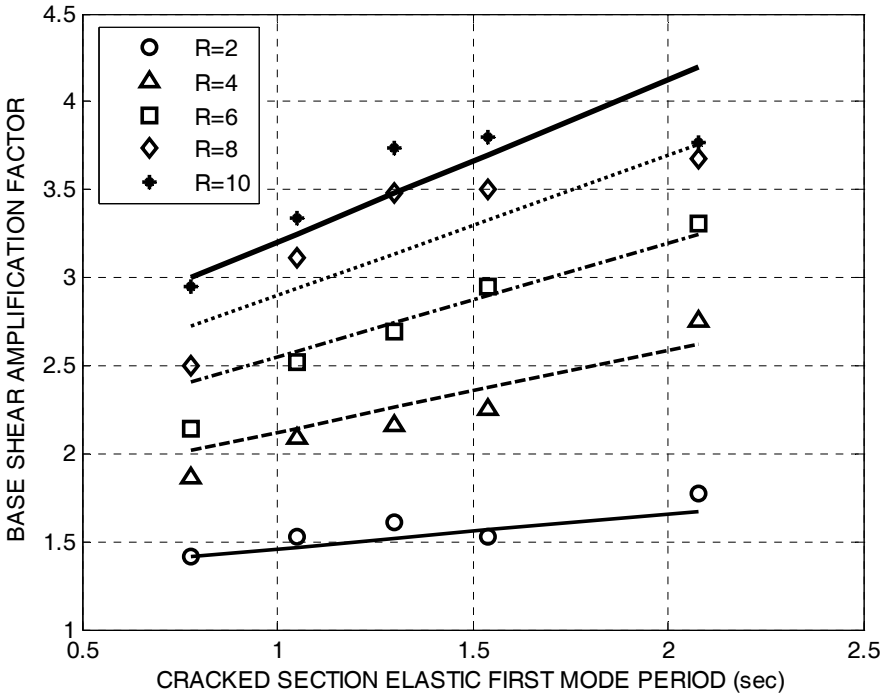

Figure 6.1. Agreement between the proposed relationship and mean base shear amplification factors

Figure 6.1 suggests that the proposed relationship is in good agreement with the mean amplification factors for strength reduction factors between 2 and 6, and overestimates the amplification factors for strength reduction factors 8 and 10 in the high period range that is believed to be acceptable in terms of a conservative approach.

6.1. Comparison of the Proposed Amplification Relationship with the Other Relationships

Proposed dynamic base shear amplification relationship given in Equation (6.2) have been compared with the relationships proposed by other researchers mentioned in Chapter 2. It should be noted that such a comparison may not be appropriate since the base shear amplification factors are highly affected by the ground motion intensity considered, number of ground motion records considered and modeling assumptions. However, it is found useful to compare the trends between the proposed relationship and those proposed by other researchers.

Figure 6.2 shows the base shear amplification factors computed for the generic walls considered in this study by using the relationship proposed by Ghosh and Markevicius (1990). In order to illustrate the deviation between the two relationships base shear amplification factors computed with Ghosh and Markevicius relationship is divided by the amplification factors obtained from the proposed relationship as shown in Figure 6.3

Figure 6.3 reveals that proposed relationship in this study provides greater base shear amplification ratios particularly in the high period range with respect to the relationship proposed by Ghosh and Markevicius, which may be attributed to lack of a period term in the Ghosh and Markevicius relationship.

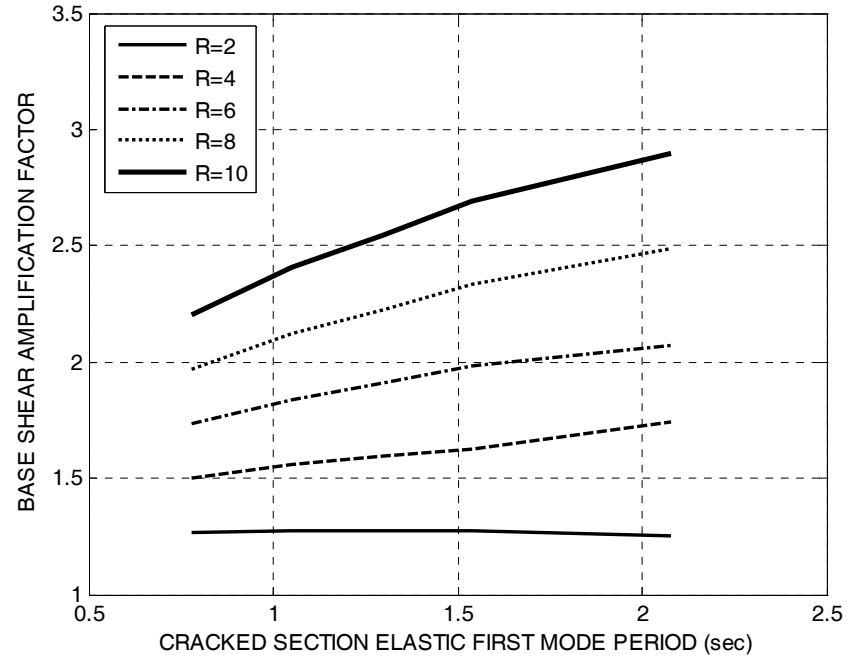

Figure 6.2. Base shear amplification factors computed by using Ghosh and Markevicius (1990) relationship

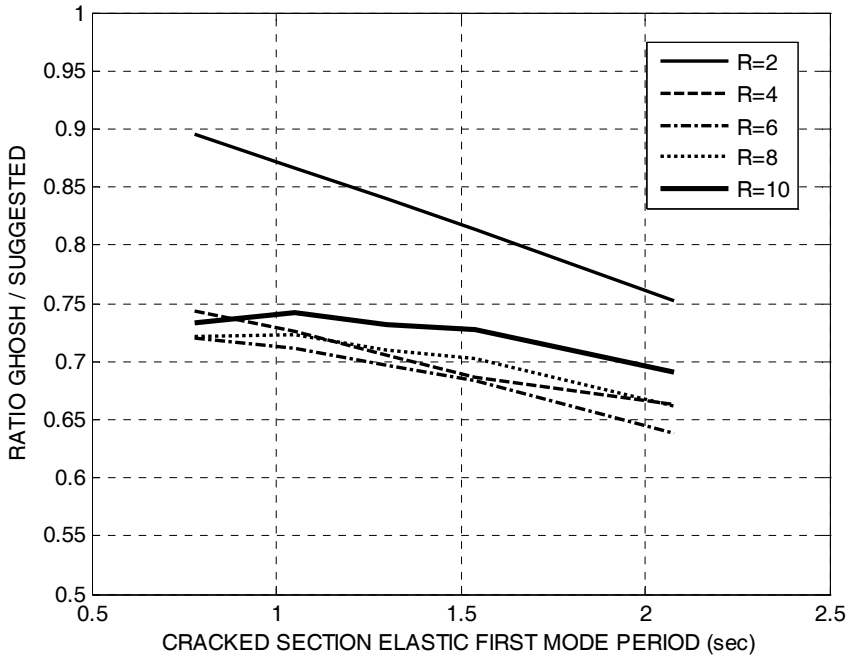

Figure 6.3. Ratio of the base shear amplification factors between the relationship suggested by Ghosh and Markevicius (1990) and this study

Figure 6.4 shows the base shear amplification factors by using the relationship proposed by Eibl and Keintzel (1988). Similarly base shear amplification factors computed with Eibl and Keintzel relationship is divided by the amplification factors obtained from the proposed relationship as shown in Figure 6.5 for comparison.

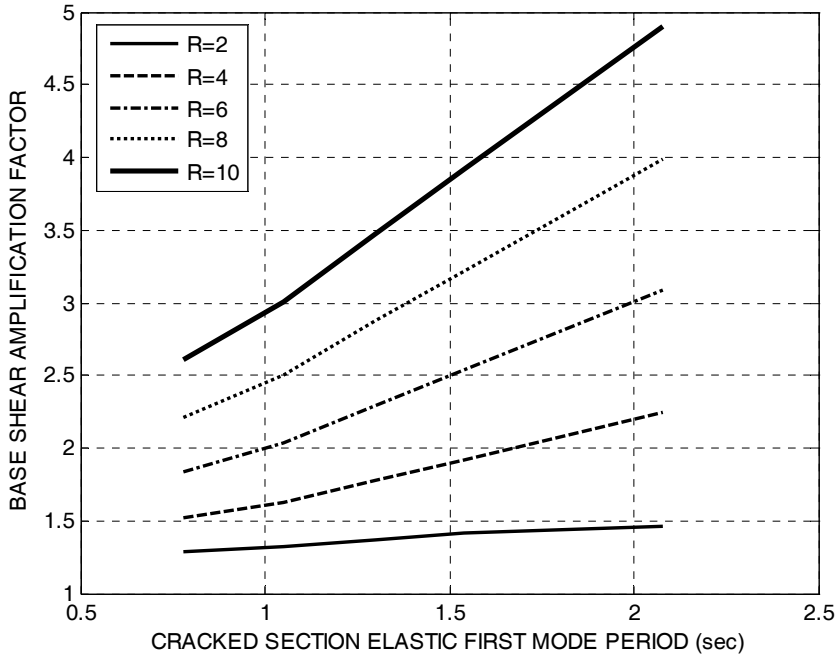

Figure 6.4. Base shear amplification factors computed by using Eibl and Keintzel (1988) relationship

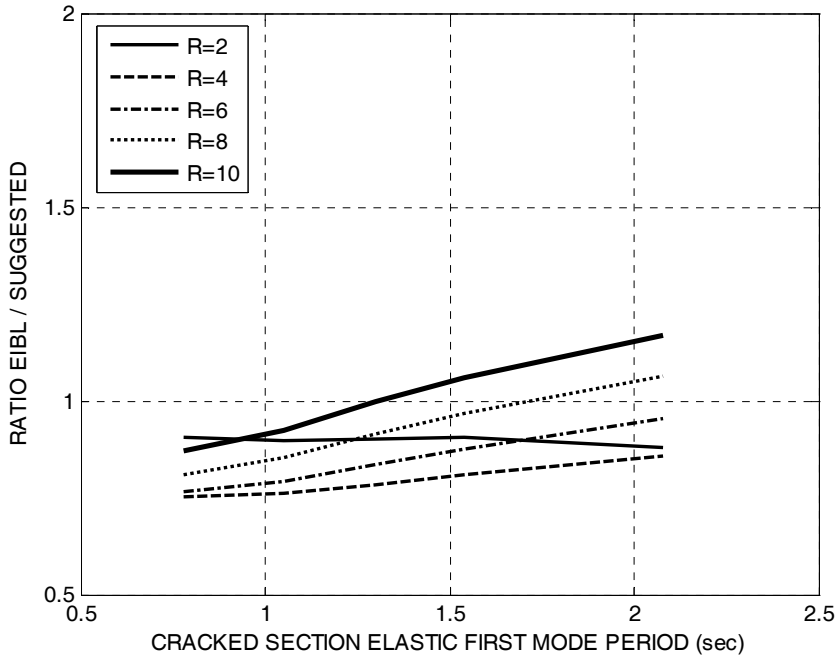

Figure 6.5. Ratio of the base shear amplification factors between the relationship suggested by Eibl and Keintzel (1988) and this study

Figure 6.5 indicates the lower amplification factors computed by Eibl and Keintzel relationship where parallel-like trends of the ratios with respect to strength reduction factors also suggests the idea that amplification factors have been affected by the different intensities of ground motion taken into account between the two studies.

Base shear amplification factors by using the relationship proposed by Rutenberg and Nsieri (2006) is illustrated in Figure 6.6, whereas the ratio between the base shear amplification factors computed with Rutenberg and Nsieri relationship and the proposed relationship is shown in Figure 6.7 for comparison.

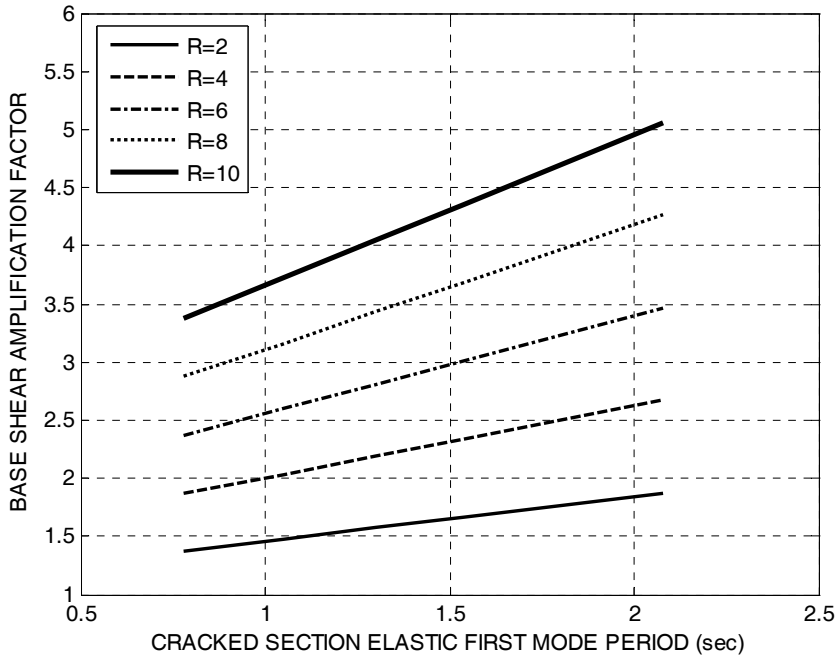

Figure 6.6. Base shear amplification factors computed by using Rutenberg and Nsieri (2006) relationship

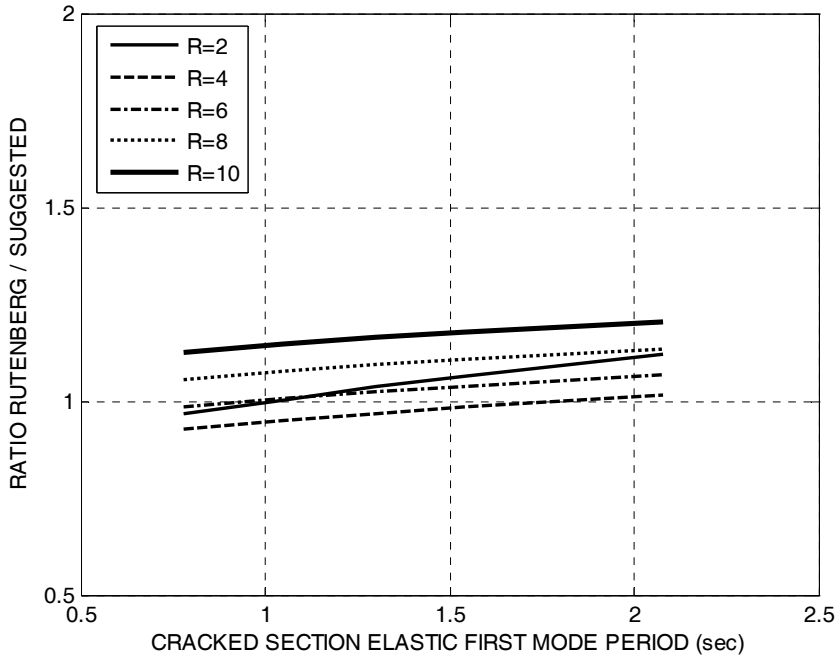

Figure 6.7. Ratio of the base shear amplification factors between the relationship suggested by Rutenberg and Nsieri (2006) and this study

Figure 6.7 depicts slightly higher amplification factors computed by Rutenberg and Nsieri in which the ratio trends are almost in a linear fashion with increasing strength reduction factor and period. This result is believed to be related to the higher intensity SAC ground motion suite (Somerville *et al.* 1997) used by Rutenberg and Nsieri in their studies.

It should be emphasized that despite the lack of consensus between the researchers on the magnitude of base shear amplification factors, the above-given results address the fact that base shear amplification factors increase with increasing strength reduction factor and increasing first mode period of structural walls. It is believed that suggested base shear amplification relationship in this study is suitable for the design of structural walls against shear failures according to Turkish Seismic Design Code (2007).

6.2. Proposed Story Shear Force Profile Along the Wall Height

Mean shear force distribution patterns derived from the non-linear time history analyses reveal that amplified shear force magnitudes drop gradually to half value at about 40 per cent of the total wall height and follow a practically uniform path up to the tip of the wall excluding the top one or two stories as shown in Figure 6.8. It is interesting to note that, normalized story shear force profiles shown in Figure 6.8 encompass all generic walls designed with the strength reduction factors considered in this study (R=2, 4, 6, 8 and 10), which indicates that amplified story shear force pattern is neither a function of first mode period nor the strength reduction factor.

It is believed that a constant shear force zone just above the base of the wall, equal to the critical wall height as per Turkish Seismic Design Code (2007) will be rational considering the tension shift effects (Paulay and Priestley, 1992) in the plastic hinge zone. Above this zone, it is suggested that the story shear forces shall linearly descend to half magnitude at the 40 per cent of the total wall height and remain constant along the rest of the wall as shown in Figure 6.9. In cases where 40 per cent of the wall height do not coincide with a story level, upper end of the linearly descending zone point may be rounded up to the nearest upper story level.

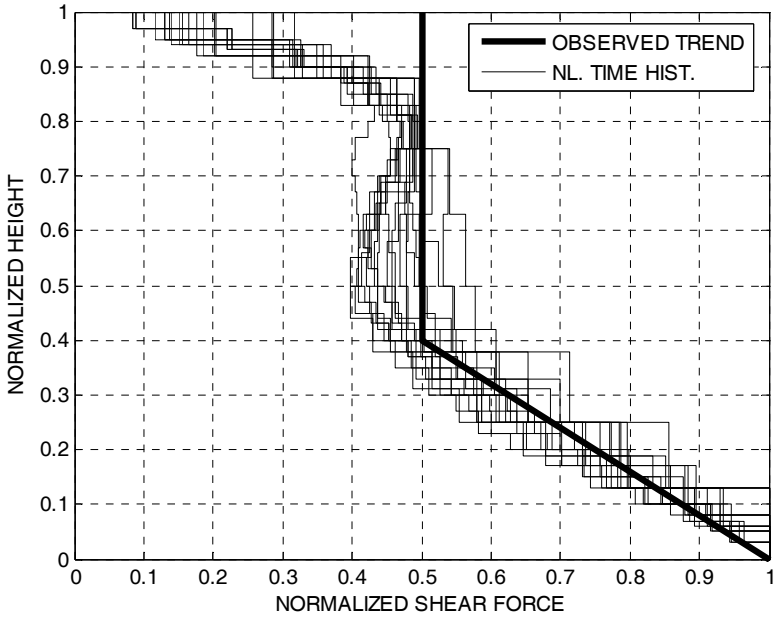

Figure 6.8. Observed trend of the shear force profile obtained from non-linear time history analyses of generic walls

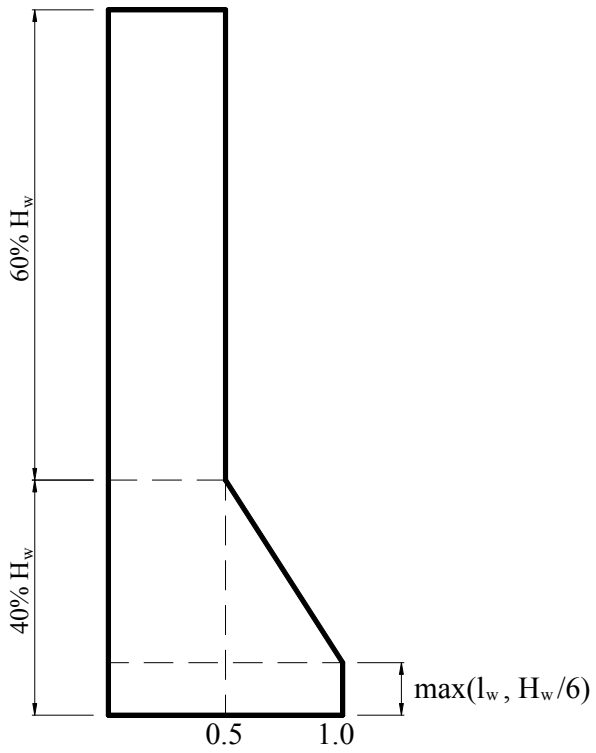

Figure 6.9. Proposed story shear force profile

Shear force profile proposed in this study is similar to that given in Eurocode 8 EN 1998-1 (CEN, 2004) in most aspects, as shown in Figure 6.10. Major notable differences

between the two profiles are the level where the shear forces drop approximately to 50 per cent of the base shear is defined as 1/3 (33 per cent) of the wall height and no constant shear in the tension shift zone at the base of the wall is taken into account.

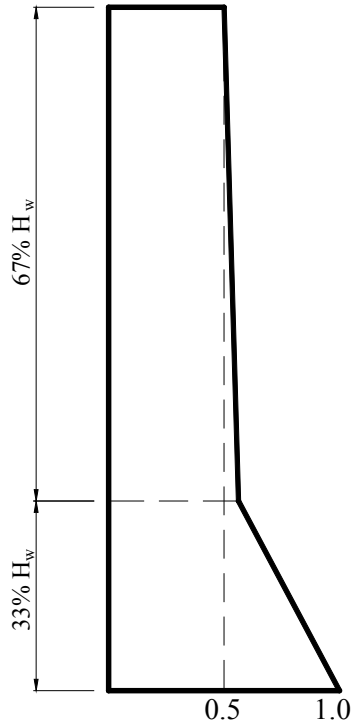

Figure 6.10. Eurocode 8.1 (CEN, 2004) story shear force profile

Rutenberg and Nsieri (2006) also recommended a similar story shear force profile based on the non-linear time history results as illustrated in Figure 6.11. The plastic hinge zone above the base has been recommended as 10 per cent of the total height by Rutenberg and Nsieri (2006) and the level where the shear forces drop 50 per cent of the base shear has been related with first mode period of the wall with the expression given in Equation (6.4)

$$\xi = 1.0 - 0.3T_1 \geq 0.50 \tag{6.4}$$

It is believed that shear force profile proposed by Rutenberg and Nsieri over punishes the structures in the medium period range, since ξ corresponds to values in the order of 70 per cent and 85 per cent of the total wall height for a structural wall with 1.0 sec and 0.50 sec period, respectively.

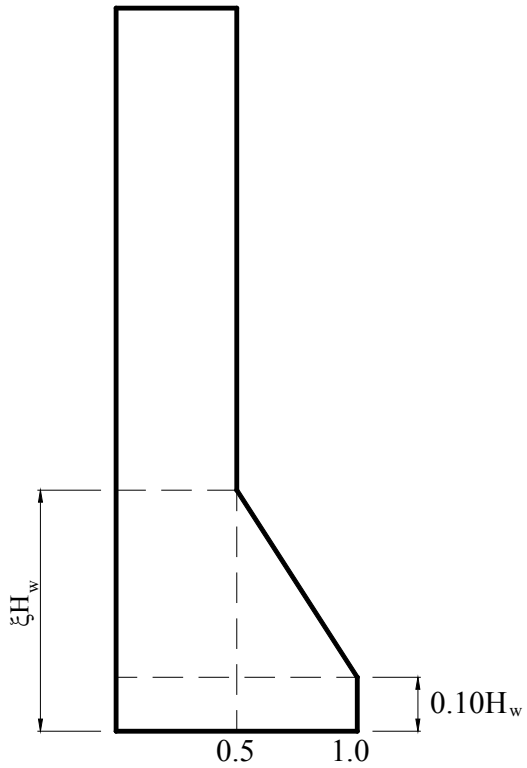

Figure 6.11. Shear force profile proposed by Rutenberg and Nsieri (2006)

6.3. Implications on Shear Design of Structural Walls

As expressed in Chapter 2, base shear amplification factors are very practical to implement in design, however they have the drawback of being related to the intensity of ground motion records they are derived from. Correspondingly, the base shear amplification relationship proposed in this study is based on the base shear amplification factors derived from ground motion records that have been scaled to fit acceleration response spectrum intensity associated with the Seismic Zone 1 of Turkey, with 10 per cent probability of exceedence in 50 years. It should be noted that the ground motion records selected in this study are recorded in the mid-range distances from the faulting plane and the designer should use the proposed relationship with caution when designing the wall systems for near field earthquakes. The proposed relationship is free of the earthquake intensity; nevertheless, it has the characteristics of the design intensity. It should be noted that for ground motion intensities higher or lower than the ground motion intensity corresponding to 10 per cent in 50 years not only the amplitudes of the ground motion may change but also the frequency content varies. Thus, it is recommended at least

few non-linear time history analyses should be performed to support the proposed relationship if the structure is complex in geometry and/or configuration or the importance level of the structure is high. It should also be noted that the proposed relationship has been derived from non-linear time history analyses of generic structural walls covering a limited period range. Thus, it is recommended that the proposed relationship should not be used for structural wall systems above 30 stories.

In majority of the cases of design practice, even flexural strength of the wall computed with minimum reinforcement ratios can well exceed the flexural strength required by analysis. This provided flexural overstrength effectively reduce the strength reduction factor used in design since the plastic hinge at the base of the wall will tend to yield at a higher moment demand than required by analysis. Thus, Equation (6.2) can be modified to take into account the aforementioned flexural overstrength as shown in Equation (6.5)

$$\beta^{b} = 1.0 + (0.281 \times T_{1\text{-cr}} + 0.394) \times (\frac{R}{\Psi^{o}} - 1.5)^{0.553} \tag{6.5}$$

where, Ψ^{o} is the flexural overstrength factor as given Equation (6.6)

$$\Psi^{o} = \frac{M_{r}^{b}}{M_{e}^{b}} \tag{6.6}$$

In Equation (6.6), M_{e}^{b} denotes the moment demand at the base of the wall obtained from code procedures and M_{r}^{b} denotes the provided moment strength of the section at the base of the wall computed with code requirements.

Application procedure of the proposed dynamic base shear amplification relationship and story shear force profile to shear design of structural walls is summarized below;

1. Obtain design base shear (V_{e}^{b}) by using the code procedures such as the equivalent seismic load method or the response spectrum method with the appropriate strength reduction factor (R)

2. Multiply the design base shear (V_e^b) with base shear amplification factor (β^b) computed by using Equation (6.5) to obtain amplified design base shear (V_a^b) as shown in Equation (6.7).

$$V_a^b = V_e^b \times \beta^b (T_{1\text{-cr}}, R) \tag{6.7}$$

3. Multiply the amplified design base shear (V_a^b) with the unitless story shear profile proposed in Section 6.2 to obtain the amplified story shear forces along the wall.

An illustrative example covering the procedure explained above is given in Appendix D.

Even though the proposed dynamic base shear amplification relationship is intended for use in design, it can be employed in the seismic assessment of structural wall systems by using linear and non-linear analysis procedures as well. Strength reduction factor obtained by using single mode pushover analysis procedures can be implemented in Equation (6.5) in order to compute the amplified base shear forces. Implementation of a dynamic base shear amplification factor is not necessary in multi-mode pushover analysis (Aydınoğlu, 2003) since the analysis procedure takes the effects of higher modes into account. For the seismic assessment of structural wall systems by using linear analysis procedures, third term in Equation (6.5) may be modified as shown in Equation (6.8).

$$\beta^b = 1.0 + (0.281 \times T_{1\text{-cr}} + 0.394) \times (R_y - 1.5)^{0.553} \tag{6.8}$$

where, R_y can be computed with:

$$R_y = \frac{M_E^b}{M_n^b} \tag{6.9}$$

In Equation (6.9), M_E^b denotes the elastic moment demand at the base of the wall obtained from code procedures and M_n^b denotes the nominal moment strength of the section at base of the wall associated with characteristic material strengths.

Some degree of sliding shear in the plastic hinge zone of walls is inevitable particularly at high ductility demands. Recent tests of walls performed on E-Defense shaking table in Japan (NIED, 2006) and UC San Diego shaking table in the US (UCSD, 2005), indicate the dominance of sliding shear in the plastic hinge zone on the wall behavior (Krawinkler, 2006). The severity of sliding shear increase with increasing ductility demand and this phenomenon causes strength deterioration as the number of cycles experienced by the plastic hinge. Thus, most of the sliding shear resistance will be provided by the dowel action of the longitudinal reinforcement as a consequence of open cracks and deteriorated concrete strength in the plastic hinge. Hence, it may be rational to define an upper bound for base shear amplifications where the behavior will be primarily governed by sliding at the base of the wall after attaining sliding shear strength.

Based on the recommendations of Paulay and Priestley (1992) for the sliding shear resistance of longitudinal reinforcement in squat walls, sliding shear resistance at the base of a of cantilever wall can be predicted by Equation (6.10);

$$V_{\mathrm{f}}^{\mathrm{b}} = 0.25 A_{\mathrm{sw}} f_{\mathrm{yk}} \tag{6.10}$$

in which, $V_{\mathrm{f}}^{\mathrm{b}}$ is the sliding resistance provided by the longitudinal reinforcement, A_{sw} is the total longitudinal reinforcement area in the web of the section at the base of the wall and f_{yk} is the characteristic yield strength of reinforcement. Thus, upper bound of the base shear amplification factor can be expressed as given in Equation (6.11)

$$\beta_{\mathrm{max}}^{\mathrm{b}} = \frac{0.25 A_{\mathrm{sw}} f_{\mathrm{yk}}}{V_{\mathrm{e}}^{\mathrm{b}}} \tag{6.11}$$

It is believed that the upper bound limitation of base shear amplifications as given in Equation (6.11) will provide rational results for design and prevent unnecessary overdesign in practice.

6.4. Proposed Moment Profile Along the Wall Height

As a side product of this study, a unitless moment profile along the wall height is suggested for the Turkish Seismic Design Code (2007), based on the regression of normalized moments obtained from non-linear time history analyses of the generic walls. It has been observed in this study that moment profile is strongly dependent on the strength reduction factor utilized, due to the increasing spread of plasticity above the base of the wall with increasing strength reduction factor. However, such a dependency was not observed for the first mode period. A tri-linear moment profile is suggested as shown in Figure 6.12.

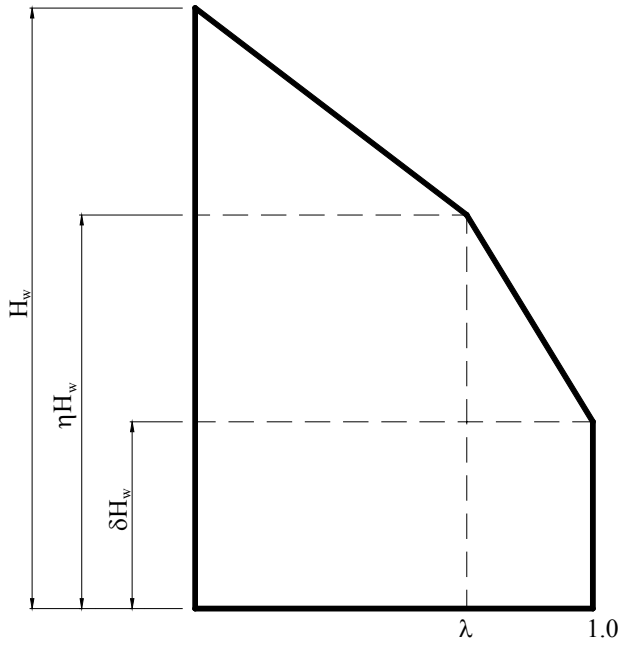

Figure 6.12. Proposed moment profile

Intermediate points on the proposed moment profile are suggested as a function of strength reduction factor as given Equation (6.12), Equation (6.13) and Equation (6.14). It should be noted that minimum value of the strength reduction factor should be taken as 2 in the equations since it has been assumed that strength reduction factors below 2 will correspond to linear response.

$$\lambda = 1.05 - 0.025 \times R \tag{6.12}$$

$$\delta = 0.003 \times (R-2)^2 + 0.025 \times (R-2) \tag{6.13}$$

$$\eta = 0.125 \times (R-2) - 0.005 \times (R-2)^2 \tag{6.14}$$

Coefficients of multiple determination of variables λ, δ and η have been calculated as 0.989, 0.999 and 0.987, respectively.

Agreement of the proposed moment profile with those obtained from non-linear time history analyses are shown in Figure 6.13 to Figure 6.17 with respect to the strength reduction factor utilized.

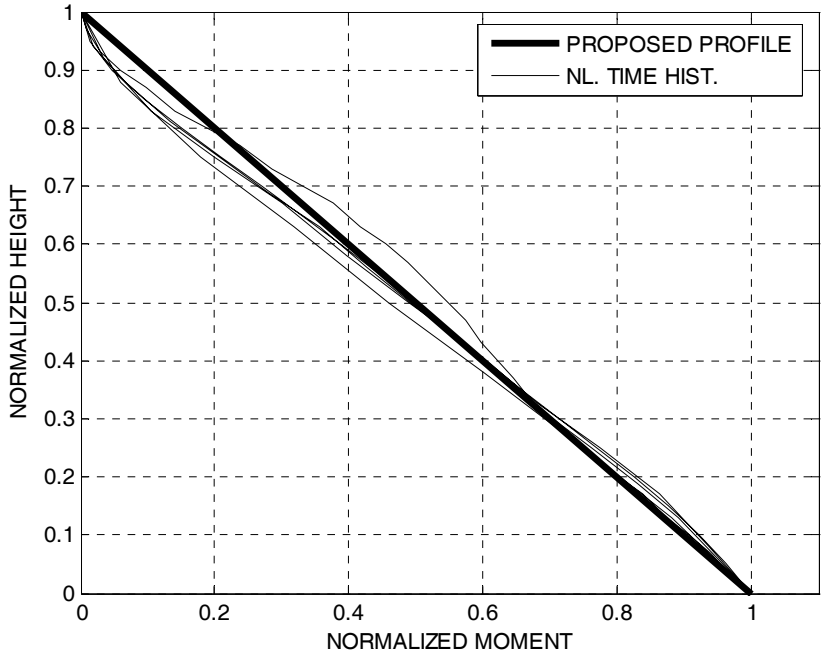

Figure 6.13. Agreement between proposed moment profile and non-linear time history analysis of the generic walls designed with R=2

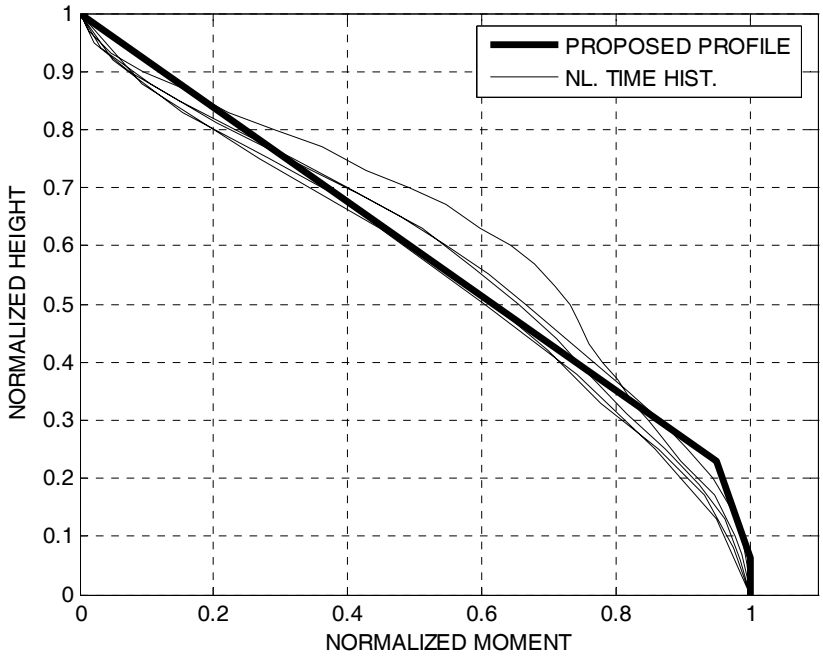

Figure 6.14. Agreement between proposed moment profile and non-linear time history analysis of the generic walls designed with R=4

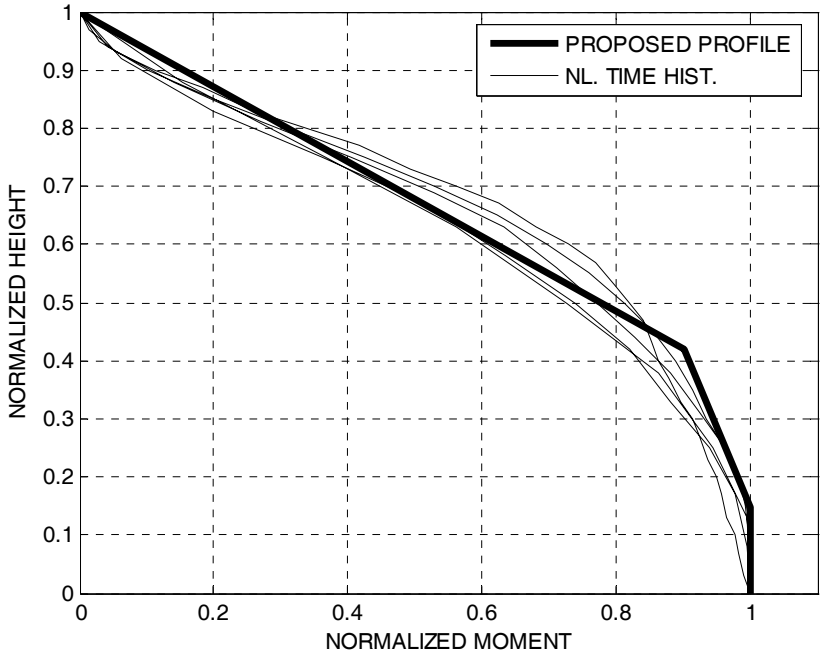

Figure 6.15. Agreement between proposed moment profile and non-linear time history analysis of the generic walls designed with R=6

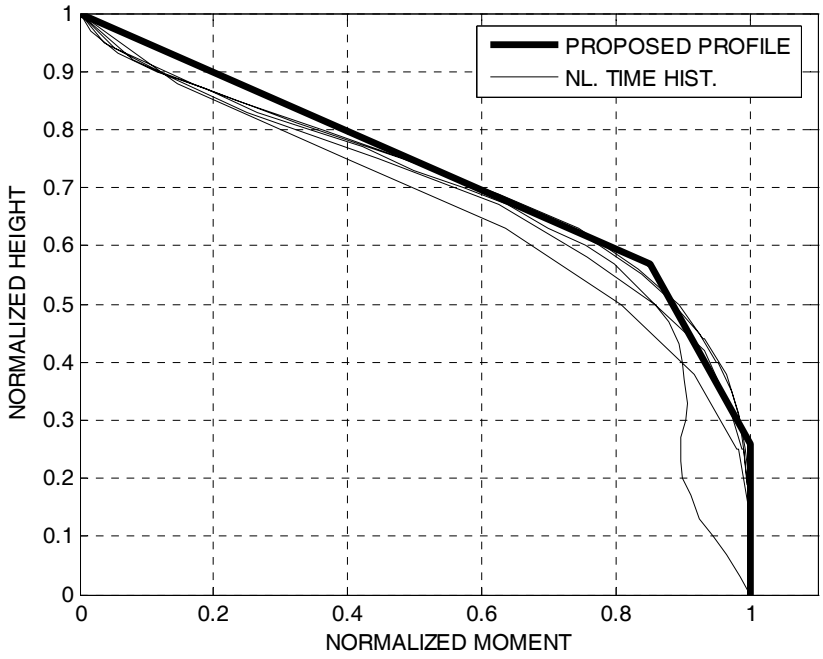

Figure 6.16. Agreement between proposed moment profile and non-linear time history analysis of the generic walls designed with R=8

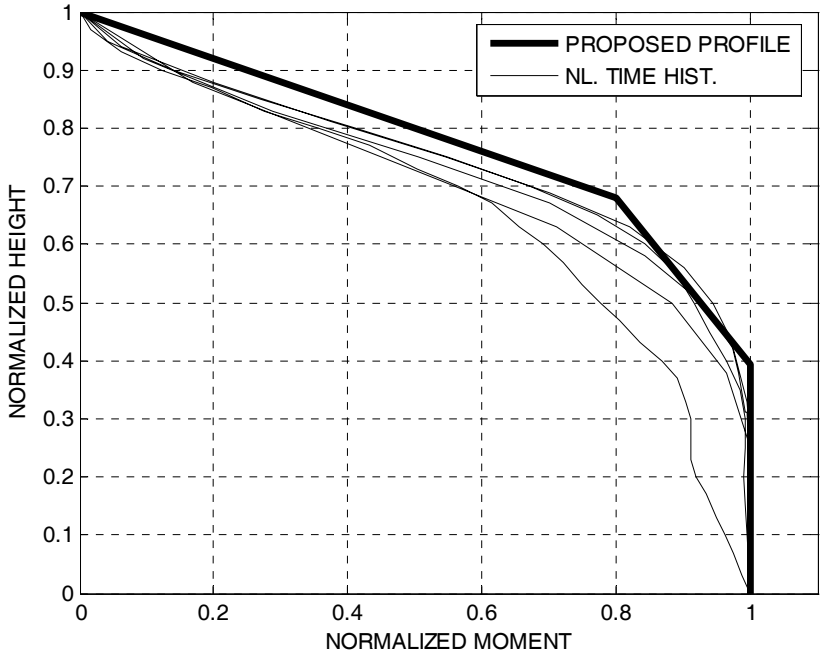

Figure 6.17. Agreement between proposed moment profile and non-linear time history analysis of the generic walls designed with R=10

It should be noted that tension shift effect (Paulay and Priestley 1992) on the proposed moment profile has not been taken into account. Equation (6.13) and Equation (6.14) should be modified as shown below to incorporate the tension shift effect in accordance with the Turkish Seismic Design Code (2007):

$$\delta = 0.003 \times (R-2)^2 + 0.025 \times (R-2) + \max(\frac{l_w}{H_w}, 0.167) \tag{6.15}$$

$$\eta = 0.125 \times (R-2) - 0.005 \times (R-2)^2 + \max(\frac{l_w}{H_w}, 0.167) \tag{6.16}$$

7. CONCLUSIONS

Dynamic shear amplification phenomenon in structural walls has been studied by limited number of researchers in the last 30 years and most of these research findings have formed the basis of code provisions in seismic prone countries. Previous research revealed that, shear forces in yielding walls are not proportional to the design moments and shear force demands are higher than predicted by the code procedures due to higher mode effects after plastic hinge formation at the base of the wall.

Amplified shear forces, particularly at the base of the wall, are probable to cause unexpected premature brittle shear failure modes of diagonal tension, diagonal compression and sliding before the intended plastic hinge development if the magnified shear forces are not taken into account. Practically dynamic shear amplification is taken into account by means of base shear amplification factors applied to the design base shear calculated with the code procedures. These amplification factors are presented principally as a function of first mode period and/or strength reduction factors. 2007 version of the Turkish Seismic Design Code considers the base shear amplification phenomena with a constant base shear amplification factor of 1.5 regardless of the first mode period and ductility level of the wall. It is believed that this must be revised with base shear amplification factors as functions of strength reduction factor and first mode period of the wall. It is also believed that a shear force profile along the height of the wall is also necessary in the Turkish Seismic Design Code (2007) not only for preventing shear failures at the base but also along the height of the structural wall.

Extensive parametric non-linear time history analyses have been performed for code designed generic structural walls, in order to suggest a base shear amplification relationship and a shear force profile for the Turkish Seismic Design Code (2007). Distribution and hysteretic characteristics of the plastic hinges have been considered in the analyses models of the parametric study, in order to investigate the effect of modeling assumptions to dynamic shear amplifications. It has been observed that dynamic shear amplifications are not dependent on the hysteretic characteristics of the plastic hinge. However, models with single plastic hinge at the base of the wall resulted in comparatively

higher story shear force amplification factors and incorrect moment patterns with respect to distributed plastic hinge models. Results of the non-linear time history analysis revealed that dynamic base shear amplification factors increase with increasing first mode period as well as with strength reduction factor. A base shear amplification relationship as functions of first mode period and strength reduction factor has been proposed based on a regression analysis of the non-linear time history analysis results. It was suggested that dynamic base shear amplifications at the base of the wall should be limited with the amplifications corresponding to the sliding shear strength during load reversals for a better characterization of the wall behavior under seismic attack. Moreover, a practical story shear force profile has been suggested, based on the non-linear time history analysis results, to be used in tandem with the Turkish Seismic Design Code (2007). It has been observed that story shear force profile is neither a function of first mode period nor the strength reduction factor. A moment profile has also been proposed for use in the Turkish Seismic Design Code (2007) as a side product of the parametric non-linear time history analyses performed in this study. Moment profiles obtained from non-linear time history analyses indicated a strong dependency on the strength reduction factor utilized but not the first mode period of the wall. A novel modal decomposition technique is presented in this study for demonstrating the individual effects of the higher modes on the dynamic shear amplification phenomenon. The technique is based on inverse extraction of modal responses from non-linear time history analyses results by using the mode superposition method. It was shown that non-linear second mode is chiefly responsible for the dynamic base shear amplifications and the effect of higher modes above the second mode has been found to be negligible. It is believed that the modal decomposition technique presented in this study demonstrates the individual contribution of higher mode effects to dynamic amplification where related studies on this subject are very limited in the literature.

Majority of the findings on dynamic shear amplification phenomenon are based on analytical studies and limited experimental research performed by Kabeyasawa (1987) and Eberhard and Sozen (1993) confirms this reality. However, recent full scale tests of walls performed on E-Defense shaking table in Japan (NIED, 2006) and UC San Diego shaking table in the US (UCSD, 2005), indicate the dominance of the sliding shear in the plastic hinge zone on the wall behavior (Krawinkler, 2006), which might be reducing the rate of amplifications as a shear fuse. It is believed that more information will be available on the

real dynamic behavior of yielding structural walls as more full-scale tests and supporting numerical research simulating the complex reinforced concrete behavior are carried out.

APPENDIX A: DESIGN MOMENTS AND STORY SHEAR FORCES OF THE GENERIC WALLS

Design Moments and Story Shear Forces of the 8 Story Wall

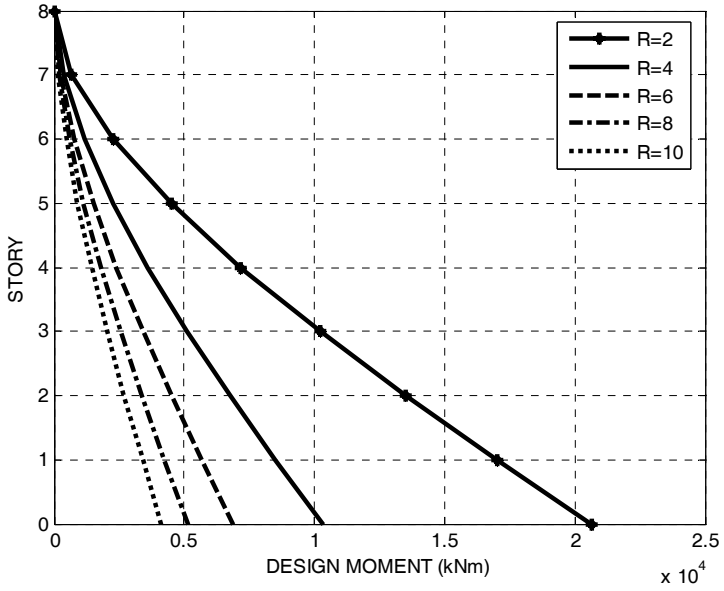

Figure A.1. Design moment profile of the 8 story wall

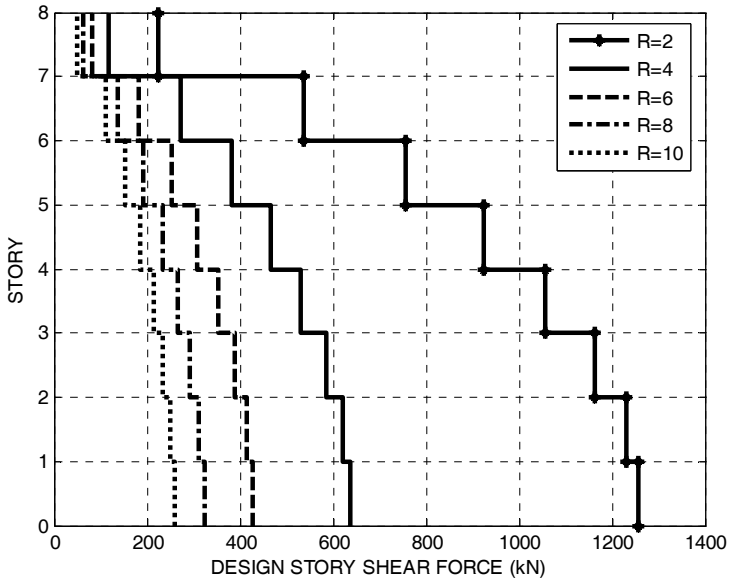

Figure A.2. Design shear force profile of the 8 story wall

Design Moments and Story Shear Forces of the 12 Story Wall

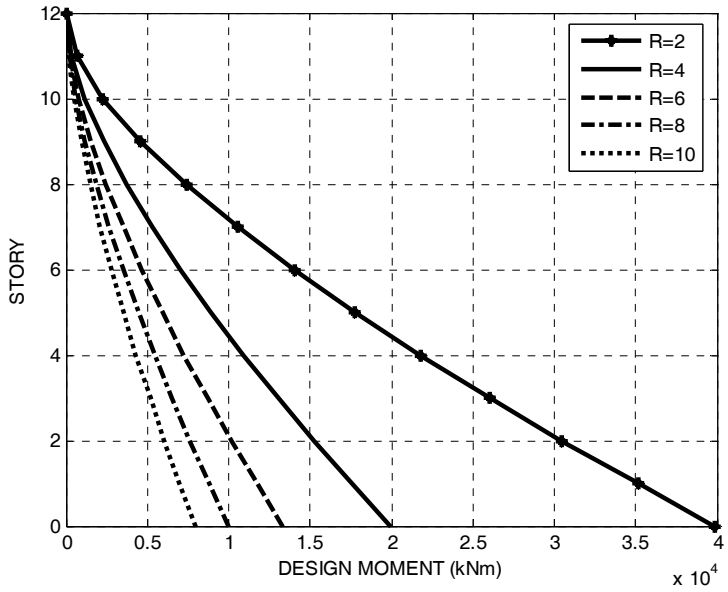

Figure A.3. Design moment profile of the 12 story wall

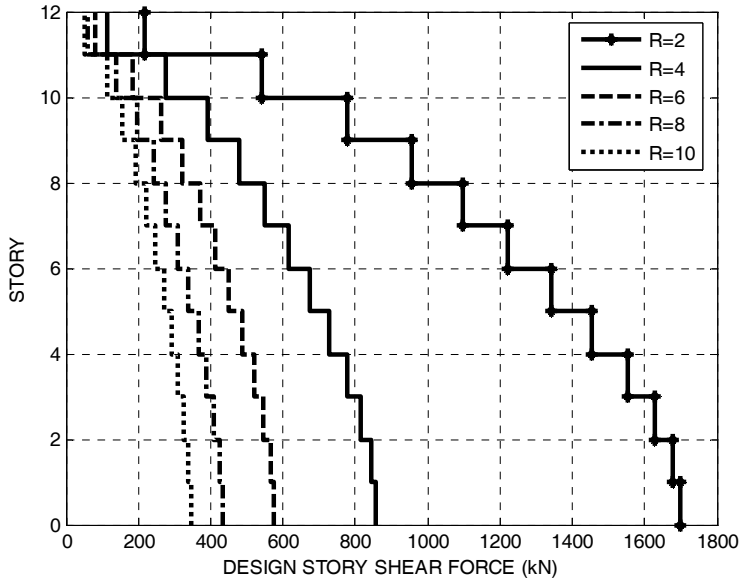

Figure A.4. Design shear force profile of the 12 story wall

Design Moments and Story Shear Forces of the 16 Story Wall

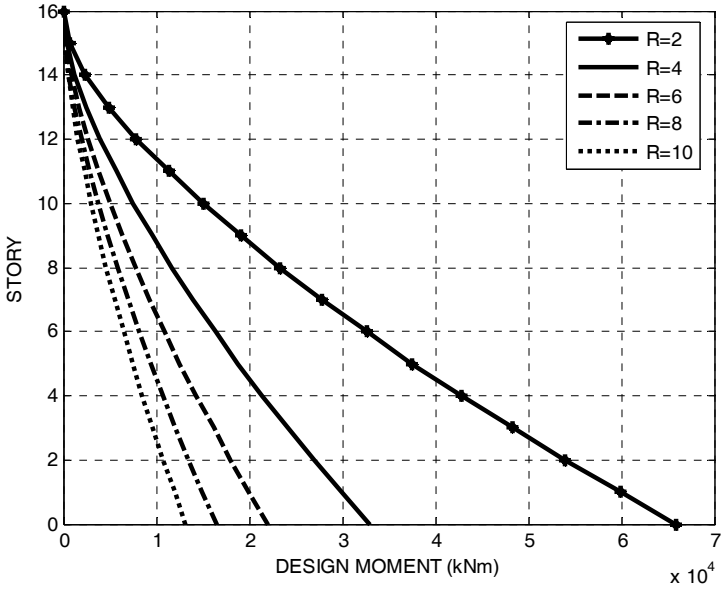

Figure A.5. Design moment profile of the 16 story wall

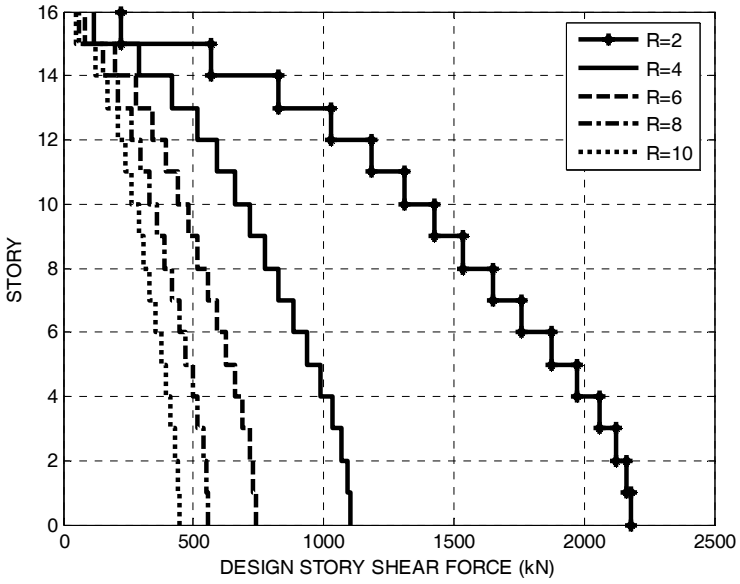

Figure A.6. Design shear force profile of the 16 story wall

Design Moments and Story Shear Forces of the 20 Story Wall

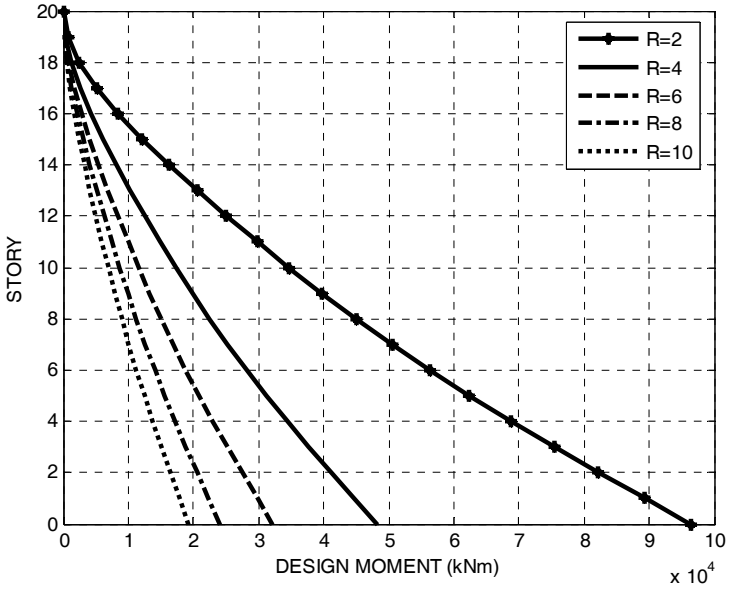

Figure A.7. Design moment profile of the 20 story wall

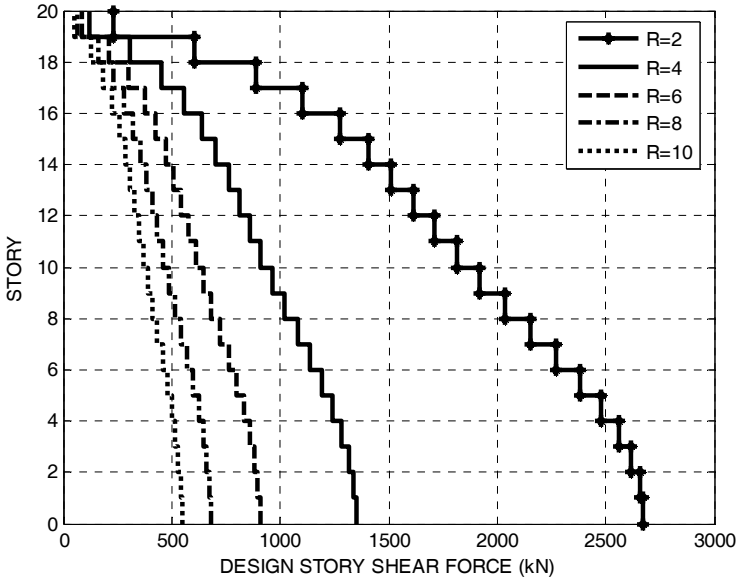

Figure A.8. Design shear force profile of the 20 story wall

Design Moments and Story Shear Forces of the 30 Story Wall

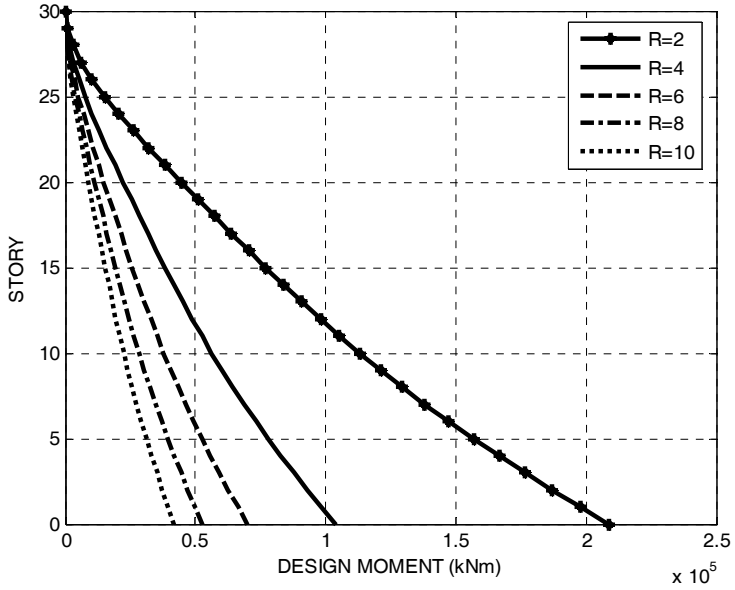

Figure A.9. Design moment profile of the 8 story wall

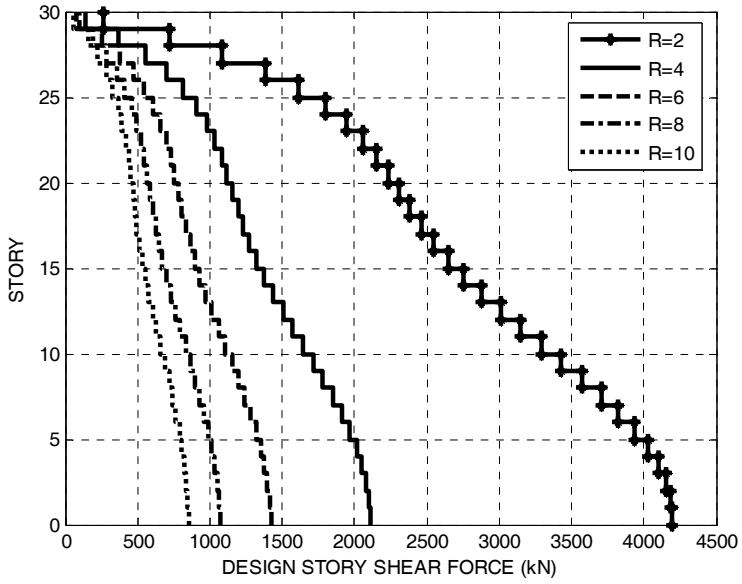

Figure A.10. Design shear force profile of the 30 story wall

APPENDIX B: LINEAR AND NON-LINEAR MODE SHAPES OF GENERIC WALL BUILDINGS

Linear and Non-Linear Modes Shapes for 8 Story Wall Building

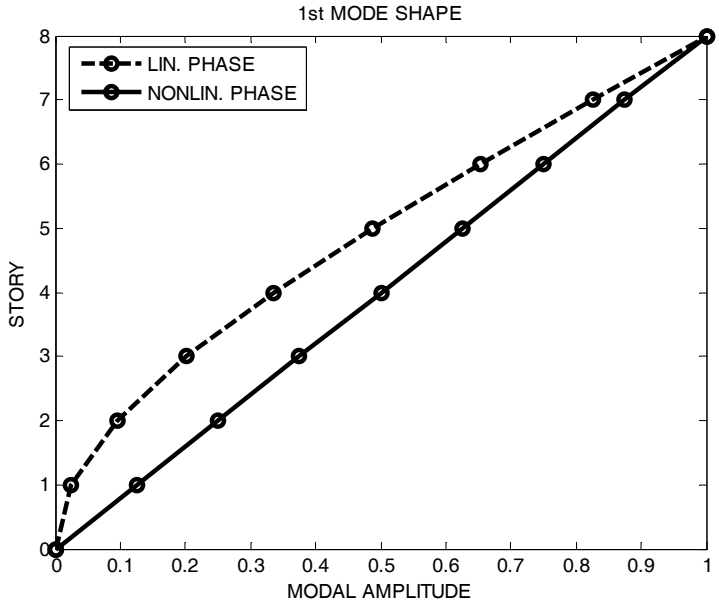

Figure B.1. Linear and non-linear 1st mode shapes of the 8 story wall building

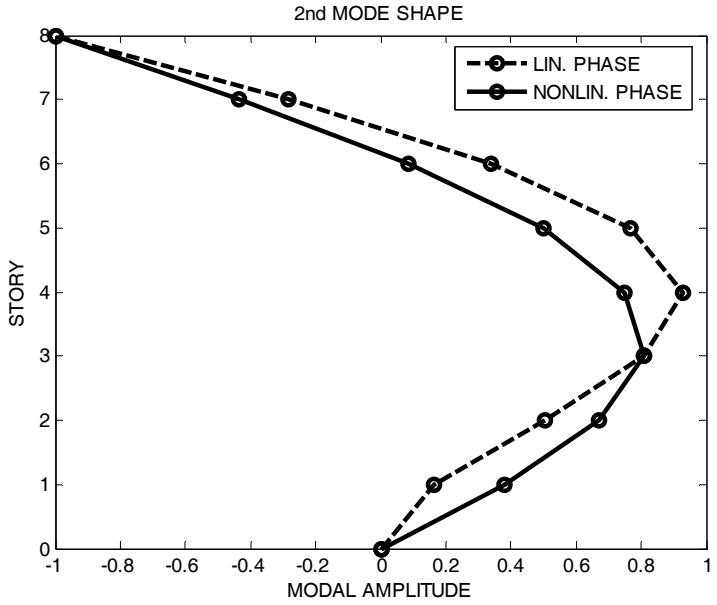

Figure B.2. Linear and non-linear 2nd mode shapes of the 8 story wall building

Linear and Non-Linear Modes Shapes for 12 Story Wall Building

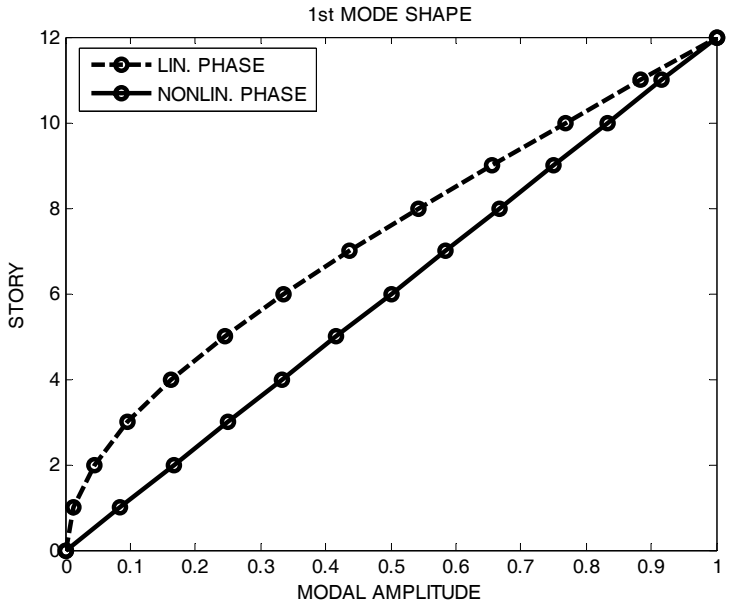

Figure B.3. Linear and non-linear 1st mode shapes of the 12 story wall building

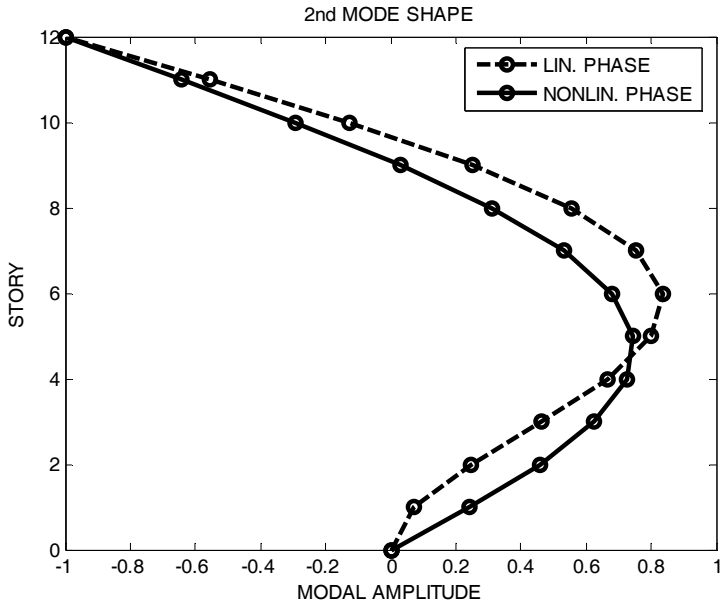

Figure B.4. Linear and non-linear 2nd mode shapes of the 12 story wall building

Linear and Non-Linear Modes Shapes for 16 Story Wall Building

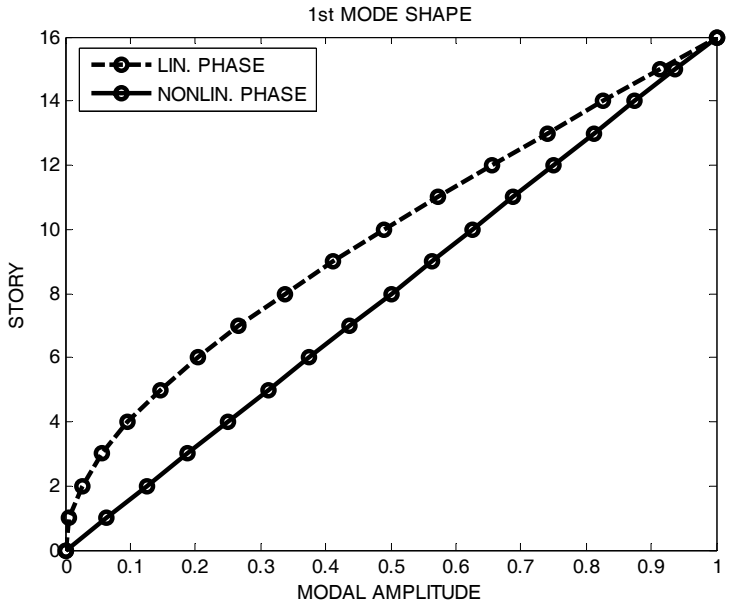

Figure B.5. Linear and non-linear 1st mode shapes of the 16 story wall building

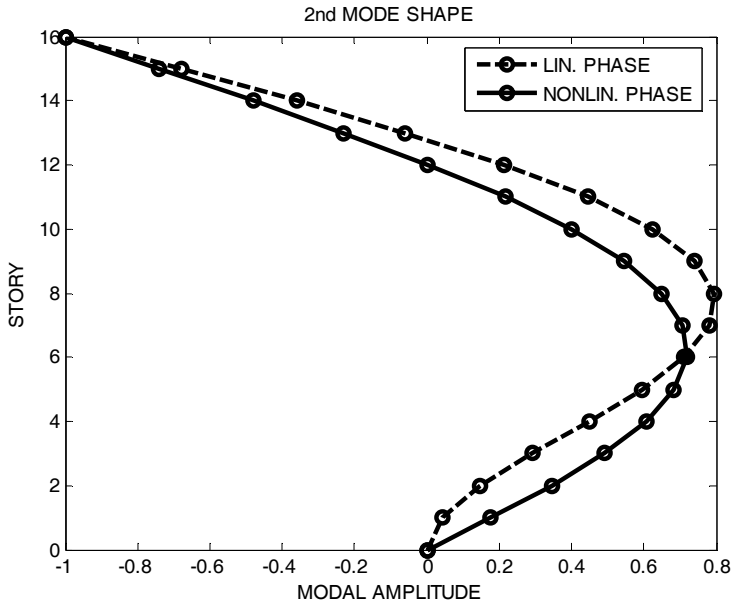

Figure B.6. Linear and non-linear 2nd mode shapes of the 16 story wall building

Linear and Non-Linear Modes Shapes for 20 Story Wall Building

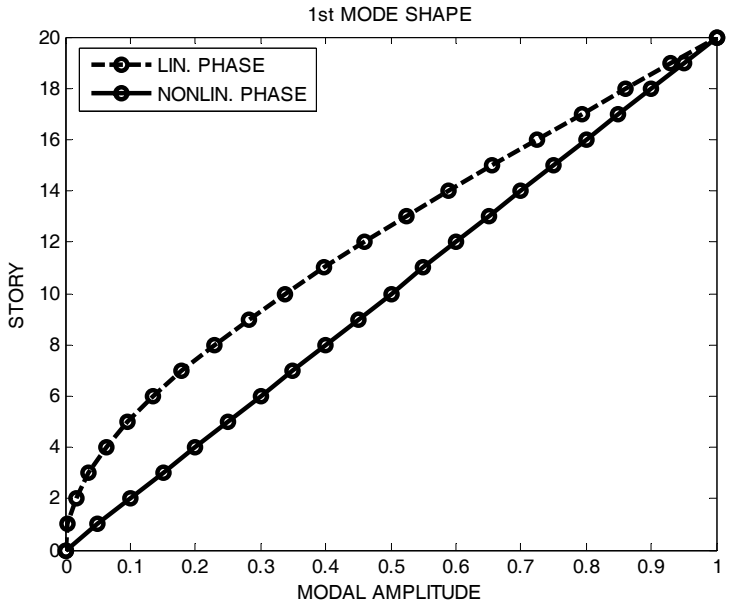

Figure B.7. Linear and non-linear 1st mode shapes of the 20 story wall building

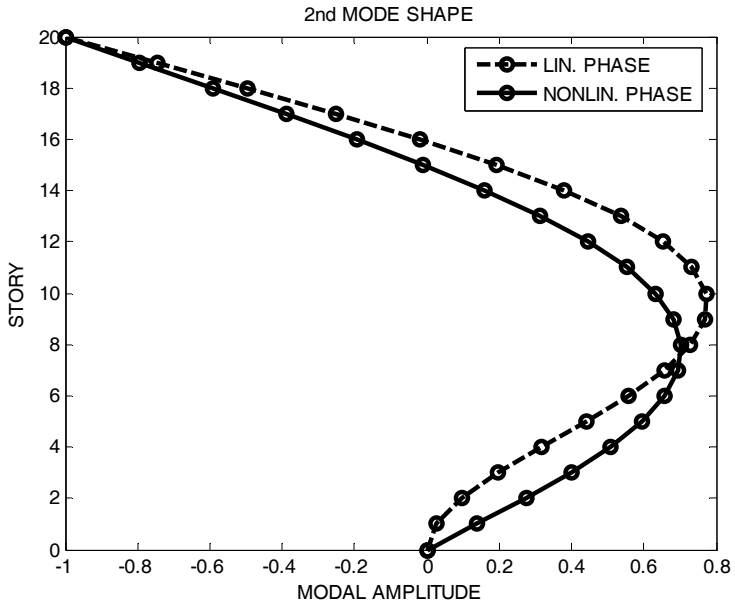

Figure B.8. Linear and non-linear 2nd mode shapes of the 20 story wall building

Linear and Non-Linear Modes Shapes for 30 Story Wall Building

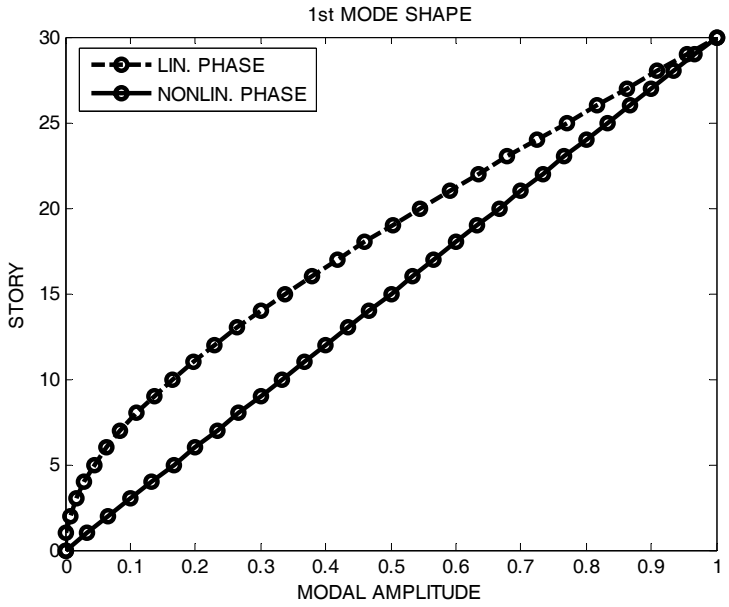

Figure B.9. Linear and non-linear 1st mode shapes of the 30 story wall building

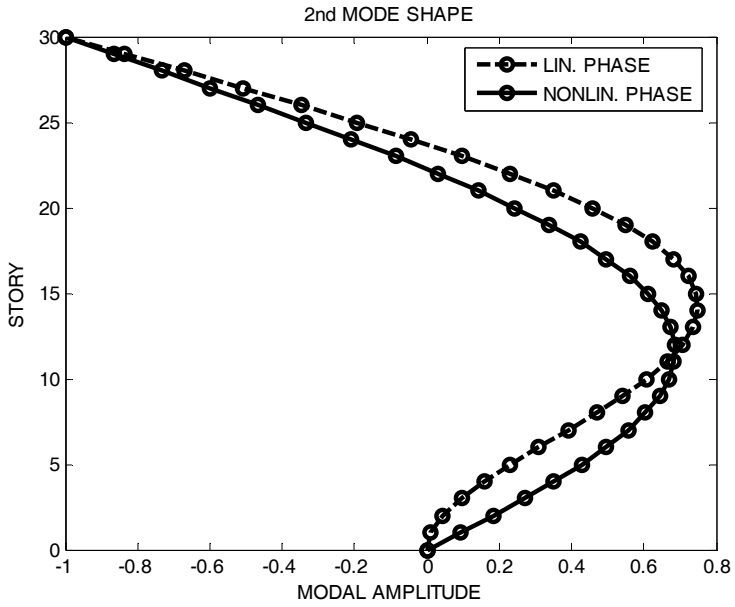

Figure B.10. Linear and non-linear 2nd mode shapes of the 30 story wall building

APPENDIX C: GROUND MOTION RECORDS FOR TIME HISTORY ANALYSES

Non-linear time history analysis is considered as the most advanced and most complicated analysis method with respect to the simplified analysis methods used in engineering practice. Simplified analysis methods have the advantage of specified ground motion characteristics mostly in the form of response spectra either in the codified or site specific forms. This eliminates the effort required by the designer to deal with the variations arising from the ground motion side of the problem and modeling assumptions and representations becomes the major concerns to deal with. However, reliable results expected from a time history analysis are also dependent on appropriately selected strong ground motion records since the ground motion characteristics will also affect the response.

Two major issues are confronted with the strong ground motion records to be incorporated in the non-linear time history analyses. First issue particularly comprises the composition of a record suite with sufficient number of ground motions records having comparable characteristics. It is evident that ground motion characteristics are primarily affected by distance to fault, magnitude of the earthquake and local site conditions. Thus, selected ground motion records should be representative of these three criteria where the structure shall be designed. Theoretically, the more the number of records incorporated in analyses, the more reliable results are obtained and an increase of number of samples allow for working with average analysis results. It is obvious that finding sufficient number of locally recorded accelerograms satisfying the three criteria is not an easy task, thus either accelerograms with similar conditions can be selected or synthetically simulated accelerograms can be developed.

Second issue relates to the standardization of accelerograms; since the frequency content and associated spectral accelerations of an accelerogram vary from record to record naturally which will eventually result in high scatters in terms of analysis results. Standardization is generally achieved by scaling the records to fit their response spectra to a target response spectrum, in most cases a code spectrum.

Selection criteria and standardization procedure of the selected accelerograms are explained in the following sections.

Selection of Strong Ground Motion Records

20 recorded accelerograms corresponding to magnitudes between M6.0 and M7.0, distance to epicenter between 15 km and 50 km and the site class similar to Z3 defined in Turkish Seismic Design Code (2007) have been selected as given in Table C.1

Table C.1. Selected ground motion records in the study

No	Earthquake	Magnitude	Station	Distance (km)	Site Condition	PGA (g)	PGV (cm/s)	PGD (cm)
1	Chalfant Valley	6.2	54428 Zack Brothers Ranch	18.7	D	0.45	36.90	7.01
2	Chalfant Valley	6.2	54429 Zack Brothers Ranch	18.7	D	0.40	44.50	8.56
3	Loma Prieta 1989	6.9	APEEL 2 - Redwood City	47.9	D	0.22	34.30	6.87
4	Loma Prieta 1989	6.9	1686 Fremont - Emerson Court	43.4	B	0.19	12.70	5.50
5	Mammoth Lakes 1980	6.0	54214 Long Valley dam	19.7	A	0.48	14.20	1.77
6	Mammoth Lakes 1980	5.7	54214 Long Valley dam	14.4	A	0.25	18.50	1.56
7	Mammoth Lakes 1980	6.0	54301 Mammoth Lakes H. S.	14.2	D	0.39	23.90	2.72
8	Morgan Hill 1984	6.2	47380 Gilroy Array #2	15.1	C	0.21	12.60	2.10
9	Morgan Hill 1984	6.2	57382 Gilroy Array #4	12.8	C	0.35	17.40	3.11
10	Northridge 1994	6.7	90074 La Habra - Briarcliff	61.6	C	0.21	12.30	1.23
11	Northridge 1994	6.7	24575 Elizabeth Lake	37.2	C	0.16	7.30	2.70
12	Northridge 1994	6.7	24611 LA - Temple &amp	32.3	B	0.18	20.00	2.74
13	Northridge 1994	6.7	90061 Big Tujunga, Angeles Nat F	24.0	B	0.25	12.70	1.12
14	Northridge 1994	6.7	90021 LA - N Westmoreland	29.0	B	0.40	20.90	2.29
15	Whittier Narrows 1987	6.0	Brea Dam (Downstream)	23.3	D	0.31	14.50	0.77
16	Whittier Narrows 1987	6.0	108 Carbon Canyon Dam	26.8	A	0.22	8.70	0.64
17	Whittier Narrows 1987	6.0	90034 LA - Fletcher Dr	14.4	C	0.21	12.60	1.45
18	Whittier Narrows 1987	6.0	90063 Glendale - Las Palmas	19.0	C	0.30	17.10	1.82
19	Whittier Narrows 1987	6.0	90021 LA - N Westmoreland	16.6	B	0.21	9.70	0.98
20	Whittier Narrows 1987	6.0	24461 Alhambra, Fremont Sch	13.2	B	0.33	22.00	2.42

It is intended that selected ground motion records suitably represent the expected ground motion characteristics for Seismic Zone 1 defined in Turkish Seismic Design Code (2007) in terms distance and magnitude. Pseudo-acceleration response spectra of the selected records are given in Figure C.1 with respect to the design response spectrum constructed for respective Site Class Z3 and the Seismic Zone 1.

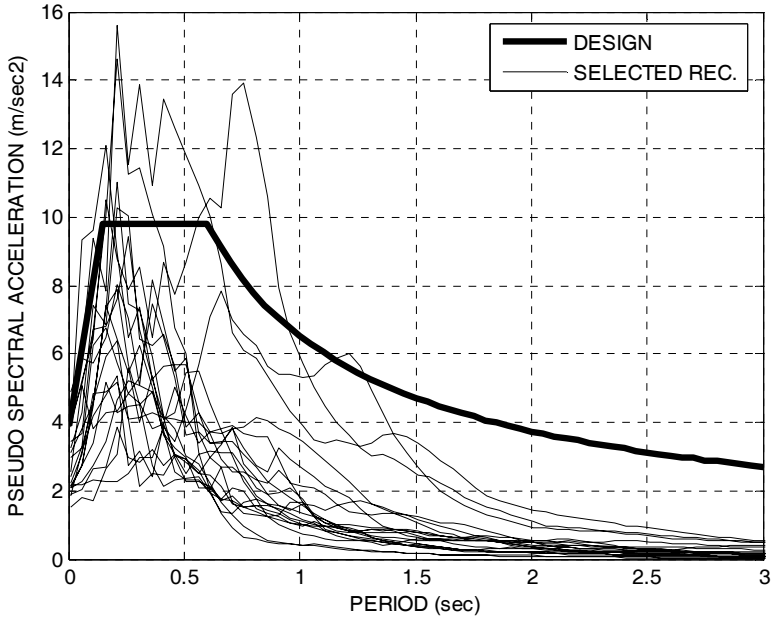

Figure C.1. Pseudo acceleration response spectra of the selected records

Standardization of Selected Ground Motion Records

Standardization of a suite of records is one of the key points for non-linear time history analyses. Standardization is principally based on scaling of real accelerograms to fit a target design ground motion level, which can be defined through design peak ground acceleration, intensity or the response spectrum itself. Although details of this subject are out of the scope of the present study, it should be reminded that any manipulation for the sake of standardization has the risk of losing the natural characteristics of the real records.

Standardization of the selected records in this study has been achieved by scaling the records to fit the target design response spectrum in all period ranges. An iterative procedure has been applied by using a program coded in MATLAB with steps given below:

1. Obtain target pseudo velocity response spectrum, for 5 per cent damping ratio($S_{pv}^{t}(f,\xi=0.05)$)
2. Obtain pseudo-velocity response spectrum of the original record, for 5 per cent damping ratio ($S_{pv}(f,\xi=0.05)$).

3. Divide the velocity response spectrum of the original record by the target pseudo-velocity response spectrum to obtain the scale factors ($\alpha(f)$) corresponding to each frequency.

$$\alpha(f) = \frac{S_{pv}(f, \xi = 0.05)}{S^{t}_{pv}(f, \xi = 0.05)}$$

4. Compute Fourier Transform of the original record. $FFT(a(t))$
5. Multiply the Fourier Transform of the original record with the scale factors obtained in Step 3 in the frequency domain, in order to obtain a Scaled Fourier Transform ($\overline{FFT}(a(t))$).

$$\overline{FFT}(a(t)) = \alpha(f) FFT(a(t))$$

6. Compute Inverse Fourier Transform of the Scaled Fourier Transform obtained in Step 5 to get the Scaled Record.

$$\bar{a}(t) = inv[\overline{FFT}(a(t))]$$

7. Repeat steps between 2 and 6 by replacing the Scaled Record in Step 6 with the original record in step 2 until a satisfactory convergence is achieved between the pseudo acceleration response spectrum of the record and the target pseudo acceleration response spectrum.

In order to illustrate the above scaling procedure, scaling applied to 90021 LA - N Westmoreland accelerogram given in Table B.1 is presented below.

Figure C.2 shows the pseudo-acceleration response spectrum of the original record with respect to target acceleration response spectrum before iteration. Figure C.3, Figure C.4 and Figure C.5 show the spectra at iteration steps 5, 10 and 20, respectively.

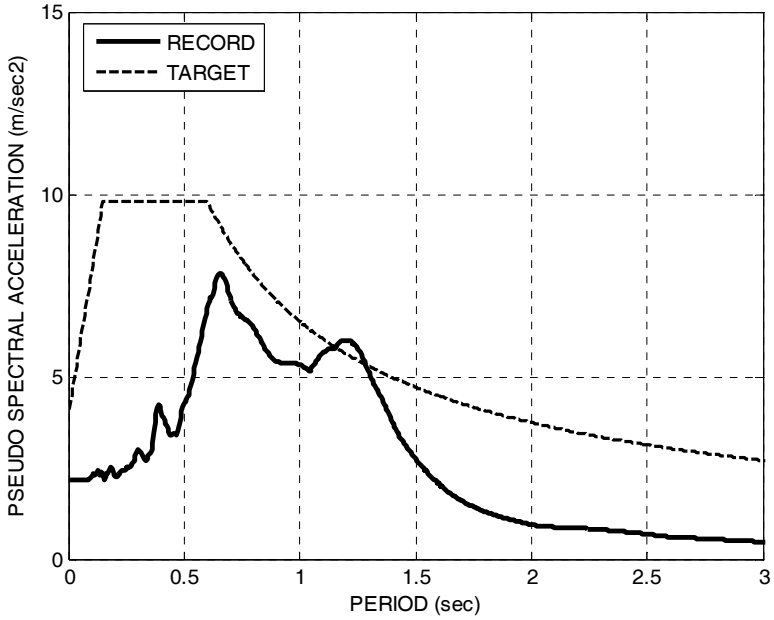

Figure C.2 . Comparison of the record spectrum with target spectrum before iteration

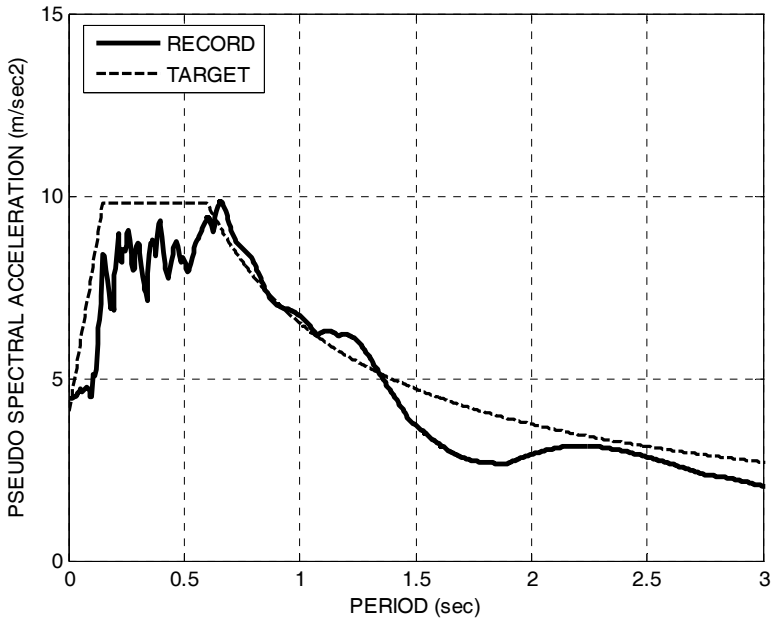

Figure C.3. Comparison of the record spectrum with target spectrum at iteration step 5

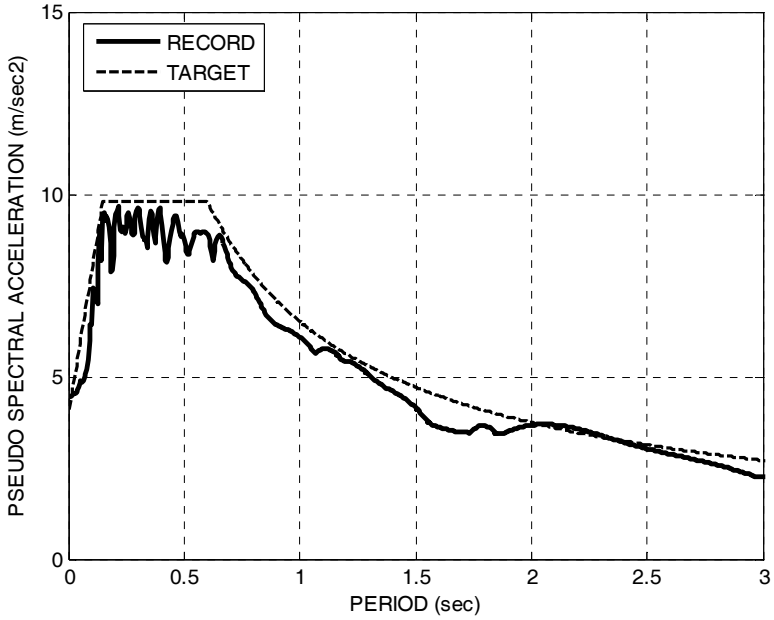

Figure C.4. Comparison of the record spectrum with target spectrum at iteration step 10

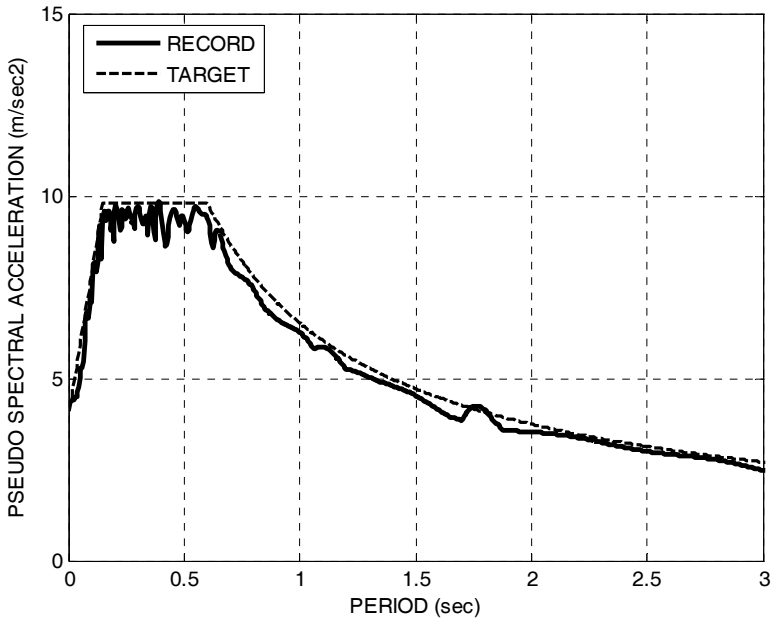

Figure C.5. Comparison of the record spectrum with target spectrum at iteration step 20

Original and scaled accelerogram of the 90021 LA - N Westmoreland station are shown in Figure C.6 for comparison.

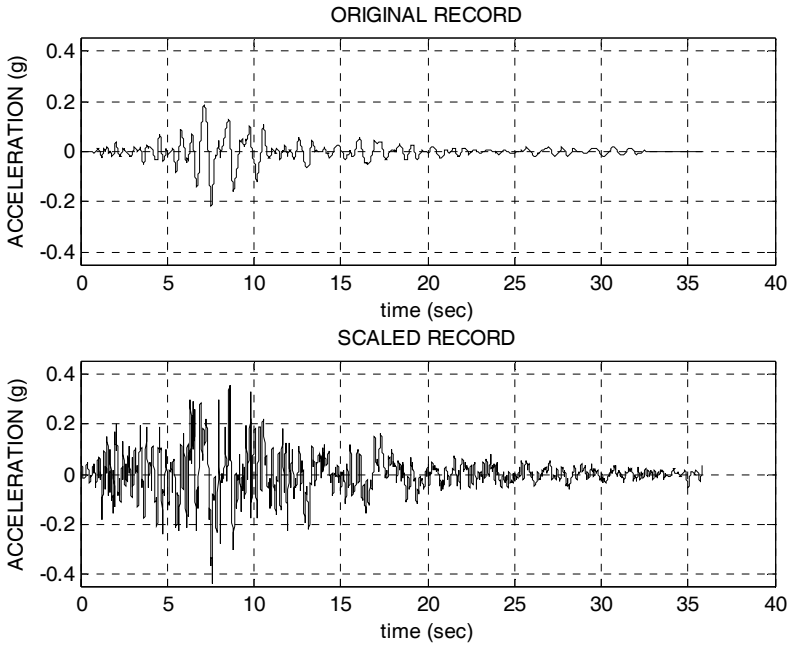

Figure C.6. Comparison of the original and scaled accelerogram of 90021 LA - N Westmoreland station

Pseudo acceleration response spectra of the selected records after scaling are given in Figure C.7 with respect to design acceleration response spectra. Accelerograms scaled by using the methodology above has been used as the ground motion data in the non-linear time history analyses of the generic walls as explained in Chapter 5.

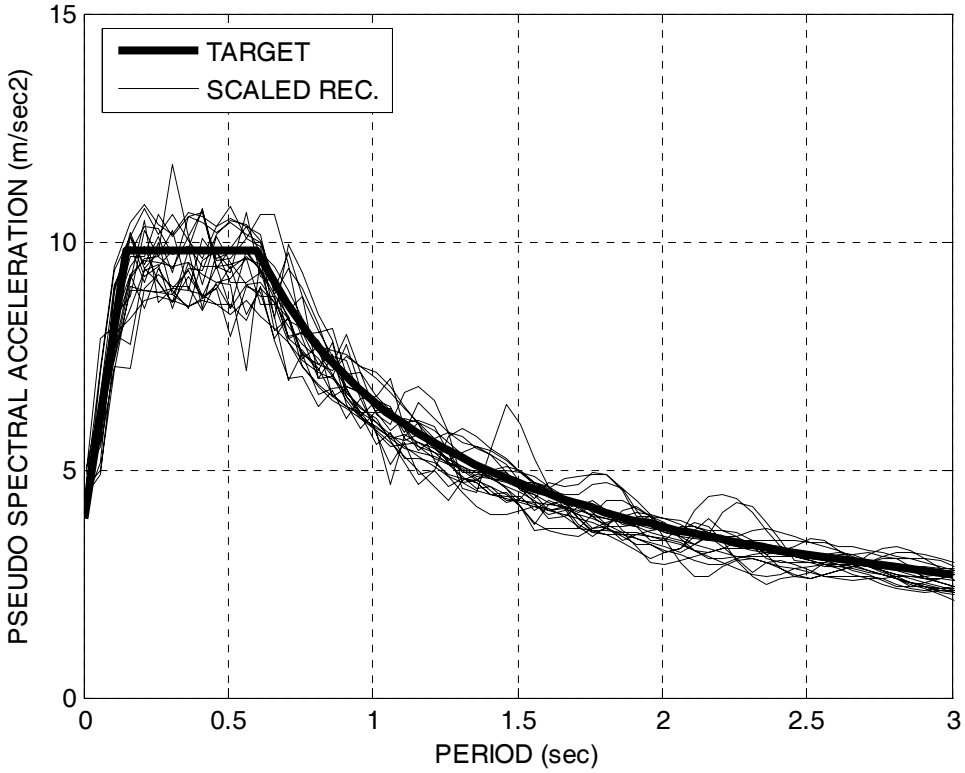

Figure C.7. Comparison of the acceleration response spectrum of the records with the target spectrum after scaling

APPENDIX D: ILLUSTRATIVE WALL DESIGN BY USING THE PROPOSED BASE SHEAR AMPLIFICATION RELATIONSHIP, SHEAR AND MOMENT PROFILE

Shear Design of the 16 Story Generic Wall Designed With a Strength Reduction Factor of R=6

The proposed shear design procedure is presented below for a 16 story generic wall designed with strength reduction factor of R = 6.

Key characteristics of the wall are summarized below;

N= 16 stories

b = 0.30 m (section width in flexure)

l_w = 7.50 m (section depth in flexure)

h = 3.00 m (Typical story height)

H_w = 48.00 m (Total wall height measured from the base)

$T_{1\text{-}cr}$ = 1.30 sec (First mode period of the wall based on cracked section stiffness properties)

Design shear forces have been obtained in Chapter 3 by using the response spectrum method as shown in Figure D.1 below;

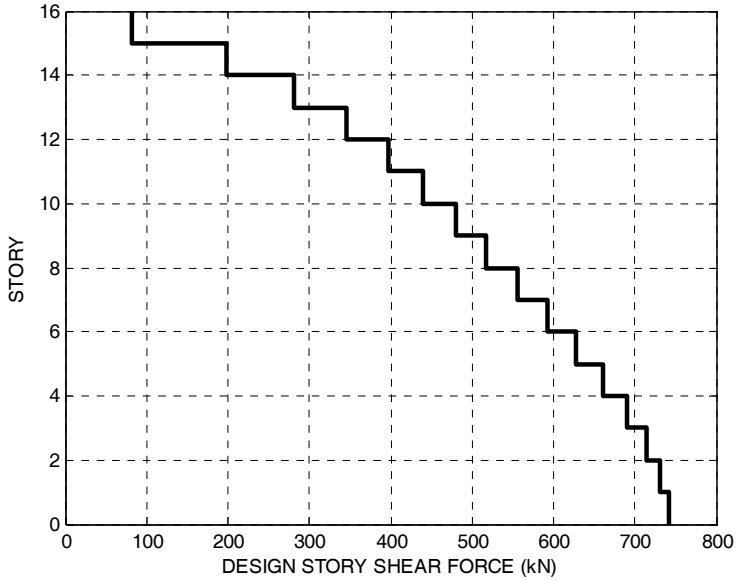

Figure D.1. Design Shear Force Diagram of the 16 Story Wall (R = 6)

Thus the design base shear obtained is;

$$V_e^b = 741 \text{ kN}$$

The base shear amplification factor is calculated by using the proposed relation given in Equation 6.5 by assuming flexural overstrength of 1.0

$$\frac{M_e^b}{M_r^b} = 1.0$$

$$\beta^b = 1.0 + (0.281 \times 1.30 + 0.394) \times (1.0 \times 6 - 1.5)^{0.553}$$

$$\beta^b = 2.744$$

The amplified design base shear is obtained from Equation 6.7 will give;

$$V_a^b = V_e^b \times \beta^b = 741 \times 2.744 = 2033.3 \text{ kN}$$

The story shear force diagram is obtained by using the suggested profile given Section 6.2

- Determine the height of the critical wall height of constant shear right above the base of wall

$$\max(l_{w,} H_w / 6) = 8.0m \rightarrow \text{App. 3 stories above the base}$$

- Determine the level where the story shear forces drop to 50 per cent of the base shear

$$0.40 \times 48.00 = 19.2m \rightarrow \text{App. 7 stories above the base}$$

Amplified story design shear force diagram obtained as above is given in Figure D.2 where it is compared with the quantities obtained from design and Group 3 non-linear time history analyses.

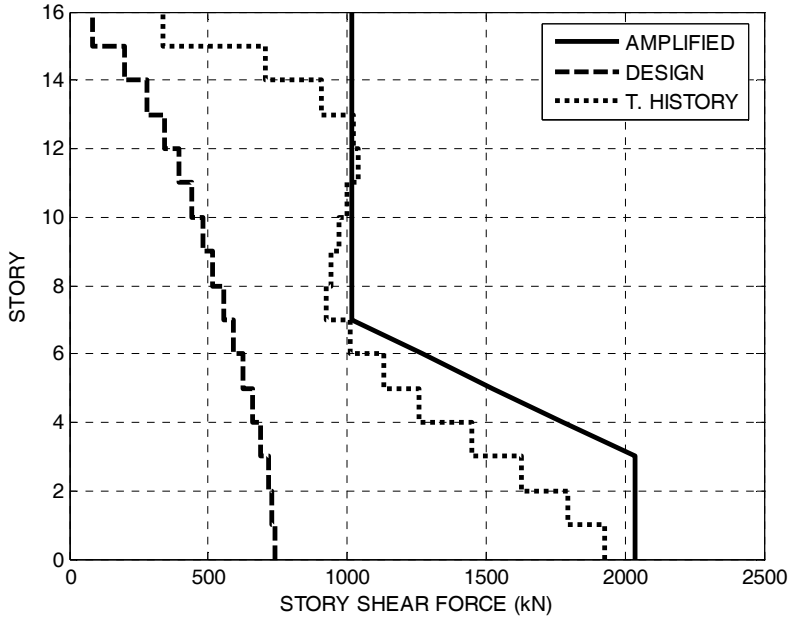

Figure D.2. Amplified design shear forces for the 16 story wall (R = 6)

Proposed Moment Diagram of the 16 Story Generic Wall Designed With a Strength Reduction Factor of R=6

Design moment at the base of the 16 story generic wall has been obtained in Chapter 3 by using the response spectrum method.

$M_e^b = 14677.34$ kNm

Intermediate points on the proposed moment profile are obtained as per Section 6.4 by considering the tension shift effects at the base of the wall.

$\lambda = 1.05 - 0.025 \times 6$ (Equation 6.12)

$\lambda = 0.90$

$\lambda M_e^b = 13209.61$ kNm

$\delta = 0.003 \times (6-2)^2 + 0.025 \times (6-2) + \max(\frac{7.50}{48.0}, 0.167)$ (Equation 6.15)

$\delta = 0.315$

$\delta H_w = 15.12$ m (Just above 5th story level)

$\eta = 0.125 \times (6-2) - 0.005 \times (6-2)^2 + \max(\frac{7.50}{48.0}, 0.167)$ (Equation 6.16)

$\eta = 0.587$

$\eta H_w = 28.18$ m (Just below 10th story level)

Proposed moment diagram with intermediate points obtained as above is given in Figure D.3 where it is compared with the quantities obtained from design and Group 3 non-linear time history analyses.

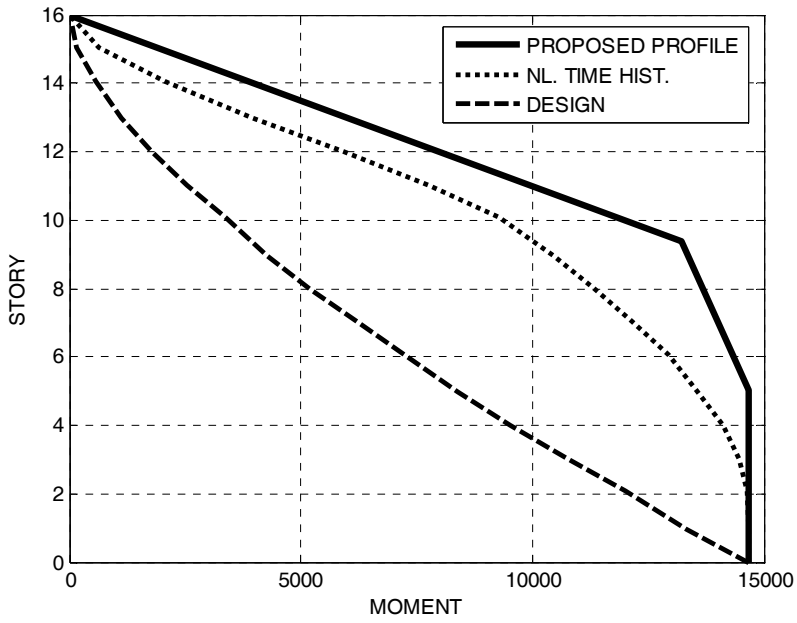

Figure D.3. Proposed moment diagram for the 16 story wall (R = 6)

REFERENCES

Aydınoğlu, M.N., 2003, "An Incremental Response Spectrum Analysis Procedure Based on Inelastic Spectral Displacements for Multi-Mode Performance Evaluation", *Bulletin of Earthquake Engineering*, Vol. 1, pp. 3-36.

Blakeley, G., C. Cooney and M. Megget, 1975, "Seismic Shear Loading at Flexural Capacity in Cantilever Wall Structures", *Bulletin of the New Zealand National Society for Earthquake Engineering*, Vol. 8, No.4, pp. 278-290.

Bathe, K-J., 1996, *Finite Element Procedures*, Prentice Hall, Upper Saddle River, NJ, USA.

Chopra, A.K., 2007, *Dynamics of Structures*, Prentice Hall, Upper Saddle River, NJ, USA.

Carr, A.J., 2000, "RUAUMOKO, Program for Inelastic Dynamic Analysis", Department of Civil Engineering, University of Canterbury, Christchurch, New Zealand.

CEN, 2004, Eurocode EC8, "Eurocode (EC) 8 Design of Structures for Earthquake Resistance-Part I General Rules, Seismic Actions and Rules For Buildings (EN 1998-1)", Comité Européen de Normalisation, Brussels.

CSI, 2006, "SAP 2000, Static and Dynamic Finite Element of Structures", Computers and Structures Inc., Berkeley, California, USA.

Derecho, A. and W. Corley, 1984, "Design Requirements for Structural Walls in Multistory Buildings", *Proceedings of Eighth World Conference on Earthquake Engineering*, San Francisco, California, July 1984, Vol. 5, pp. 541-548.

Eberhard, M. and M. Sözen, 1993, "Behavior Based Method to Determine Design Shear in Earthquake-Resistant Walls", J*ournal of the Structural Division, American Society of Civil Engineers (ASCE)*, Vol. 119(2), pp. 619-640.

Eibl, J. and E. Keintzel, 1988, "Seismic Shear Forces in RC Cantilever Shear Walls", *Proceedings of Ninth World Conference on Earthquake Engineering*, Kyoto, Japan, 2 August-9 August 1991,Vol. VI, pp. VI/5-VI/10.

Filiatrault, A., D. D'Aronco and R. Tinawi, 1994, "Seismic Shear of Ductile Cantilever Walls: A Canadian Code Perspective", *Canadian Journal of Civil Engineering*, Vol. 21, pp. 363-376.

Gosh, S. and P. Markevicius, 1990, "Design of Earthquake Resistant Shearwalls to Prevent Shear Walls", *Proceedings of Fourth U.S. National Conference on Earthquake Engineering*, Palm Springs, California, 20 May-24 May 1990, Vol. 2, pp. 905-913.

Kabeyasawa, T., 1987, "Ultimate-state Design of Reinforced Concrete Wall-Frame Structures", *Proceedings of Pacific Conference on Earthquake Engineering*, Auckland, New Zealand, Vol. 4, pp. 431-440.

Krawinkler, H., 2006, "Importance of Good Nonlinear Analysis", *The Structural Design of Tall and Special Buildings*, Vol. 15, pp. 515-531.

NIED, 2006, "Test of a Six Story R/C Building", Hyogo Earthquake Research Center, E-Defense Facility, National Research Institute for Earth Science and Disaster Prevention, Japan, www.bosai.go.jp.

Paulay, T. and M.J.N. Priestley, 1992, "Seismic Design of Reinforced Concrete and Masonry Buildings", John Wiley & Sons, New York, USA.

Rutenberg, A. and E. Nsieri, 2006, "The Seismic Shear of Ductile Cantilever Wall Systems and the EC8 Provisions", *Bulletin of Earthquake Engineering*, Vol. 4, pp.1-21.

SEAOC, 1999, "Recommended Lateral Force Requirements and Commentary", Structural Engineers Association of California, Sacramento, CA, USA.

Senaviratna, K. and H. Krawinkler, 1994, "Strength and Displacement Demands for Seismic Design of Structural Walls", *Proceedings of Fifth U.S. National Conference on Earthquake Engineering*, Chicago, Illinois, 10 July-14 July 1994, Vol. II, pp.181-190.

Somerville, P., N. Smith, S. Puntamurthula and J. Sun, 1997, "Development of Ground Motion Time Histories for Phase-2 of the FEMA/SAC Steel Project", *SAC Background Document*, SAC/BD-97/04, SAC Joint Venture, Richmond, CA, USA.

Standards New Zealand, 1982, "NZS 4203 Code of Practice for Structural Design and Design Loadings for Buildings", Wellington, New Zealand.

Standards New Zealand, 2006, "Concrete Structures Standard: Part I-The Design of Concrete Structures, Part II-Commentary on the Design of Concrete Structures", Wellington, New Zealand.

Takeda, T., M. Sözen and N. Nielsen, 1970, "Reinforced Concrete Response to Simulated Earthquakes", J*ournal of the Structural Division, American Society of Civil Engineers (ASCE)*, Vol. 96(12), pp 101-113.

The MathWorks Inc., 2004, MATLAB, *The Language of Technical Computing*, USA.

Turkish Seismic Design Code, 2007, "Specification for Buildings to be Built on Seismic Areas", in Turkish, Ministry of Public Works and Settlement, Ankara, Turkey.

Turkish Seismic Design Code, 1997, "Specification for Structures to be Built on Disaster Areas", in English and Turkish, Ministry of Public Works and Settlement, Ankara, Turkey.

UCSD, 2005, "Shake Table Test of a Full-Scale Seven Story Structural Wall", Englekirk Center, Powell Structural Research Laboratories, University of California, San Diego, USA, www.jacobsschool.ucsd.edu/Englekirk.

Wilson, E., 2006, “The Eigenvalue Problem”, Technical Papers, www.csiberkeley.com.

REFERENCES NOT CITED

Clough , R.W. and J. Penzien, 1993, *Dynamics of Structures*, 2nd International Edition, McGraw Hill Inc., Singapore.

Kappos, A.J. and P. Antoniadis, 2007, "A Contribution to Seismic Shear Design of R/C Walls in Dual Structures", *Bulletin of Earthquake Engineering*, Vol. 5, pp. 443-466.

Linde, P., 1998, "Evaluation of Structural Walls Designed According to Eurocode 8 and SIA 160", *Earthquake Engineering and Structural Dynamics*, Vol. 27, pp. 793-809.

Priestley, M.J.N., 2003, "Myths and Fallacies in Earthquake Engineering, Revisited", *The Mallet Milne Lecture*, IUSS Press, Pavia, ITALY.

Riva, P., A. Meda and E. Giuriani, 2003, "Cyclic Behavior of a Full Scale RC Structural Wall", *Engineering Structures*, Vol. 25, pp. 835-845.

Senaviratna, K. and H. Krawinkler, 1997, "Evaluation of Inelastic MDOF Effects for Seismic Design", *The John A. Blume Earthquake Engineering Center*, Report No. 120, June 1997, Department of Civil and Environmental Engineering, Stanford University, CA, USA.